5-2024

Emergency vehicle prioritization in connected and autonomous traffic.

Mohamadreza Haghani
University of Louisville

EMERGENCY VEHICLE PRIORITIZATION IN CONNECTED AND AUTONOMOUS TRAFFIC

By

Mohamadreza Haghani
M.Sc., Civil and Environmental Engineering, Iran University of Science and Technology, Iran, 2016
B.Sc., Civil and Environmental Engineering, Shahid Bahonar University of Kerman, Iran, 2013

A Dissertation submitted to the Faculty of the
J. B. Speed School of Engineering of the University of Louisville
in Partial Fulfillment of the Requirements for the Degree of

Doctor of Philosophy in Civil Engineering

Department of Civil and Environmental Engineering
University of Louisville
Louisville, Kentucky

May 2024

EMERGENCY VEHICLE PRIORITIZATION IN CONNECTED AND AUTONOMOUS TRAFFIC

By

Mohamadreza Haghani
M.Sc., Road and Transportation Engineering, Iran University of Science and Technology, Iran, 2016
B.Sc., Civil and Environmental Engineering, Shahid Bahonar University of Kerman, Iran, 2013

A Dissertation Submitted on

April 26, 2024

By the following Dissertation Committee:

Dr. Robert Kluger, Committee Chair

Dr. Zhihui Sun

Dr. Richard Li

Dr. Lihui Bai

DEDICATION

I would like to dedicate this dissertation to my lovely wife, Farzaneh,

whose unwavering support and love kept me going on,

to my parents, Hasan and Shahnaz,

who sacrificed so much to give me this opportunity,

and to my beloved brother, Javad,

who left us far too soon.

ACKNOWLEDGMENTS

Primarily, I would like to extend my heartfelt appreciation to Dr. Robert Kluger, my committee chair and advisor. His patient guidance throughout my Ph.D. journey, along with unwavering support during challenging moments, has left an indelible mark. As I embark on my academic path, I am fortunate to have him as a perfect model of a mentor, a scientist, and an exceptional individual.

I wish to express my sincere gratitude to my committee members: Dr. Zhihui Sun, Dr. Richard Li, and Dr. Lihui Bai, for their thorough evaluation of my work and constructive feedback. Ultimately, this research owes its existence to the financial support provided by the School of Interdisciplinary and Graduate Studies and the Department of Civil Engineering at the University of Louisville.

Finally, I wish to thank my wife whose belief in my abilities kept me going during tough moments. Thank you for being my rock and my inspiration. I would like to express my gratitude to my parents, Hasan and Shahnaz, whose sacrifices, love, and unwavering faith in my dreams have been instrumental. They have been my pillars of strength. I also wish to extend my gratitude to my siblings, Saeid, Javad, Fatemeh and Amin, whose unwavering encouragement kept me motivated during challenging times. Although my dear brother, Javad, won't be here to witness my graduation, I hope his memory lives on through my dedication to science and research. May he rest in peace.

ABSTRACT

EMERGENCY VEHICLE PRIORITIZATION IN CONNECTED AND AUTONOMOUS TRAFFIC

Mohamadreza Haghani

April 26, 2024

Introduction:

Reducing the response time of emergency vehicles (EV) is highly important due to the relationship between response time and fatality rate. Emerging technologies can help reduce response time by warning vehicles to an approaching EV and harmonizing the movement of vehicles to decrease the lane-changing interference. On the other hand, EV prioritization can negatively impact general traffic especially in cross streets of signalized intersections. In this research, three main objectives were followed. Firstly, creation and dissipation of EVP disruption on arterial cross streets was studied to recommend solutions to prevent this disruption. Secondly, lane-changing and stopping behavior of CAVs were studied in EV prioritization to identify the best lane-changing behavior through minimizing delay. Thirdly, a cooperative behavior framework was developed for CAVs to optimize their trajectories when prioritizing EV to minimize lane-changing conflict.

Methods:

In the first section of this research, a shockwave-based queue length estimation model was developed to determine how EVP affects cross street queue length during and after EVP. Using the developed model, the influence of signal timing adjustments during EVP and transition algorithms on the queue length of cross streets was investigated. The developed model was validated in simulation on an isolated signalized intersection in SUMO to investigate the sensitivity of queue length to influencing variables. In the second section, a driving behavior algorithm specifying what CAVs should do when alerted to an approaching EV and when they should return to normal driving behavior were developed to guide how technology should be used to provide the advance warnings of approaching EVs. A preemption algorithm was also developed to prioritize EVs at signalized intersection. Then, the algorithms were used in different microsimulation scenarios to study the influence of lane-changing and stopping behaviors on the delays of EV and surrounding traffic. At the end, the proposed algorithm was compared with an existing algorithm. In the third section, an optimization algorithm was developed to minimize the delay of the EV and surrounding CAVs by minimizing a lane-changing cost function. A control algorithm was also developed to facilitate CAV movements during emergencies using the optimization results. The trajectory optimization method and the control algorithm together form a proposed cooperative behavior framework for CAVs to facilitate EV passage. The developed framework was evaluated in traffic microsimulation on a three-lane freeway with a right shoulder.

Results:

In the first part, simulation results showed by increasing the traffic flow of cross street in uncongested traffic, maximum and minimum queue lengths of the preemption cycle increased with a constant slope. It was also observed that increasing preemption time reached in increased maximum and minimum queue lengths of preemption cycle. The results verified the model was able to quantify how the disruption created by EVP should be counteracted by adjusting signal timing in transition cycles. In the second part, it was concluded using both lane-changing and stopping behaviors was more favorable as it resulted in lower CAVs delay. An optimum lane-changing threshold was recognized which was accompanied by minimum EV delay. The proposed algorithm proved its ability to induce more reduction in EV delay compared to the existing algorithm. In the third part, the results showed using the cooperative algorithm reduced EV travel time and improved EV travel time reliability compared to other tested algorithms in the scenarios in which EV was on the lanes not adjacent to shoulder. The cooperative algorithm was successful in reducing CAV delay compared to the non-cooperative algorithm in most of scenarios with EV on the lane not adjacent to shoulder. Small increases in EV travel time and CAV delay when EV moved on the lane adjacent to shoulder was a trade-off for the intelligent use of shoulder in the cooperative algorithm intending to minimize shoulder use.

Conclusions:

This research shows that shockwave theory can quantify the disruption created by EVP and investigating solutions to counteract the disruption. The influence of different parameters including preemption, transition, signal timing, and traffic can be investigated on the

disruption. Using the developed queue estimation model, the strategies to prevent the disruption can be designed, and if the disruption is not preventable, the solutions to aid the approaches recover quickly after EVP can be investigated. The results of cooperative behavior framework indicate that if EVs move on the rightmost road lane, adjacent to shoulder, the cooperative algorithm can clear EV's lane and have minimal adverse impact on CAV delay as it can wisely open shoulder to CAVs when required. The developed framework could be implemented to enhance EV movements in traffic networks and reduce the negative impact of EV prioritization on traffic. Intelligent use of shoulder enables the cooperative algorithm to avoid using shoulder when there are obstacles in shoulder which can be studied in future research. As very little is known about human behaviors during EV encounters, in future research, the human aspect of behaviors could be studied to enable the simulation of human drivers in emergencies so that the improvement of CAVs can be measured compared to human drivers. Our cooperative approach was developed and tested in fully connected and autonomous traffic. This approach could be adopted to consider human driving behavior in mixed traffic with different market penetration rates.

TABLE OF CONTENTS

LIST OF TABLES

LIST OF FIGURES

CHAPTER 1

INTRODUCTION

1.1 Introduction and contribution

The response time of emergency medical service (EMS) activations strongly correlates to positive health outcomes (O'Keeffe et al., 2011). EMS vehicle is referred as emergency vehicle (EV) in the following. The response time of EV is the duration between when an emergency call is received and when an EV reaches the scene (Blanchard et al., 2012). Based on EMS call records, the average response time in the United States was estimated to be 7.9 minutes (Mell et al., 2017). It was also observed that reducing the response time to less than 5 minutes was accompanied with a substantial decrease in the fatality rate of EMS, while slight variations in the fatality rate were associated with the response times in the range of over 5 minutes (Blackwell & Kaufman, 2002).

Prioritizing the movement of EVs is highly important in transportation management as it directly influences EV response time. Emergency vehicle preemption (EVP) is used to ensure the safe and fast passage of EVs at signalized corridors. While improving safety and reducing the response time of EVs, EVP can have detrimental influences on general traffic. The performance of EVP algorithms is highly dependent on the preemption threshold that activates the EV's prioritization at traffic signal. If a short threshold is implemented, the EV can be delayed at the intersection. While using large thresholds results in high disruption for general traffic, especially movements other than the EV's approach. Arterial cross streets perpendicular to the EV's movement receive a red light during EVP, and, after EV departure, may require several cycles to fully discharge the residual queue created by EVP. To aid cross streets recover sooner after EVP, transition algorithms are implemented to adjust signal timing. Therefore, the first goal of this research is to quantify the effect on

the queue length of arterial cross streets during and after EVP and provide recommendations to lessen the EVP disruption.

One of the main barriers to reducing EV response time is interference from other vehicles (Lenné et al., 2008). Vehicles ceding right of way to an EV may interfere with each other while changing lanes. As emerging technologies has demonstrated benefits to transportation networks for different purposes such as traffic safety (Papadoulis et al., 2019; Sahebi et al., 2024; Virdi et al., 2019; Ye & Yamamoto, 2019), emergency evacuation (Y. Chang & Edara, 2017, 2018; Ekram & Rahman, 2018; Mirjalili et al., 2023) and intersection management (Khayatian et al., 2020; Khayatian et al., 2018; Qiang Lu & Kim, 2019; Yu et al., 2019) among other applications, they can be beneficial in helping drivers to recognize approaching EVs and, hence, reduce EV response time. Promising technologies include connected vehicles (CV) and connected and autonomous vehicles (CAV) that implement different communication tools such as vehicle to vehicle (V2V) (R. Wang et al., 2019; Zheng et al., 2021) and vehicle to infrastructure (V2I) (Afdhal & Elizar, 2015; Olaverri-Monreal et al., 2018; Zheng et al., 2021). CAVs can leverage communication and advanced computing to aid in reducing the lane-changing inference. CAVs operate by broadcasting positions and speeds to other CAVs and infrastructure. V2V communications can potentially be used to alert vehicles to an approaching EV, without relying on limitations associated with lights and sirens. V2I communications can help relay messages between vehicles and infrastructure and enable infrastructure such as connected traffic signals to engage in preemption.

While previous research investigated the applications of new technologies to facilitate the movement of EVs through varying conditions (Hannoun et al., 2018; Lenné et al., 2008; Weinert & Düring, 2015; J. Wu et al., 2020), none was identified that focused on comparing different combinations of vehicles lane-changing and stopping behavior to preclear the EV's lane in a connected and autonomous traffic environment. CAV technologies can be implemented to improve lane changing behavior to cede the right of way more efficiently to EVs. Hence, the second goal of this research is to explore the lane-changing and stopping behaviors of CAVs on arterial corridors to investigate how these behaviors affect the delay of EV and CAV traffic.

Independent behavior of vehicles while clearing EV's way is a factor contributing to increasing lane-changing conflict. Utilizing autonomous vehicles, a traffic fleet can behave cooperatively to clear the way for an EV. Using cooperative behavior algorithms, positions and speeds of CAVs can be transmitted to a central processor, where optimization methods are implemented to improve the chance EVs are unimpeded in responding to emergencies and limit the impact of the encounter on surrounding traffic. Therefore, the third goal is to establish a cooperative behavior framework for harmonizing the trajectories of CAVs to cede the right of way for EVs on multilane freeways.

The contributions of this research are as follows:

1. A queue estimation model was developed based on shockwave theory to study the influence of EVP on arterial cross streets. Using the developed model, the sensitivity of residual queue created by EVP was investigated to contributing parameters including signal timing, preemption and transition settings and traffic

volume. The developed model can estimate EVP disruption and required number of cycles to dissipate the disruption with the current preemption and transition settings. It also can recommend what preemption and transition settings are required to eliminate EVP disruption in a desired number of cycles.

2. A driving behavior algorithm was developed to identify the desired behavior of CAVs in preclearing EV's lane. A preemption algorithm was also devised to prioritize EVs at signalized intersections. Using the developed algorithms, the desired lane-changing and stopping behavior of CAVs in emergencies was investigated with the aim of minimizing EV and general traffic delay in arterial corridors.
3. A binary linear programing model was developed to optimize trajectories of CAVs when clearing EV's way with the aim of minimizing lane-changing disruption. A control algorithm was implemented to control lane changes and speed changes of CAVs based on optimization output. The optimization approach and the control algorithm together form a cooperative behavior framework harmonizing CAVs movements in emergencies on multilane freeways. The developed framework can allow CAVs to move to shoulder when clearing EV's way is not feasible using freeway main lanes.

1.2 Structure of the dissertation

This dissertation includes five other chapters. Chapter 2 provides a summary of related literature focused on EV prioritization. This chapter is divided into three parts focusing on EVP methods, CAVs lane-changing and stopping behavior and cooperative behavior of

CAVs. Chapters 3, 4 and 5, each includes a research paper and has objectives, methodology, results, discussions, and conclusions sections.

Chapter 3 aimed to quantify the effect on the queue length of arterial cross streets during and after EVP and provide recommendations to reduce the EVP disruption. A shockwave-based queue length estimation model was developed to determine how EVP affects cross street queue length during and after EVP. Using the developed model, the influence of signal timing adjustments during EVP and transition algorithms on the queue length of cross streets was investigated. The developed model was validated in simulation on an isolated signalized intersection in SUMO to investigate the sensitivity of queue length to influencing variables.

Chapter 4 investigated how the lane-changing and stopping behaviors of CAVs affect the delay of EV and CAV traffic on arterial corridors in microsimulation. A driving behavior algorithm specifying what CAVs should do when alerted to an approaching EV and when they should return to normal driving behavior were developed to guide how technology should be used to provide the advance warnings of approaching EVs. A preemption algorithm was also developed to prioritize EVs at signalized intersection. At the end, the proposed algorithm was compared with an existing algorithm.

Chapter 5 aimed to establish a methodology for optimizing CAVs trajectories when an EV enters a freeway segment. An optimization algorithm was developed to minimize the delay of the EV and surrounding CAVs by minimizing a lane-changing cost function. A control algorithm was also developed to facilitate CAV movements during emergencies using the optimization results. The trajectory optimization method and the control algorithm together

form a proposed cooperative behavior framework for CAVs to facilitate EV passage. The developed framework was evaluated in traffic microsimulation on a three-lane freeway with a right shoulder.

Chapter 6 summarizes the research, provide contributions and applications of the developed models, and recommend future research topics based on our limitations.

CHAPTER 2

BACKGROUND

2.1 Introduction

Researchers have widely investigated approaches to prioritize EVs in traffic networks (Akdoğan et al., 2018; Hannoun & Menendez, 2022; Y. Liu et al., 2016; Park et al., 2019). EV prioritization approaches have been studied in both real-world settings and simulation environments. Simulation enables the testing of microscopic effects of EVs on traffic conditions while controlling for factors that cannot be easily controlled for in the real world (Gomes, 2022; Hassannayebi et al., 2020; Xu et al., 2017). A summary of literature focused on EV prioritization is provided in the following. The related research was divided into three sections. In the first section, different EVP approaches used to prioritize EVs and minimize adverse influence on general traffic at signalized corridors were provided. In the second section, a summary of research investigating lane-changing and stopping behavior of CAVs to facilitate EV movement were summarized. In the third section, the related research on CAV cooperative behavior with the aim of clearing EV's way was highlighted.

2.2 Emergency Vehicle Preemption

EVP allows a traffic signal to dynamically adjust phases and timings to prioritize EV movements safely. Sanderson et al. and Roberson et al. were among the first researchers to investigate the ability of local controllers to initiate green waves to facilitate the movement of EV as computer controllers were being first developed in the late 1970s (Robertson & Glassbrook, 1979; Sanderson & Lord, 1978). More attention was brought to EVP when it was reported that 60 percent of EV traffic accidents at signalized intersections were right angle crashes against perpendicular traffic when EV crossed the red light (Cleal, 1982).

The preemption threshold, which is used to activate preemption, is one of the challenging parameters in EVP algorithms. If a short threshold is used, queue may not be fully discharged before EV arrival. On the other hand, using a longer threshold results possibly large disruptions for general traffic. Approaches that face red light during EVP may encounter large residual queues at the end of preemption. Hence, researchers aimed to improve EVP algorithms by accurate preemption threshold identification (Mu et al., 2018; Noori, 2013; Noori et al., 2016; Qin & Khan, 2012; Viriyasitavat & Tonguz, 2012) and devise preemption strategies that accounted for both EV delay and traffic delay due to the disruptions in signal timings (Qiang Lu & Kim, 2017; Qin & Khan, 2012; Su et al., 2023; Yun et al., 2011).

Different emerging technologies including vehicular ad hoc network (VANET) (Nellore & Hancke, 2016; Noori, 2013), dedicated short-range communications (DSRC) (Noori et al., 2016), and internet of things (IOT) (Chowdhury, 2016) have been employed to improve EVP and EV routing performance. Qin et al. developed an EVP algorithm which used V2I communications to obtain the arrival time of EV and the discharge time for the intersection queue to improve preemption threshold estimation accuracy. In addition to the queue dispersal time, then also added a safety time parameter to create a period of guaranteed safe passage for the EV. By calibrating these parameters, EVPs could be triggered only when necessary, reduce the amount of unused green time and ended once the EV has passed (Qin & Khan, 2012). Wang et al. developed a model to estimate the travel time of EVs with EVP and compare different preemption strategies in microsimulation (J. Wang et al., 2013). Noori et al. developed a VANET communication strategy to implement EVP in

SUMO (Noori, 2013). In another study, Noori et al. identified the proper time to start preemption for EV by estimating the queue length of intersection using V2I communications in SUMO. They created a beaconing algorithm that introduced further refinements to improve the queue discharge time calculation. Startup and saturation times and estimated queue was used to evaluate discharge time (Noori et al., 2016).

To lessen the negative influence of EVP on the vehicles surrounding EV, Kang et al. proposed a coordination system for optimizing EVPs. The results of traffic simulations showed the developed system was able to decrease the delay of EVs without having noticeable effects on other vehicles' delay (Kang et al., 2014). Viriyasitavat and Tonguz developed a self-organized system to prioritize EVs at intersections using virtual traffic lights (Viriyasitavat & Tonguz, 2012). Lu and Kim developed an intersection control algorithm to identify the best vehicle sequence which prioritizes EV passing and minimizes adverse impact on CAV traffic. A genetic algorithm approach was utilized to optimize vehicle sequence. Simulation results in SUMO revealed that the proposed algorithm reduced the response times of EVs without causing substantial delays for other vehicles (Qiang Lu & Kim, 2017). Karmakar et al. developed an EV priority framework to prioritize emergency services based on incident's severity and type. EV's route and required signal interventions then were identified through minimizing EV's travel time and negative influence on traffic (Karmakar et al., 2020). Shelke et al. implemented Fuzzy logic to develop a framework considering real-time congestion in EV routing to improve signal control and EV prioritization (Shelke et al., 2019). Su et al. developed a decentralized

reinforcement learning strategy to improve the real-time integration between EVP and EV routing (Su et al., 2022).

As EVP disrupts coordination with upstream signals in coordinated corridors, different transition algorithms have been developed in the literature to resync the coordinated signals after EVP and to aid the recovery of corridors. Nelson and Bullock discussed the disruptive influence of EVP on general traffic as one of EVP's drawbacks. Their research aimed to quantify this disruption by investigating different transition methods designed to recover from EVP. Smooth, dwell and add-only methods were compared, and smooth transition was identified as the best performing method in their research (Nelson & Bullock, 2000). Later, Shelby and Bullock preformed comprehensive research on signal transition and confirmed smooth transitioning as a promising method while the short way method showed the best results (Shelby et al., 2006). Yun et al. investigated the optimized transition from the preemption state of a traffic signal to normal state to reduce delay (Yun et al., 2011). In another study, they concluded that the implementation of short way method with 2 to 3 transition cycles reached minimum average delay (Yun et al., 2012).

Queue length is a performance measure that can reflect the instantaneous impact of external factors on an approach's performance. Hence, the variation of queue length can be investigated to quantify the disruption created by EVP and evaluate the performance of transition methods in eliminating this disruption. To this end, queue estimation models have been developed. According to the literature, queue estimation models can be divided into two general groups. The first group called input-output models were proposed by Webster (Webster, 1958) and expanded by other researchers (Sharma et al., 2007; Strong

et al., 2006; Vigos et al., 2008). These models are based on using the input and output traffic flow of an approach to estimate queue. The main drawback of input-output models is their inability to explain the spatial variation of queue length over time (Michalopoulos et al., 1981). Sharma et al. concluded that input-output models are simple and cost-effective but are unable to work properly when there is inflow or outflow traffic between the stop line and traffic detector or when queue spills back over the detector (Sharma et al., 2007). Liu et al. also noted input-output models fail when congestion overtakes the detector's location (H. X. Liu et al., 2009).

The second group of queue estimation models are based on shockwave theory proposed by Lighthill and Whitham (Lighthill & Whitham, 1955) and Richards (Richards, 1956) and improved by Stephanopolos and Michalopoulos (Michalopoulos et al., 1981; Stephanopoulos et al., 1979). In shockwave theory, it is assumed that shockwaves cause the process of queue creation and dissipation at signalized intersections. Hence, in these models, queue estimation is performed by following the trajectory of shockwaves. Liu et al. developed a shockwave-based queue estimation model able to explain the spatiotemporal characteristics of queue using high-resolution event-based data as input (H. X. Liu et al., 2009).

With the advent of new technologies, researchers began implementing real-time vehicle trajectory data to develop shockwave-based queue estimation models. Ban et al. used vehicle travel time collected by smartphone as inputs in their queue estimation model. Two new concepts of Queue Front No-delay Arrival Time (QFNAT) and Queue Rear No-delay Arrival Time (QRNAT) were defined according to shockwave theory. Their model

estimated queue length based on queueing delay, QFNAT and QRNAT (Ban et al., 2011). Cheng et al. developed a shockwave-based model to estimate queue length using only vehicle trajectory data as input. Trajectory data were collected using V2V and V2I communication tools. A new concept of the Critical Point (CP) was defined as a point where vehicle dynamics change. Shockwave speeds were calculated through identifying CPs and used for queue estimation (Y. Cheng et al., 2011). Cetin used probe vehicles trajectories to determine shockwaves speeds and intercepts. Then, a shockwave-based model was implemented to estimate the trajectory of tail of queue over time (Cetin, 2012). Wang et al. improved the performance of shockwave-based queue estimation models using multi-source data. The recorded trajectories of probe vehicles were combined with traffic detector data to calculate shockwaves speeds and estimate queue length (Z. Wang et al., 2017). Cycle-based queue estimation using shockwave-based models relies on the accurate identification of arrival traffic characteristics and the residual queue remained from previous cycle. Zhang et al. integrated low-penetration rate probe vehicles trajectory data to calibrate these two parameters to improve queue estimation accuracy (H. Zhang et al., 2019).

Despite producing high-fidelity results, shockwave-based models depend on the identification of critical breakpoints in the shockwave diagram. Breakpoints are the points in space-time diagram at which queue crosses traffic detector. Breakpoint identification is not feasible in specific traffic states including oversaturation, undersaturation with short queues or when vehicles arrive in large platoons from upstream. To overcome the deficiency of breakpoint identification, An et al. added two input-output models to a

shockwave-based model. The authors also developed frameworks for breakpoint and queue-over-detector misidentification checking. The results showed a Mean Absolute Error (MAE) reduction in maximum queue length estimation (from 105.6 ft to 35.7 ft) using the proposed model compared to using only the shockwave-based model (An et al., 2018). Wu and Liu developed a comprehensive model called Shockwave Profile Model (SPM) to estimate queue in saturated and oversaturated intersections. Their model considered the changes in shockwave speeds when residual queue spills over to the upstream intersection (X. Wu & Liu, 2011). Shockwave-based models assume three traffic states including arrival, saturated and jam states. Shockwaves are created at the intersection of each pair of these states. In well-coordinated corridors, vehicles move in large platoons which makes it hard to distinguish between arrival and saturated traffic states. Therefore, tracking shockwaves and implementing shockwave-based models for queue estimation become infeasible. To address this limitation, Shen et al. integrated shockwave theory to platoon dispersion models to develop a new queue estimation model assuming truncated normal distribution for speed (Shen et al., 2022). Chang et al. noted that the disadvantages of shockwave-based models were their complexity and dependence on detailed event-based data that might not be available in real-time. They developed a queue estimation model comparing the average occupancy recorded by a traffic detector with two thresholds corresponding to free flow traffic with no queue and congested traffic with queue spilling over the detector (J. Chang et al., 2013).

2.3 Lane-Changing and Stopping Behavior

Understanding how vehicles react to approaching EVs is critical to both accurate simulation and designing technology. By analyzing video data, Weinert and Düring observed that nearly 25% of drivers reacted to approaching EVs exceeding 50 meters from their vehicles, about 50% of drivers reacted to an approaching EV between 20 and 50 meters from their vehicles, and the other 25% reacted when the EV was less than 20 meters away (Weinert & Düring, 2015). Bieker-Walz et al. utilized SUMO software to simulate the driving behavior of EVs and surrounding traffic in a microscopic traffic environment. 25 meters was used, in this software, as the threshold distance at which vehicles recognized an approaching EV and reacted to it. This distance corresponds to the sound pressure level of 100 dB(A), at which, the sound of siren is audible for an average driver (Bieker-Walz et al., 2018).

Driving behavior models have been explored to replicate the real behavior of vehicles in emergencies in simulation environments. Generally, driving behavior models have two components: car following and lane changing models (Sun & Elefteriadou, 2014). Interference while lane-changing is the primary source of delay when vehicles clear a lane for an EV in road segments (Hannoun et al., 2018; Lenné et al., 2008; J. Wu et al., 2020). Therefore, to study the driving behavior of EVs and other vehicles, the focus of research should be on lane-changing models. Moussa developed a cellular atomation model to simulate vehicles lane-changing behavior when evacuating EV's lane in highways. The additional rule in this model was the pull-over of vehicles (Moussa, 2009).

Emerging technologies are already changing the way that an EV can operate through a traffic fleet. Obenauf et al. developed a framework to estimate the influence of CAV implementation on EV response time and mortality rate (Obenauf et al., 2019). Lenné et al. investigated the impact of utilizing advanced warning device (AWD) on the responses of vehicles to EVs in different scenarios in a driving simulator study. AWD helped drivers to detect an approaching EV up to 400 meters away. The results showed that the use of AWD was accompanied by an earlier speed reduction at intersections while it was associated with an earlier lane-changing on road segments compared to no AWD (Lenné et al., 2008). Few studies have linked lane-changing behavior and technologies in emergencies. Weinert and Düring's research is one of these studies in which the lane-changing behavior of CAVs was investigated to make a rescue lane for EV (Weinert & Düring, 2015). And among these few studies, none investigated the desired combination of lane-changing and stopping behaviors of CAVs to facilitate EV's movement.

2.4 Cooperative Behavior

With the advent of autonomous vehicles, cooperative behavior has been implemented for CAV fleets to improve safety and efficiency of traffic networks. In a multi-agent environment, cooperative behavior is defined as a behavior algorithm enabling agents to move towards the common benefit of group (Fujii et al., 2010). Miculescu and Karaman developed a coordination control algorithm to adjust autonomous vehicles speeds with the goal of reducing delay and prohibiting crash at intersection (Miculescu & Karaman, 2019). Zheng et al. also developed a rule-based cellular automation model to simulate the cooperative driving using V2V communications (Zheng et al., 2021). Bai et al. developed

a cooperative behavior model for CAVs to eliminate conflicting lane-changings and decrease traffic oscillation in weaving areas (Bai et al., 2022). Nageshrao et al. developed a decision-making method using reinforcement learning to enable autonomous vehicles make better real-time decisions in different scenarios (Nageshrao et al., 2019). Zhou et al. developed a framework to model the cooperative lane-changing behavior of autonomous vehicles using multi-agent reinforcement learning (Zhou et al., 2022).

Cooperative behavior has also been employed to facilitate EV movement. Humayun et al. developed an emergency vehicle management system to prioritize EVs in traffic networks. Their algorithm is able to identify the efficient sequence of autonomous traffic to simultaneously prioritize several EVs and considers ordering vehicles to move to shoulder to clear EV's lane (Humayun et al., 2022). Buckman et al. implemented game theory to develop semi-cooperative behavior for autonomous EVs and used the social value orientation metric to model EV's impact on the behavior of non-automated traffic (Buckman et al., 2021). So et al. developed a driving control strategy controlling autonomous EV movements and signal preemption to improve EV's safety and efficiency. The focus of their study was on EV automated driving without considering evasive maneuvers for surrounding vehicles to clear EV's lane (So et al., 2020).

Parada et al. developed a decentralized multi-agent optimization method to create cooperative behavior for autonomous vehicles with the goal of increasing safety and efficiency of EV movements (Parada et al., 2023). Decentralized methods improve the efficiency and processing time of optimization as gathering and transferring data to a central processor is not required. On the other hand, centralized optimization methods can

better minimize the objective function as they have access to a larger amount of data ad can create larger solution sets. Hence, the behavior of a traffic fleet could be controlled and optimized by a central unit to improve the performance of cooperative behavior. Integer linear programming (Hannoun et al., 2018) and mixed-integer nonlinear programming (J. Wu et al., 2020) were used by Hannoun et al. and Wu et al., respectively, for optimizing the behavior of connected vehicles to clear a lane for EV using discrete cell trajectory models.

Because the cooperative behavior algorithms presented by (Hannoun et al., 2018; J. Wu et al., 2020) were developed based on discrete cell simulations, they did not consider microsimulation car-following and lane-changing models. In discrete cell simulations, traffic variables including position and speed are discrete. Since discrete speed might lead in unrealistic traffic movements, an integer variable is defined for speed in discrete simulations (Hannoun et al., 2018). Hence, developing and evaluating cooperative behavior in microsimulation is necessary as it enables cooperative frameworks better adopt to real-world applications. Additionally, as realistic lane-changing processes cannot be effectively modeled in discrete cell simulations, real-world lane-change conflicts cannot be addressed in discrete simulations. Hence, the literature lacks a cooperative behavior model optimizing CAV trajectories to prioritize EV which goes beyond the limitations of discrete cell simulations and considers more realistic driving behavior models in traffic microsimulation.

2.5 Research Gaps

In this dissertation, a comprehensive study was performed on prioritizing EV in CAV traffic which was a gap in the literature. EV prioritization impacts traffic on main approach and cross approaches. Firstly, the negative impact on cross streets can be counteracted by improving preemption and transition strategies. However, the relationship between preemption and transition parameters and EV disruption has not been investigated before. Secondly, the negative influence of EV on main approach can be counteracted by improving lane-changing behavior of CAV traffic. The literature lacks a study investigating the best lane-changing and stopping behavior of CAVs to minimize EV and traffic delay. As the next step, the literature also lacks a cooperative behavior framework able to optimize CAVs trajectories to minimize lane-changing disruption. A summary of research gaps identified in the literature is provided:

1. The first gap was the lack of a model able to explain the creation and dissipation queues on minor streets during EVP. Hence, a queue estimation model was developed based shockwave theory. The developed model can estimate EVP disruption and can be used to recommend solutions for minor streets to recover sooner.
2. The second gap was the lack of a research investigating lane-changing and stopping behaviors of CAVs while clearing way for EV. By studying different combinations of CAVs lane- changing and stopping behaviors, the best behavior setting can be identified to facilitate EV's movement. To investigate CAV behavior, a CAV

behavior control algorithm and a preemption algorithm were developed to prioritize EV on urban arterials.

3. The third gap was the lack of a cooperative behavior framework for CAVs which can optimize CAV trajectories to clear EV's lane. Previous cooperative frameworks for CAVs in emergencies was developed based on discrete cell-based simulations. Cell-based simulations do not consider car-following and lane-changing details of vehicle movements. Traffic microsimulation tools, on the other hand, implement car-following and lane-changing models. These models can address the potential conflicts happening in real-world maneuvers when CAVs intend to clear EV's way and improve the performance of cooperative framework. To address this gap, an optimization approach was developed to optimize vehicle trajectories, and a control algorithm was developed to direct CAVs based on optimized trajectories.

CHAPTER 3

USING SHOCKWAVE THEORY TO QUANTIFY THE DISRUPTION CREATED BY EMERGENCY VEHICLE PREEMPTION

3.1 Objective

The objective of this research was to quantify the effect on the queue length of arterial cross streets during and after EVP and provide recommendations to lessen the EVP disruption. A shockwave-based queue length estimation model was developed based on shockwave theory (Lighthill & Whitham, 1955; Richards, 1956) to determine how EVP affects cross street queue length during and after EVP. Using the developed model, the influence of signal timing adjustments during EVP and transition algorithms on the queue length of cross streets was investigated. The developed model was validated in simulation on an isolated signalized intersection in SUMO microsimulation software (Lopez et al., 2018) to investigate the sensitivity of queue length to influencing variables.

3.2 Methodology

3.2.1 Queue Length Estimation Model

EVP and transition algorithms modify signal timing to prioritize EV during EVP and accelerate corridor recovery after EVP, respectively. As the goal of this research is to quantify the disruption created by EVP, the developed queue estimation model should be able to capture the influence of signal timing parameters on queue length. The model was developed based on an observable initial queue to prevent the limitation of break point identification infeasibility (H. X. Liu et al., 2009). All the variables used in the queue estimation model and their definitions are provided in Table 3.1. As described in Liu et al.'s study, shockwave theory can be used to explain the creation and dissipation process of queue at signalized intersections. Four shockwaves, defined in Liu et al.'s research, take

part in this process with the speeds calculated using Equations 3.1, 3.2, 3.3 and 3.4 (H. X. Liu et al., 2009). Comparing Equations 3.2 and 3.4, it can be observed that shockwaves v_2 and v_4 have the same speed magnitude.

Table 3.1. Variables used in the queue estimation model.

Variable symbol	Definition
v_1	The speed of the queue creation shockwave (meters per second)
v_2	The speed of the queue dissipation shockwave (meters per second)
v_3	The speed of the queue reduction shockwave (meters per second)
v_4	The speed of the residual queue shockwave (meters per second)
q_a	The flow of arrival traffic (vehicles per second)
k_a	The density of arrival traffic (vehicles per meter)
q_m	The flow of saturated traffic (vehicles per second)
k_m	The density of saturated traffic (vehicles per meter)
k_j	The density of jammed traffic (vehicles per meter)
$Q_{min\_obs}^{n-1}$	The observed minimum queue length of cycle $n-1$ (meters)
T_{min}^{n-1}	The time at which the observed minimum queue of cycle $n-1$ occurred (seconds)
Q_{max}^{n}	The estimated maximum queue length of cycle n (meters)
T_{max}^{n}	The time at which the estimated maximum queue length of cycle n occurred (seconds)
Q_{min}^{n}	The estimated minimum queue length of cycle n (meters)
T_{min}^{n}	The time at which the estimated minimum queue length of cycle n occurred (seconds)
T_r^n	The start of effective red time in cycle n (Seconds)
T_g^n	The start of effective green time in cycle n (Seconds)
T_g^n	The adjusted start of effective green time in cycle n (Seconds)
T_r^{n+1}	The start of effective red time in cycle $n+1$ (Seconds)
T_r^{n+1}	The adjusted start of effective red time in cycle $n+1$ (Seconds)
T_a^n	The time when v_1 crosses the horizontal axis (Seconds)
T_b^n	The time when v_3 crosses the horizontal axis (Seconds)
R	The effective red time assigned to the studied approach in one cycle (Seconds)
G	The effective green time assigned to the studied approach in one cycle (Seconds)
s	The number of transition cycles
ΔQ_{max}^0	The induced change in Q_{max} in the preemption cycle compared to before preemption
ΔQ_{min}^0	The induced change in Q_{min} in the preemption cycle compared to before preemption
ΔQ_{max}^s	The induced change in Q_{max} in s transition cycles compared to before preemption
ΔQ_{min}^s	The induced change in Q_{min} in s transition cycles compared to before preemption
ΔR_P	The change in the effective red time of the preemption cycle
ΔG_{T0}	The change in the effective green time of the preemption cycle
ΔR_{Tl}	The change in the effective red time of the lth transition cycle
ΔG_{Tl}	The change in the effective green time of the lth transition cycle
x	It is 1 if s is equal or more than 1. Otherwise, it is 0.
y	It is 1 if s is equal or more than 0. Otherwise, it is 0.

$$v_1 = \frac{0 - q_a}{k_j - k_a} \quad (3.1)$$

$$v_2 = \frac{q_m - 0}{k_m - k_j} \quad (3.2)$$

$$v_3 = \frac{q_m - q_a}{k_m - k_a} \quad (3.3)$$

$$v_4 = \frac{0 - q_m}{k_j - k_m} \quad (3.4)$$

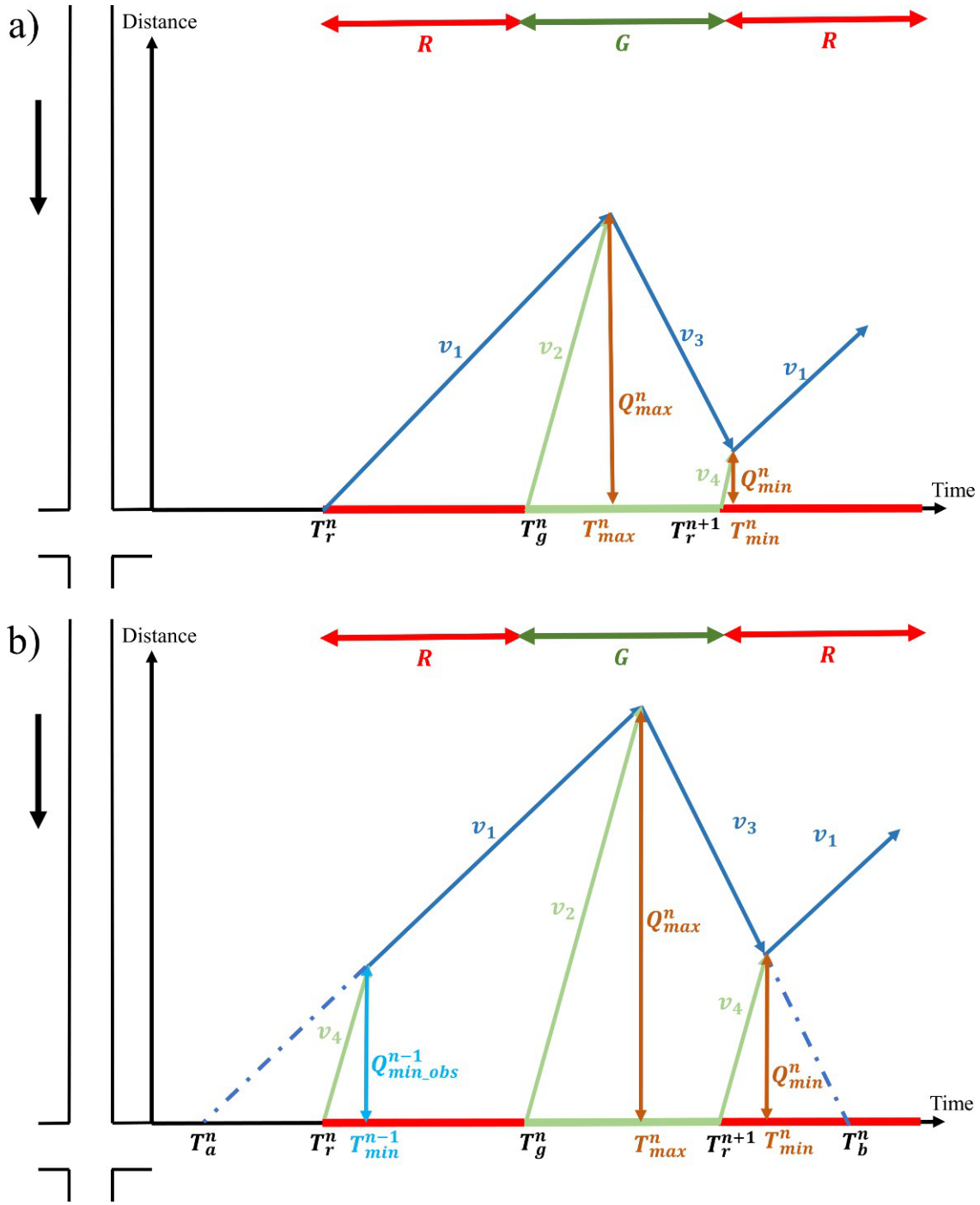

Figure 1. (a) Shockwave profiles of a signalized intersection without initial residual queue (H. X. Liu et al., 2009)
(b) with initial residual queue.

In this study, queue length is considered as the distance between the stop line and the rear bumper of the last stopped vehicle in queue. Figure 1 shows shockwave profiles of a signalized intersection with and without initial residual queue remained from the previous cycle, $Q_{min\_ob}^{n-1}$. n represents the number of the studied cycle for which the maximum and minimum queue lengths are estimated. Figure 1 (a) is a special case of Figure 1 (b) when $Q_{min\_ob}^{n-1}$ is equal to 0. Hence, the queue estimation model was developed for a cycle with $Q_{min\_ob}^{n-1}$. Figure 1 (a) is derived from Liu et al.'s study. Liu et al.'s queue estimation model was based on identifying the breakpoints at which queue crosses the detector's position (H. X. Liu et al., 2009). However, our model is based on the points at which shockwaves v_1 and v_3 intersect the horizontal axis. Therefore, the points T_a^n and T_b^n were added in Figure 1 (b). According to Figure 1 (b), Equations 3.5, 3.6, 3.7 and 3.8 were derived to calculate Q_{max}^n, T_{max}^n, Q_{min}^n and T_{min}^n, respectively. The details of deriving these equations are provided in Appendix A.

$$Q_{max}^n = \frac{R + Q_{min\_obs}^{n-1}\left(\frac{1}{v_1} - \frac{1}{v_2}\right)}{\left(\frac{1}{v_1} - \frac{1}{v_2}\right)} \quad 3.5$$

$$T_{max}^n = T_r^n + \frac{Q_{min\_obs}^{n-1}}{v_2} + \frac{\left(Q_{max}^n - Q_{min\_obs}^{n-1}\right)}{v_1} \quad 3.6$$

$$Q_{min}^n = \frac{Q_{max}^n\left(\frac{1}{v_1} + \frac{1}{v_3}\right) - Q_{min\_obs}^{n-1}\left(\frac{1}{v_1} - \frac{1}{v_2}\right) - (R+G)}{\left(\frac{1}{v_2} + \frac{1}{v_3}\right)} \quad 3.7$$

$$T_{min}^n = T_{max}^n + \frac{\left(Q_{max}^n - Q_{min}^n\right)}{v_3} \quad 3.8$$

According to Equations 3.5, 3.6, 3.7 and 3.8, Q^n_{max}, T^n_{max}, Q^n_{min} and T^n_{min} are dependent on shockwave speeds (v_1, v_2 and v_3), signal timing parameters (R and G), and the observed initial residual queue ($Q^{n-1}_{min\_ob}$). Based on Equations 3.1, 3.2 and 3.3, shockwave speeds are dependent on traffic conditions. Hence, Equations 3.5 and 3.7 explain how traffic conditions indirectly influence Q^n_{max} and Q^n_{min} through shockwave speeds. EVP algorithms are used to clear a signal's approach before EV's arrival. The preemption threshold influences the red time, R, for cross streets. According to Equations 3.5 and 3.7, Q^n_{max} and Q^n_{min} are dependent on R which is influenced by preemption threshold. Transition algorithms adjust signal timing parameters (R and G) for several cycles after EVP to clear the disruption created by EVP. According to Equations 3.5 and 3.7, Q^n_{max} and Q^n_{min} are dependent on R and G which are identified by the transition algorithm.

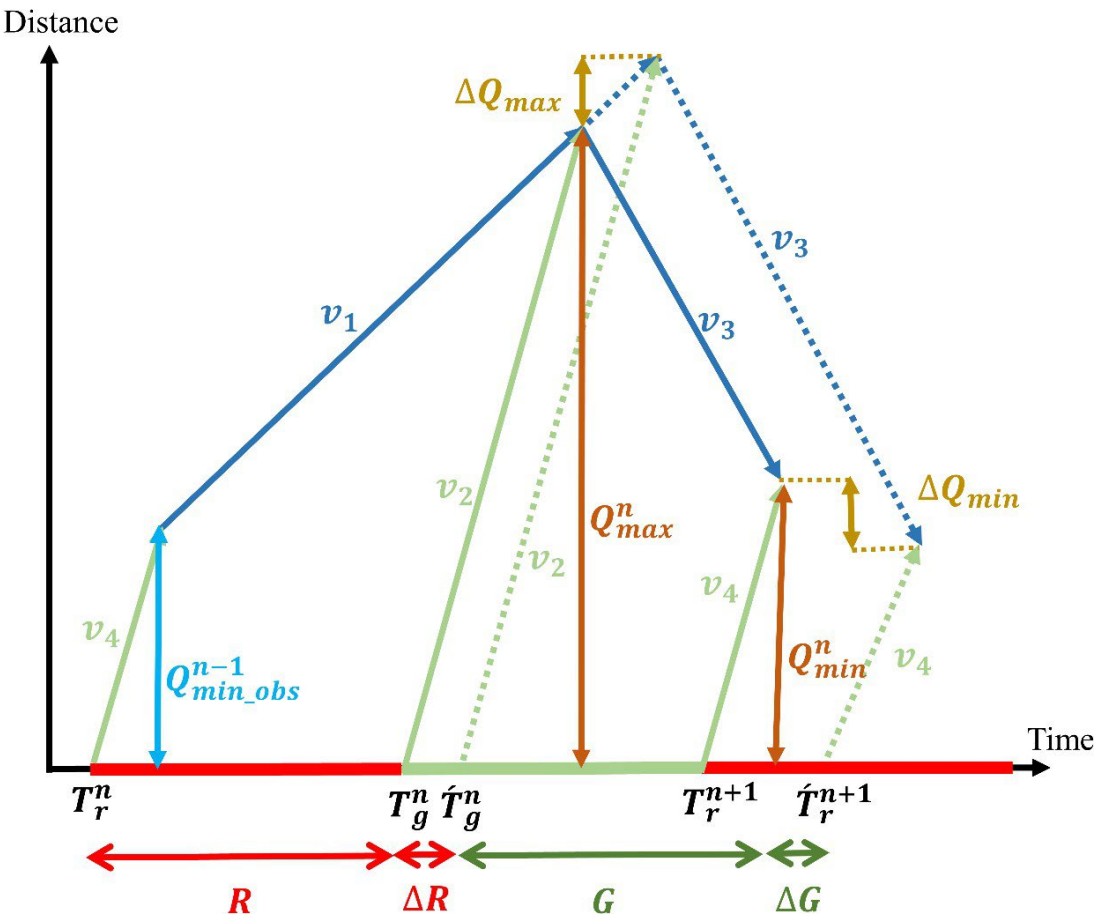

Figure 2. Induced variations in Q_{max} and Q_{min} due to changes in R and G

Figure 2 shows how queue length is influenced by R and G extensions in 1 cycle. Equations 3.9 and 3.10 are derived from Equations 3.5 and 3.7 to calculate the induced changes in Q_{max} and Q_{min} due to changes in R and G after s transition cycles when all other variables are kept constant.

$$\Delta Q^s_{max} = \frac{\Delta R_P}{\Delta R_{T_l}} + x\left(\sum_{l=1}^{s} \frac{\Delta R_{T_l}}{\left(\frac{1}{v_1}-\frac{1}{v_2}\right)} - \sum_{i=0}^{s-1} \frac{\Delta G_{T_i}}{\left(\frac{1}{v_2}+\frac{1}{v_3}\right)}\right) \quad 3.9$$

$$\Delta Q^s_{min} = \frac{\Delta R_P}{\Delta R_{T_l}} + x\sum_{l=1}^{s} \frac{\Delta R_{T_l}}{\left(\frac{1}{v_1}-\frac{1}{v_2}\right)} - y\sum_{i=0}^{s} \frac{\Delta G_{T_l}}{\left(\frac{1}{v_2}+\frac{1}{v_3}\right)} \quad 3.10$$

The residual queue at the end of transition cycles can be used to identify whether the transition algorithm is able to completely clear the disruption created by EVP. To identify the required transition settings for this objective, ΔQ_{min}^{s} is set to 0 in Equation 3.10. Hence, Equation 3.11 shows the required relationship between the EVP red time, ΔR_P, the transition red time, ΔR_T, and the transition green time, ΔG_T, extensions to fully discharge the residual queue at the end of s transition cycles.

$$\Delta R_P = \sum_{i=2}^{m} \Delta R_{Ti} - \frac{\left(\frac{1}{v_1} - \frac{1}{v_2}\right)}{\left(\frac{1}{v_2} + \frac{1}{v_3}\right)} \sum_{i=1}^{m} \Delta G_{Ti} \qquad 3.11$$

3.2.2 Validation of the Developed Model in EVP Simulation

As the aim of this research is to study the variation of queue as an indicator of arterial cross streets disruption induced by EVP, the developed queue estimation model was validated using EVP simulation. SUMO, an opensource traffic microsimulation software, was used to simulate EVP in an isolated signalized intersection, and the model was implemented to estimate queue at arterial cross streets (Lopez et al., 2018). The simulation network is shown in Figure 3.

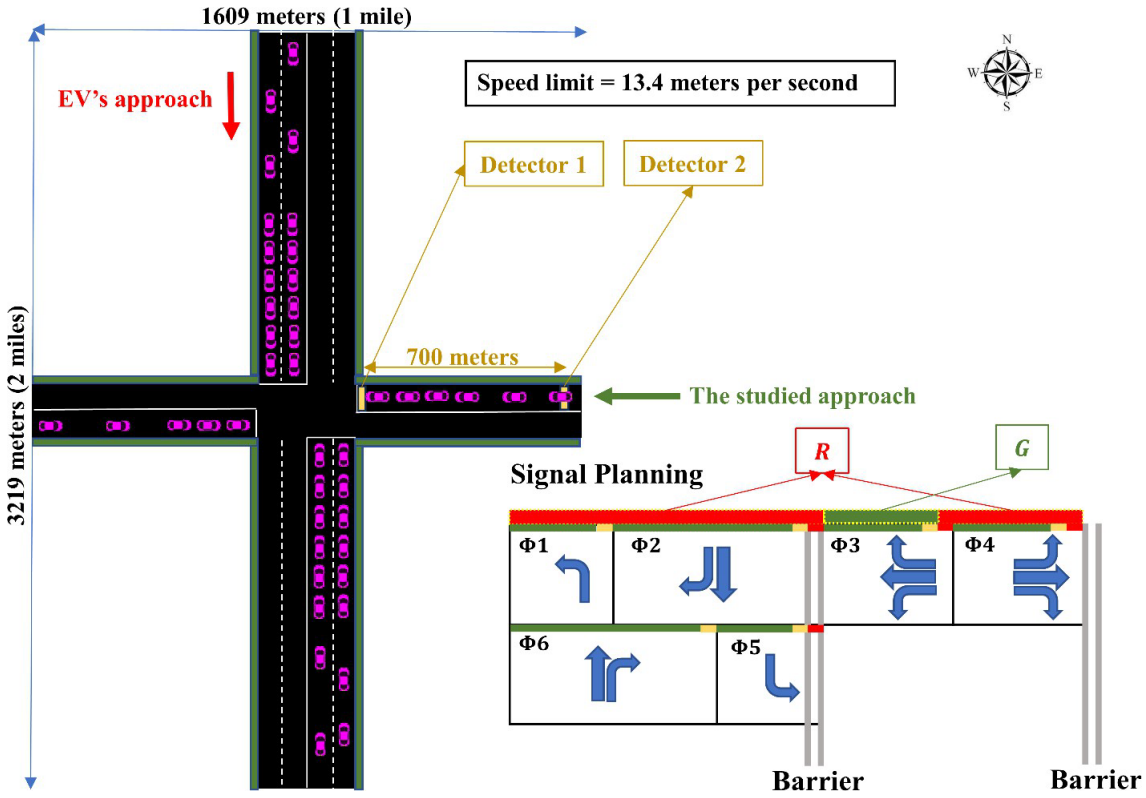

Figure 3. Simulation network

As shown in Figure 3, the simulated network has 2 approach lanes in major approaches and 1 approach lane in minor approaches. The length of each major approach is 1609 meters (1 mile), and the length of each minor approach is 805 meters (0.5 mile). The speed limit is 13.4 meters per second (30 miles per hour); however, EV can move 4.5 meters per second (10 miles per hour) faster than general traffic. The signal has a normal cycle length of 90 seconds. Figure 3 shows that the effective green time, G, is defined as the addition of phase 3's green and yellow time. The effective red time, R, is the rest of cycle length.

Event-based data collected by traffic detectors was used to quantify arrival and saturated traffic states. For this context the EV used the Southbound (SB) approach of the arterial, and the performance of cross-street's Westbound (WB) approach was recorded during and

after EV passage. Two traffic detectors were placed in the WB approach to obtain the flow and density of saturated and arrival traffic. Detector 1 was placed right before the stop line to measure the characteristics of vehicles moving in saturated traffic. Detector 2 was placed 700 meters before the stop line to record the characteristics of arrival traffic. The position of Detector 2 was calibrated for the network to ensure queue does not reach this detector.

According to the developed model, the sensitivity of Q^n_{max} and Q^n_{min} to each influencing variable was studied. Equations 3.5 and 3.7 show that Q^n_{max} and Q^n_{min} are dependent on shockwave speeds, v_1, v_2 and v_3. It was assumed that q_m, k_m and k_j are constant in our simulation settings. Hence, based on Equation 3.2, v_2 is constant. According to Equations 3.1 and 3.3, v_1 and v_3 are dependent on the values of q_a and k_a. The value of q_a, which is the WB approach's traffic flow, can be directly manipulated in simulation. Therefore, different values of q_a, which influences v_1 and v_3, were used in simulation to study the sensitivity of Q^n_{max} and Q^n_{min} to q_a.

EVP was used to clear the SB approach before EV reaches the stop line. As preemption threshold identification was not the focus of our research, the value of preemption threshold was set directly in simulation to study the influence of preemption threshold on queue length. According to Equations 3.5 and 3.7, Q^n_{max} and Q^n_{min} are dependent on R which is directly related to preemption threshold. In our simulation settings, it was assumed as preemption threshold increased x seconds, x seconds was also added to the duration of red phase of WB approach, R. Therefore, different values of R were tested in simulation environment to investigate the sensitivity of Q^n_{max} and Q^n_{min} to R.

In this research, a transition method was implemented to aid cross streets discharge the residual queue created by EVP. According to Equation 3.7, Q_{min}^{n} is dependent on G. Hence, the implemented transition method increased WB approach's green phase duration, G, for three cycles after EVP. Different values of G were used in simulation to study the sensitivity of Q_{max}^{n} and Q_{min}^{n} to G.

MAE and Mean Absolute Percentage Error (MAPE) measures were used to evaluate the performance of the developed model. Equations 3.12 and 3.13 were used to calculate these performance measures.

$$MAE = \frac{1}{m}\sum_{i=1}^{m}|O_i - E_i| \tag{3.12}$$

$$MAPE = \frac{1}{m}\sum_{i=1}^{m}\left(\left|\frac{O_i - E_i}{O_i}\right| \times 100\right) \tag{3.13}$$

Where, O_i is the i^{th} observed value, E_i is the i^{th} estimated value, and m is the number of observations.

3.3 Results and discussion

Each simulation run lasted 6000 seconds, and EV entered the network 3000 seconds after the simulation started. It was assumed that demand was constant spanning an individual simulation run. Additionally, it was assumed $Q_{min\_ob}^{n-1}$ is 0 for the preemption cycle, i.e., traffic was uncongested. 15 simulation runs with different traffic flows on the study approach, q_a, were taken. The variations of shockwaves speeds are illustrated in Figure 4. Figure 4 shows v_1 increased, v_2 remained constant, and v_3 reduced as q_a increased. The

maximum and minimum queue lengths, Q^n_{max} and Q^n_{min}, during the preemption cycle were recorded in each simulation run and provided in Figure 5 (b) along with the estimated values. Figure 5 (a) illustrates the estimated and observed values of Q^n_{max} and Q^n_{min} in the preemption cycle. For each simulation run, with a specific q_a, these values were obtained and shown in Figure 5 (b). As it is observed in Figure 5 (b), both Q^n_{max} and Q^n_{min} increased with a constant slope as q_a increased. The induced increases in Q^n_{max} and Q^n_{min} due to the changes in $v_1$and v_3, keeping all other variables in Equations 3.5 and 3.7 constant, can be explained using shockwave theory, shown in Figure 6. According to Figure 6, as $Q^n{}_{max}$ occurs at the intersection of v_1 and v_2, keeping v_2 constant, an increase in v_1 accelerates the queue creation process and leads in higher Q^n_{max}. Additionally, Figure 6 shows Q^n_{min} occurs at the intersection of v_3 and v_4. It is deducted that keeping v_4, which has the same speed magnitude as v_2, constant and reducing v_3 slows down the queue reduction process and results in higher Q^n_{min} values. Figure 5 (b) also illustrates the linear regressions fitted to observed Q^n_{max} and Q^n_{min}. The fitted regression lines show the high accuracy of the developed model as the regression lines closely follow the estimated queue. The R^2 values of regression lines are provided in Table 3.2.

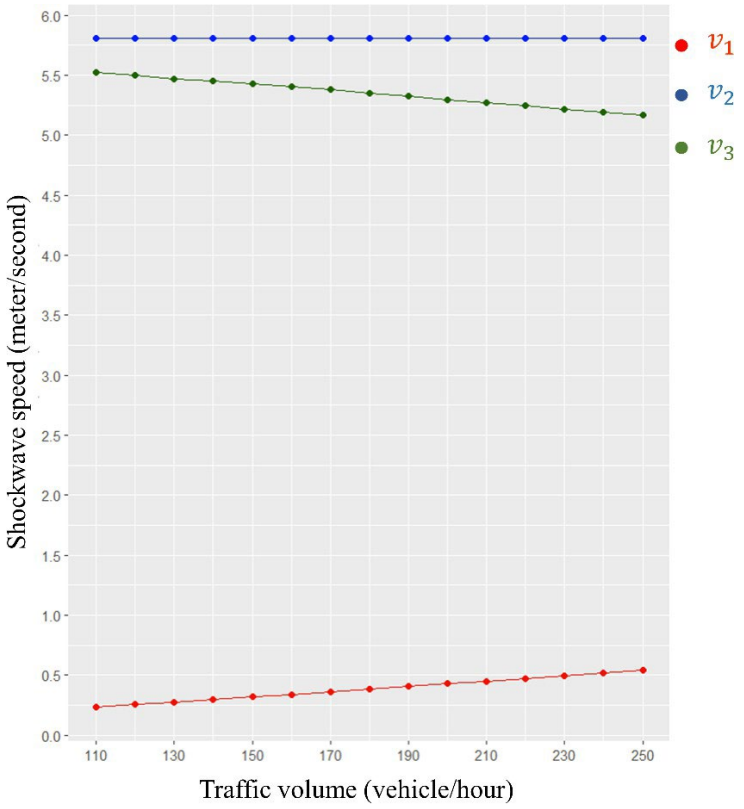

Figure 4.Variations of v_1, v_2 and v_3 of the preemption cycle based on q_a.

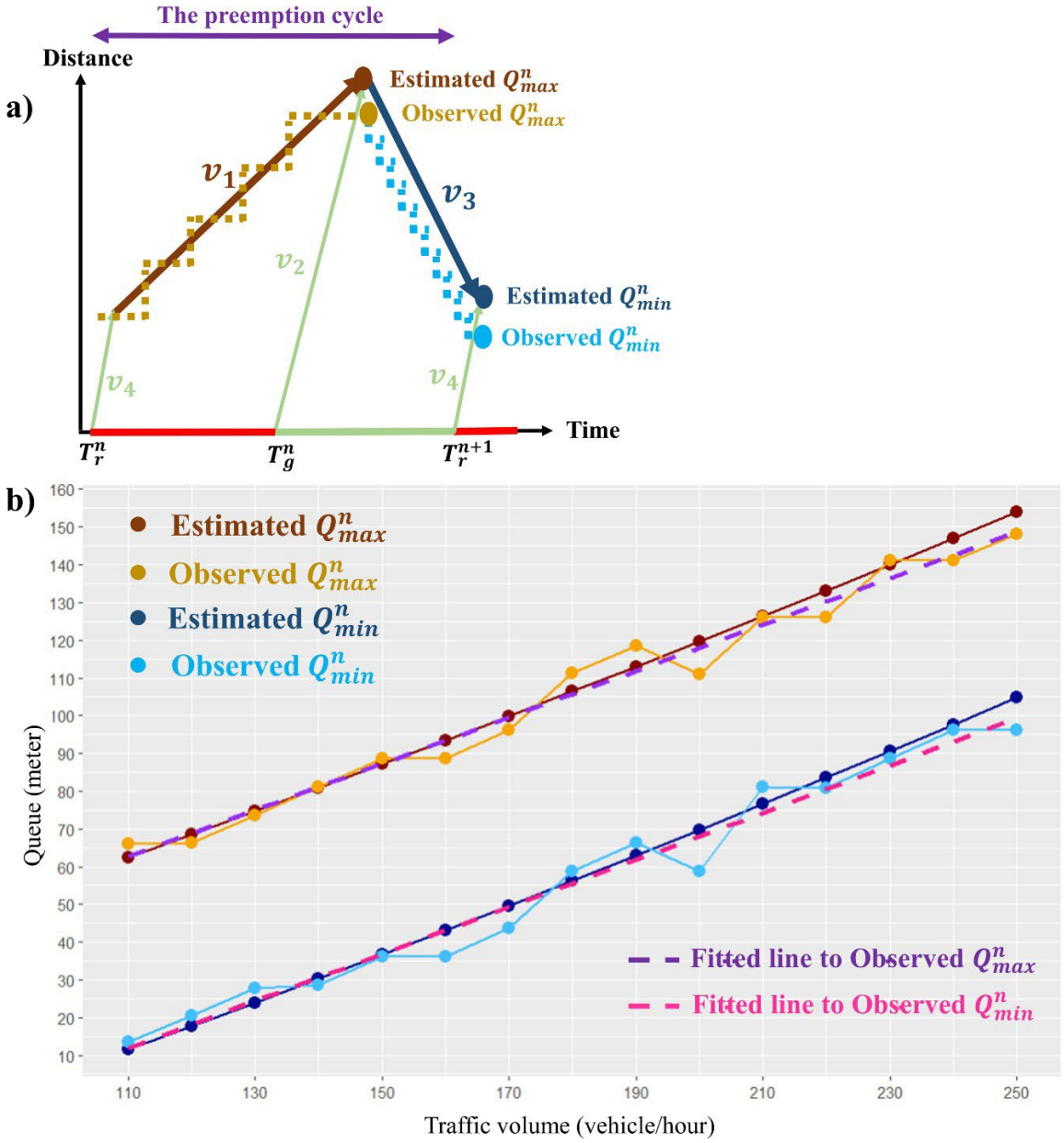

Figure 5. Variations of Q^n_{max} and Q^n_{min} of the preemption cycle based on q_a.

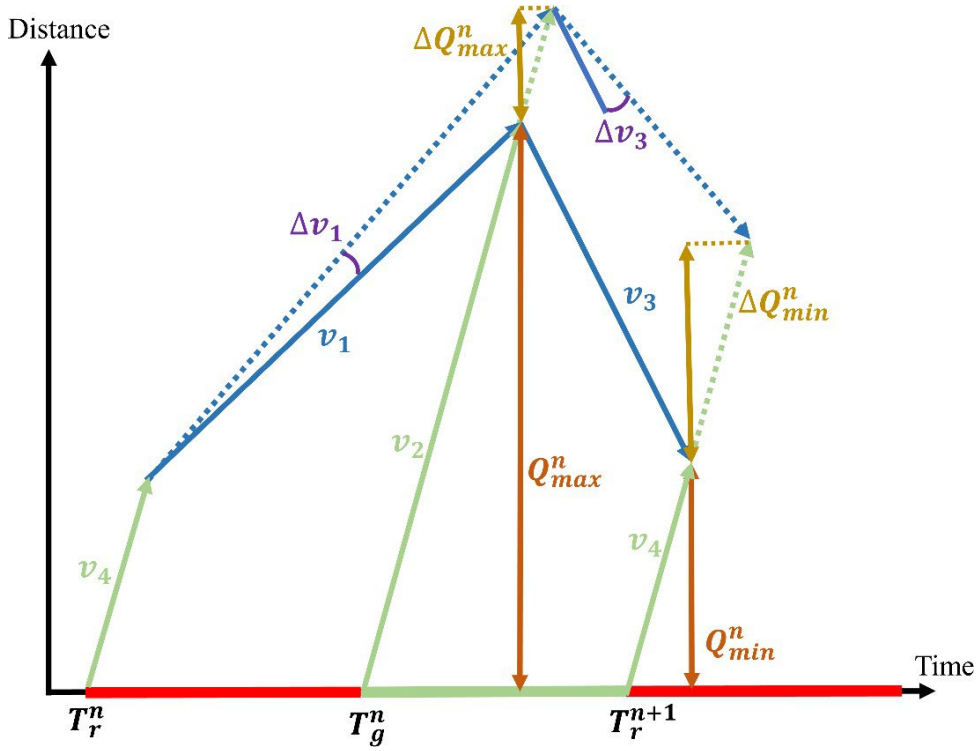

Figure 6. Variations of Q^n_{max} and Q^n_{min} while increasing v_1 and reducing v_3

The MAPE and MAE are provided in Table 3.2. The calculated MAE and MAPE values show higher estimation error in Q^n_{min} than in Q^n_{max}. The higher error in Q^n_{min} estimation can be explained with shockwave theory. As stated before, Q^n_{max} is occurs at the intersection of shockwaves v_1 and v_2, and Q^n_{min} occurs at the intersection of shockwaves v_3 and v_4, equal to $|v_2|$. Eliminating v_2 since it is common in both Q^n_{max} and Q^n_{min}, it can be deducted that the speeds of v_1 and v_3 influence Q^n_{max} and Q^n_{min}, respectively. It is observed in Figure 4 that v_3 generally has higher speed than v_1. Assuming v_3 and v_1 are estimated using the same process, higher magnitude of v_3 should lead in higher estimation error than v_1. Hence, as v_3 identifies the coordinates of Q^n_{min} in the queue diagram, higher errors are observed in the estimation of Q^n_{min} than Q^n_{max}.

Table 3.2. Q^n_{max} and Q^n_{min} estimation errors of the preemption cycle in simulations with different q_a.

	MAE (meters)	MAPE (percent)	R^2
Q^n_{max}	3.68	3.51	0.98
Q^n_{min}	3.76	8.24	0.97

33 simulation runs were taken with different red time (R) values, and the results are provided in Figure 7. As illustrated in Figure 5 (a) the estimated and observed values of Q^n_{max} and Q^n_{min} of the preemption cycle in each simulation run, with a specific R, were obtained and shown in Figure 7. Figure 7 shows that there is an overall increasing trend for Q^n_{max} and Q^n_{min} in response to increasing R. According to Equations 3.9 and 3.10, for the preemption cycle ($S = 0$) when the green time extension, ΔG_{T_0}, is 0, ΔQ^0_{max} and ΔQ^0_{min} becomes equal that verifies the observed trend in Figure 7. Figure 7 also shows the linear regressions fitted to observed Q^n_{max} and Q^n_{min}. The fitted lines verify the model's performance as they are very close to the estimated results. The fitted regression lines R^2 values are provided in Table 3.3.

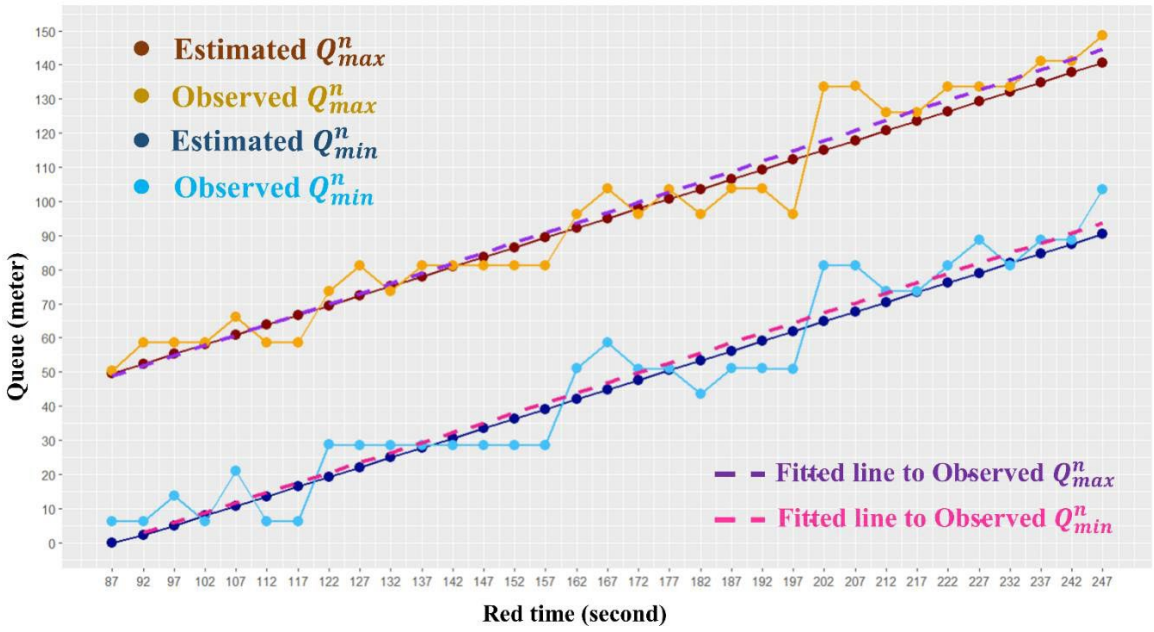

Figure 7. Variations Q^n_{max} and Q^n_{min} of the preemption cycle based on R

Estimation errors of Q^n_{max} and Q^n_{min} in simulation runs with different R values were measured and provided in Table 3.3. It is observed that the estimation error in Q^n_{min} is more than in Q^n_{max}. The same explanation provided for the estimation error of simulation runs with different q_a is viable here. 6 simulation runs were taken with different values of G extensions in transition cycles. Figure 8 illustrates the trajectory of observed and estimated queue lengths during preemption and transition cycles for each value of G.

Table 3.3. Q^n_{max} and Q^n_{min} estimation errors of the preemption cycle in simulations with different R.

	MAE (meters)	MAPE (percent)	R^2
Q^n_{max}	5.63	5.93	0.94
Q^n_{min}	6.72	28.82	0.92

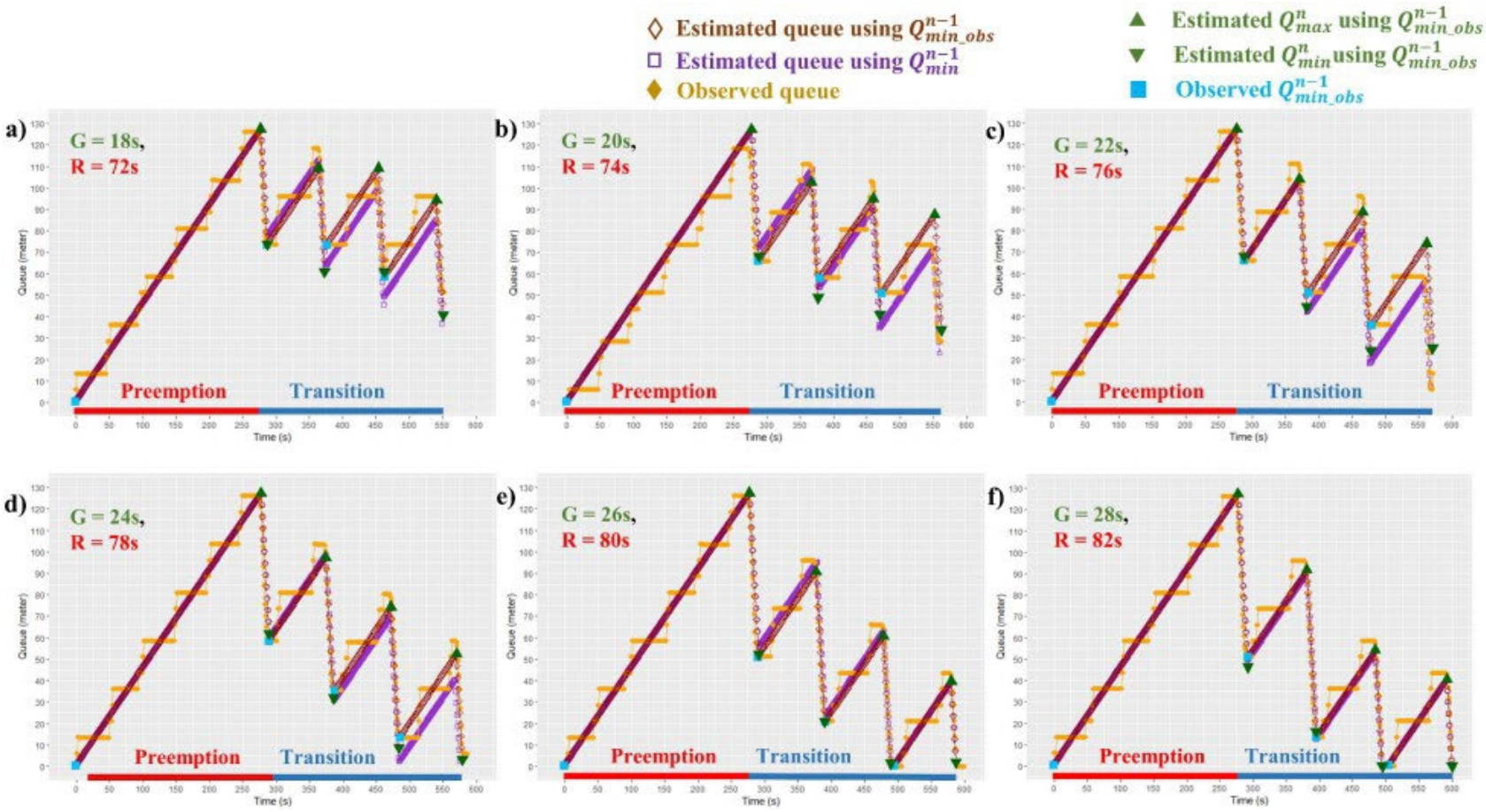

Figure 8. Queue trajectory in preemption and transition cycles for different values of G.

Figure 8 illustrates how the model estimates the trajectory of the tail of queue. This figure verifies the developed queue estimation model can identify the number of required transition cycles to discharge the residual queue created by EVP. The developed model can be used to estimate queue for several consecutive cycles. In the first cycle, using Equations 3.5 and 3.7, Q^1_{max} and Q^1_{min} are estimated based on the initial queue, $Q^0_{min\_obs}$ which was 0 in our simulation settings as traffic was assumed to be uncongested. Then, the estimated Q^1_{min} is used as $Q^1_{min\_obs}$ in Equations 3.5 and 3.7 to estimate Q^2_{max} and Q^2_{min} in the second cycle. The same process is repeated for next transition cycles. In this way, the residual queue at the end of transition cycles can be estimated without requiring the observed initial queue for every cycle. The drawback of this method is that the estimation error aggregates as the estimated values of a cycle are used to estimate the queue of the next cycle. To reduce the aggregated estimation error, the developed model can be calibrated using the observed initial queue at the beginning of every cycle, i.e., the observed residual queue at the end of cycle $n-1$, $Q^{n-1}_{min\_obs}$, is used to estimate Q^n_{max} and Q^n_{min}. The estimation results of both methods are provided in Figure 8. In Figure 8 (a) to (f), each section shows the results of simulation with a different G value, varying between 18 (the default value in signal timing) and 28. Moving from Figure 8 (a) to (f), in each simulation, 2 seconds were added to the green time of each cross street in transition cycles, i.e., both G and R increased 2 seconds for the WB approach. It is observed in Figure 8 (e) that by adding 8 seconds to G, the residual queue created by EVP at the end of the preemption cycle was completely discharged in 2 transition cycles.

The trend of residual queue dissipation during preemption and transition cycles is illustrated in Figure 9. When residual queue, ΔQ^s_{min}, becomes 0, EVP's disruption is completely dissolved, and the approach is recovered. ΔQ^s_{min} was calculated for different values of ΔG based on Equations 3.9 and 3.10 and illustrated in Figure 9 along with the observed values. Figure 9 (a) shows the residual queue created by EVP, ΔQ^0_{min}, at the end of the preemption cycle. Figure 9 (b), (c) and (d) show ΔQ^s_{min} for the 1st, 2nd and 3rd cycles of transition. Figure 9 illustrates as ΔG increases, more stopped vehicles are discharged, and ΔQ^s_{min} decreases. The calculated errors are provided in Table 3.4. According to Figure 9, the estimation error of the method using Q^{n-1}_{min} were aggregated cycle by cycle as the model were not calibrated using $Q^{n-1}_{min\_ob}$. However, low MAE values of less than 10 meters verify the application of Equations 3.9 and 3.10 in identifying the required transition settings to discharge the EVP's disruption.

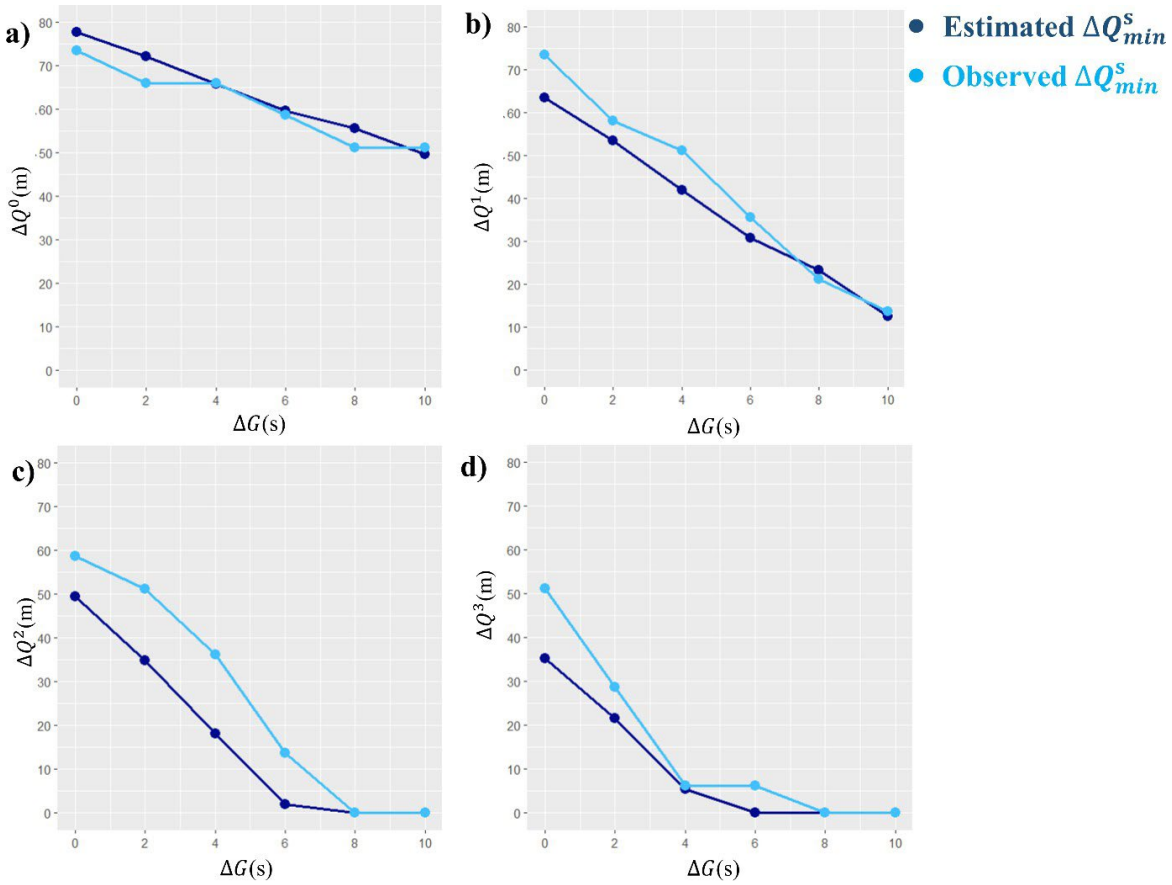

Figure 9. ΔQ^s_{min} in preemption and transition cycles for different values of ΔG

Table 3.4. ΔQ^s_{min} estimation errors in simulations with different ΔG in preemption and transition cycles

Cycle		MAE (meters)	MAPE (percent)
Preemption cycle	ΔQ^0_{min}	2.9	4.75
Transition cycle 1	ΔQ^1_{min}	5.33	11.88
Transition cycle2	ΔQ^2_{min}	9.26	46.17
Transition cycle 3	ΔQ^3_{min}	4.96	42

3.4 Conclusions

The aim of this research was to quantify the disruption induced by EVP in arterial cross streets at signalized intersections and provide recommendations to aid cross streets in discharging the disruption. Queue length was considered as the representative of the induced disruption. Hence, a queue estimation model was developed based on shockwave theory to investigate the disruption. Then, the developed model was validated though simulating EVP at an isolated signalized intersection in SUMO. The model was used to estimate the maximum and minimum queue lengths of preemption and transition cycles, and estimation errors were calculated. Additionally, the sensitivity of residual queue created by EVP to the influencing parameters were investigated. Using the results of sensitivity analysis, recommendations were provided to aid arterial cross streets in clearing the disruption created by EVP.

The results showed by increasing the traffic flow of cross street in uncongested traffic, maximum and minimum queue lengths of the preemption cycle increased with a constant slope. It was also observed that increasing preemption time reached in increased maximum and minimum queue lengths of preemption cycle. By comparing the regression lines fitted to the observed values and the estimated values, it was verified that the developed model can accurately estimate the sensitivity of queue to traffic flow and signal timing settings. The results also verified the model was able to quantify how the disruption created by EVP should be counteracted by adjusting signal timing in transition cycles. The model estimated

the residual queue at the end of transition to evaluate the transition method in eliminating the residual queue.

This research showed that shockwave theory can quantify the disruption created by EVP and investigate solutions to counteract the disruption which was a gap in the literature. The goal was to develop a model able to explain the creation and dissipation of EVP disruption on minor streets which was addressed using the obtained model. The developed model can be used in transportation network management to adjust EV routing and EVP algorithms to lessen the disruption. The influence of different parameters including preemption, transition, signal timing, and traffic can be investigated on the disruption. Using the developed model, the strategies to prevent the disruption can be designed, and if the disruption is not preventable, the solutions to aid the approaches recover quickly after EVP can be investigated. The results obtained in this research can be validated in future studies with different networks and different traffic conditions. The proposed model is limited to one lane approaches with the current formulation. Future research can investigate the required adaptations to enable the model to estimate queue in multi-lane approaches. Additionally, the influence of initial residual queue can be investigated on the EVP disruption in future studies. The developed model can be further evaluated in corridors with various geometries and signal timing strategies, and the estimated results can be validated with real queue data.

CHAPTER 4

LANE-CHANGING BEHAVIOR OF CONNECTED AND AUTONOMOUS VEHICLES IN EMERGENCIES

4.1 Objective

In this chapter, the lane-changing and stopping behaviors of CAVs were explored on an arterial corridor to investigate how these behaviors affect the delay of EV and CAV traffic. The objective was to establish and tune an algorithm specifying the driving behavior and parameters associated with the EV's and CAVs' movements in an urban arterial corridor using microsimulation. This algorithm specified what CAVs should do when alerted to an approaching EV and when they should return to normal driving behavior to guide how technology should be used to provide the advance warnings of approaching EVs. Then, this algorithm was used in different microsimulation scenarios to study the influence of lane-changing and stopping behaviors on the delays of EV and surrounding traffic. At the end, the proposed algorithm was compared with an existing algorithm.

4.2 Methodology

In this study, simulations were performed in SUMO software. SUMO is an open-source microscopic traffic simulation software in which some characteristics for EVs to simulate their particular driving behavior are already defined (Lopez et al., 2018). In SUMO, some permissions are given to EVs. For approaching EVs, the vehicles in the leftmost lane move to the leftmost sublane of their lanes, and the vehicles in all other lanes move to the rightmost sublane of their lanes. The result is an open space between the left lane and other lanes, denoted as the emergency lane. Only EVs can pass through the emergency lane (Bieker-Walz et al., 2018). In SUMO, each lane is divided to several sublanes. Vehicles can move between different sublanes to change their lateral position inside a lane.

With the advent of CAVs, control of vehicles can be improved with the objective of minimizing impact of EVs on overall network performance while simultaneously ensuring a safe and efficient passage of a vehicle with priority status. Additionally, CAVs can transmit messages to alert each other of an approaching EV at far distances, reducing or eliminating human errors and sub-optimal behaviors.

In this research, the desired behavior of CAVs in emergencies in an arterial road network is investigated. One objective of this research was to establish a driving behavior algorithm for CAVs to preclear an EV's lane on an arterial corridor. Since the studied simulation traffic network included road segments passing through signalized intersections, a preemption algorithm was required to prioritize EVs in signal phasing. By testing different scenarios in microscopic traffic simulation, the sensitivity of travel time delays of EVs and surrounding traffic to the driving behavior and traffic conditions can be investigated in a connected and autonomous traffic environment.

4.2.1 Simulation network

Simulations were performed on a 6437 m (4-mile) urban divided arterial road network. The corridor had 2 lanes in each direction and three intersections with 183 m (600 ft) left-turn lane on the main approaches. The perpendicular approaches had the length of 183 m. The simulation network is shown in Figure 10. Signal phasing, intersection areas, and exclusive left-turn lanes are also shown in this figure. The speed limit was 13.4 meters per second (30 miles per hour) on all road segments. In this study, as well as in the literature, EVs were allowed to move with a maximum speed 4.5 meters per second (10 miles per hour)

higher than the road segment's posted speed limit (Henchey et al., 2014; Weinert & Düring, 2015).

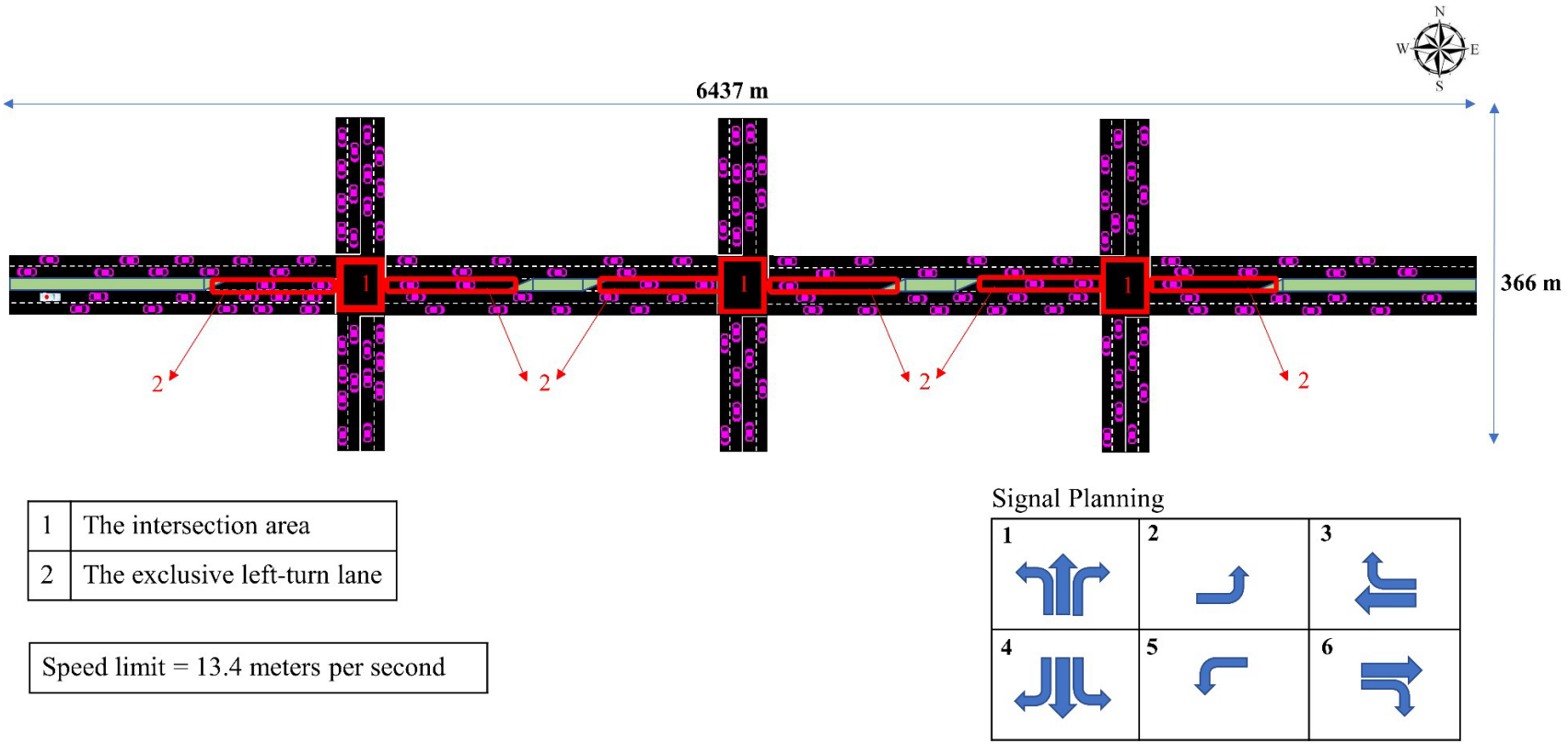

Figure 10. Simulation network

4.2.2 The driving behavior algorithm

An algorithm was written to establish the driving behavior of CAVs in the presence of an approaching EV. It was assumed that the EV enters the simulation network from the left lane and continues moving in this lane. Clearing the EV's path is completed in two steps. Two new threshold distance parameters were defined, relative to the front of the EV, including the lane-changing and stopping thresholds. The area between the EV and the stopping threshold distance creates stopping area while the distance between the stopping threshold and the lane changing threshold creates the lane-changing area. CAVs that enter the lane-changing area move to the right lane. Then, when CAVs enter the stopping area, they move to the rightmost sublane and stop. One of the benefits of CAVs is that both threshold distances are not limited by the limitations of human senses (for example hearing and locating the siren), therefore we assume that all vehicles are aware of the approaching EV and behave uniformly based on the threshold. Figure 11 (a) and (b) visualized the stopping and lane-changing areas, respectively.

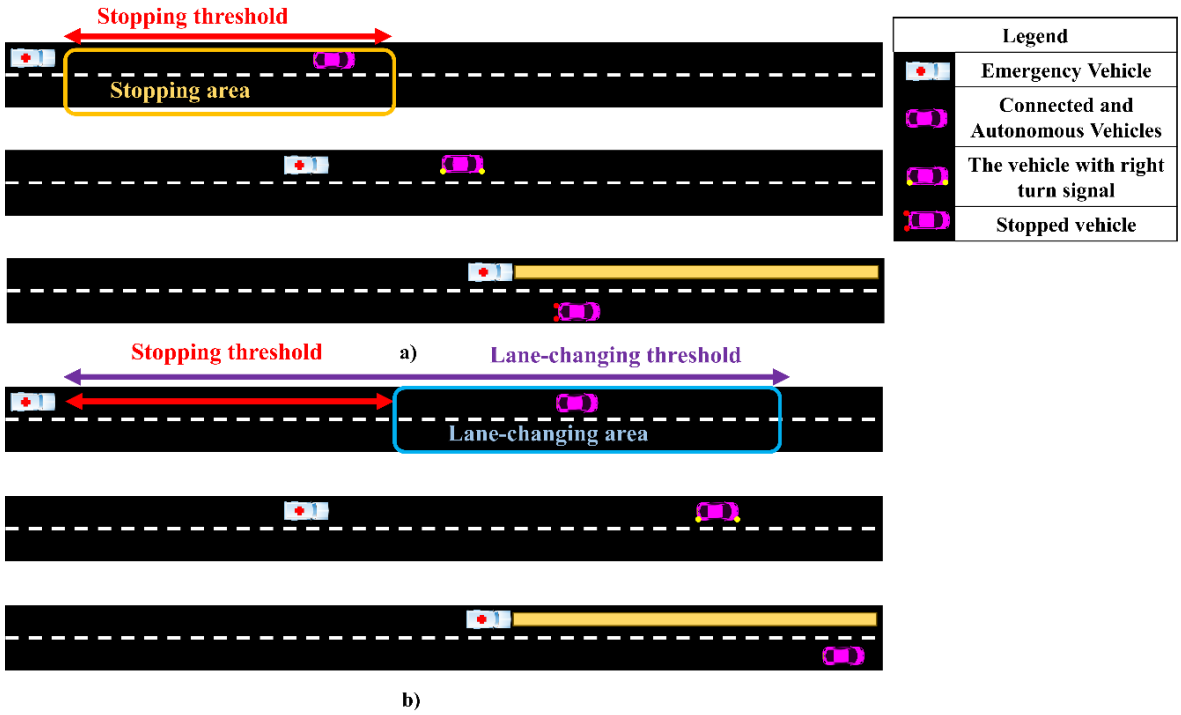

Figure 11. Stopping and lane-changing thresholds and areas

The new variables used in the driving behavior algorithm are provided in Table 4.1.

Table 4.1. Variables used in the driving behavior algorithm

Variable symbol	Definition
l(i, t)	The index of the lane on which CAV *i* is at time step *t* (0 refers to the right lane, 1 to the left lane, and 2 to the exclusive left-turn lane, which is present only near intersections in EB/WB approaches). The lane indices are shown in Figure 12.
p(i, t)	The lateral sublane position of CAV *i* at time step *t* (Three lateral sublane positions were considered including "*Right*," "*Center*," and "*Left*"). Different lateral sublane positions are shown in Figure 13.
s(i, t)	The desired speed of CAV *i* at time step *t*.
d(i, t)	The longitudinal distance between CAV *i* and the EV at time step *t* (positive when the CAV is in front of the EV and negative when the CAV is behind the EV).
tr_1	The stopping threshold is a threshold distance of CAVs to an EV in which the CAVs that are in the right lane move to the rightmost sublane and stop.
tr_2	The lane-changing threshold is a threshold distance beyond the stopping threshold in which CAVs move to the right lane and continue moving on this lane.
c	A coefficient (between 0 and 1) that is multiplied by tr_2 and results in tr_1.
di(i, t)	The longitudinal distance between CAV *i* and the center of intersection at time step *t* (positive when the CAV has passed the intersection and negative when the CAV has not passed the intersection).
r	The distance between the stop line and the center of the intersection.
inf	The vector of the CAVs whose behaviors were influenced by an EV. This vector contains all the CAVs whose distances to the EV were once between 0 and tr_2.
et(i)	The time step at which the EV passes CAV *i* (the time at which $d(i, t) = 0$).

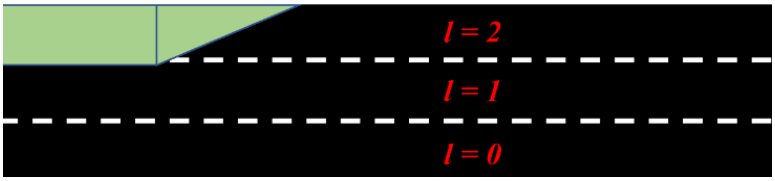

Figure 12. Lane indices

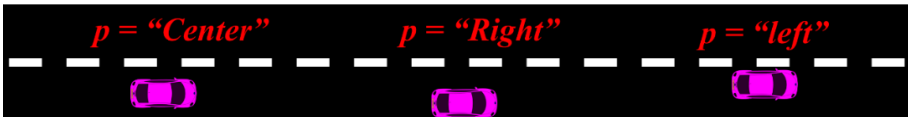

Figure 13. Lateral positions

To study the delay of EV and surrounding traffic in a connected and autonomous traffic environment, different stopping and lane-changing threshold values were tested in microsimulation environment. The relationship between stopping threshold, tr_1, and lane-changing threshold, tr_2, is defined in equation.

$$tr_1 = \mathrm{c} \times tr_2 \qquad 4.1$$

In this research, three values of 0, 0.5 and 1 were used for c. Hence, three threshold settings including using only a stopping area (stopping threshold equal to lane-changing threshold), using both stopping and lane-changing areas (stopping threshold equal to half lane-changing threshold), and using only lane-changing area (stopping threshold equal to 0) were tested.

The driving behavior algorithm of the CAVs interacting with an EV is provided in Figure 14.

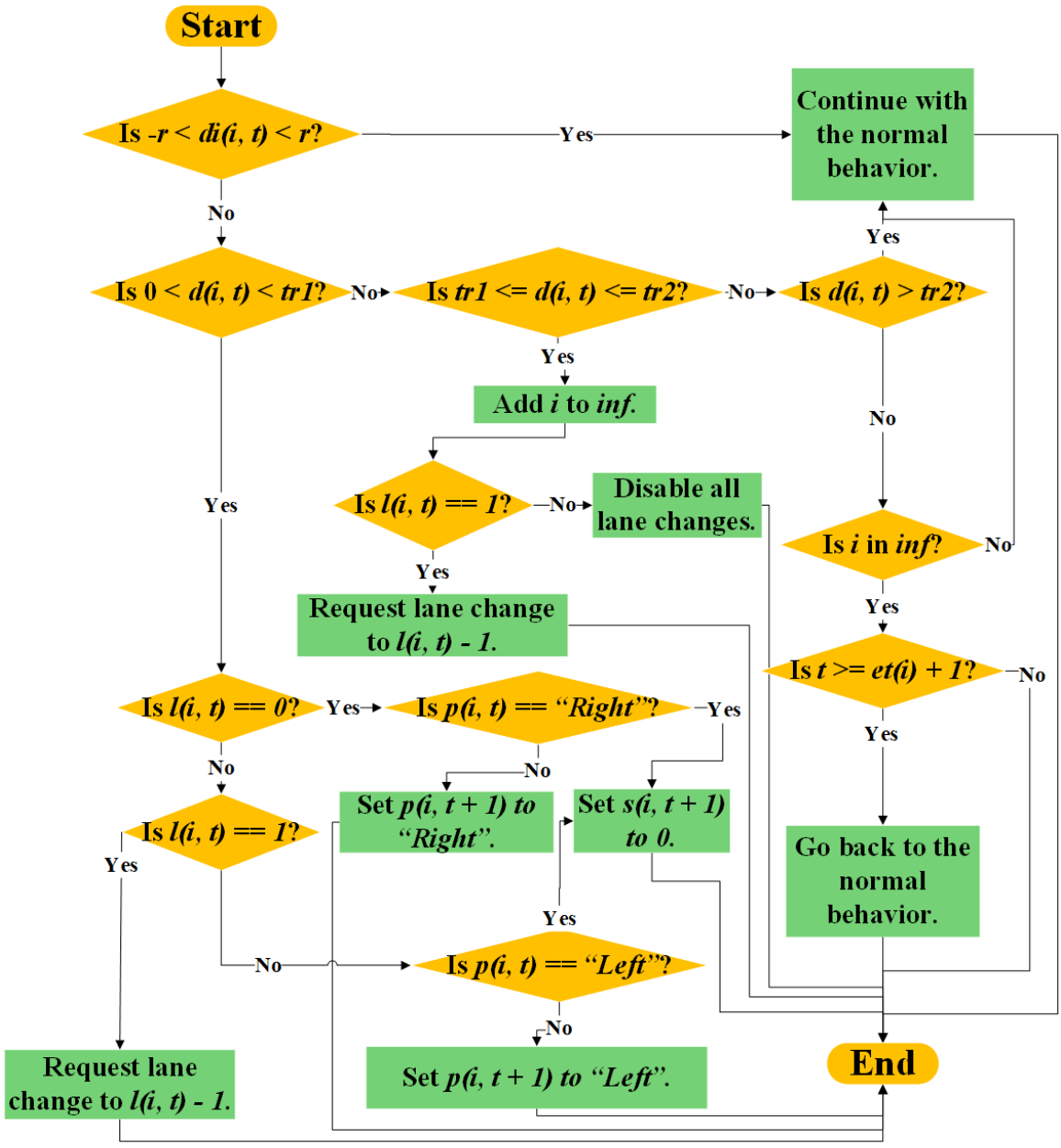

Figure 14. Driving behavior algorithm for the CAVs interacting with an EV

Based on Figure 5, first, the algorithm checks whether the vehicle is inside the intersection. If it is inside the intersection, the algorithm does not send lane change or speed change requests to the vehicle to prevent blocking the intersection. Next, it checks whether the vehicle is in the lane-changing or stopping areas. If the vehicle is in one of the areas, lane change, lateral sublane position change and/or speed change requests are sent to it based

on its lane index. At the end, when the EV passes the stopped vehicles, they start moving after one second. These checks are performed at each simulation time step.

The driving behavior algorithm sends the requests of lane change orders when they are necessary. These requests are checked by the SUMO lane-changing model, SL2015 (Erdmann, 2015). If a lane change was recognized to be feasible by the model, a lane change command is executed. SUMO's lane-changing model may recognize lane-changing is not feasible at time *i*. Therefore, it may take several time steps until the CAV starts changing lane. The same is true for changing lateral sublane position and speed. The algorithm sends speed change requests. Then, the request is checked by SUMO car following model, Krauss model (Krauß, 1998) to execute a speed change command. This process is shown in Figure 15.

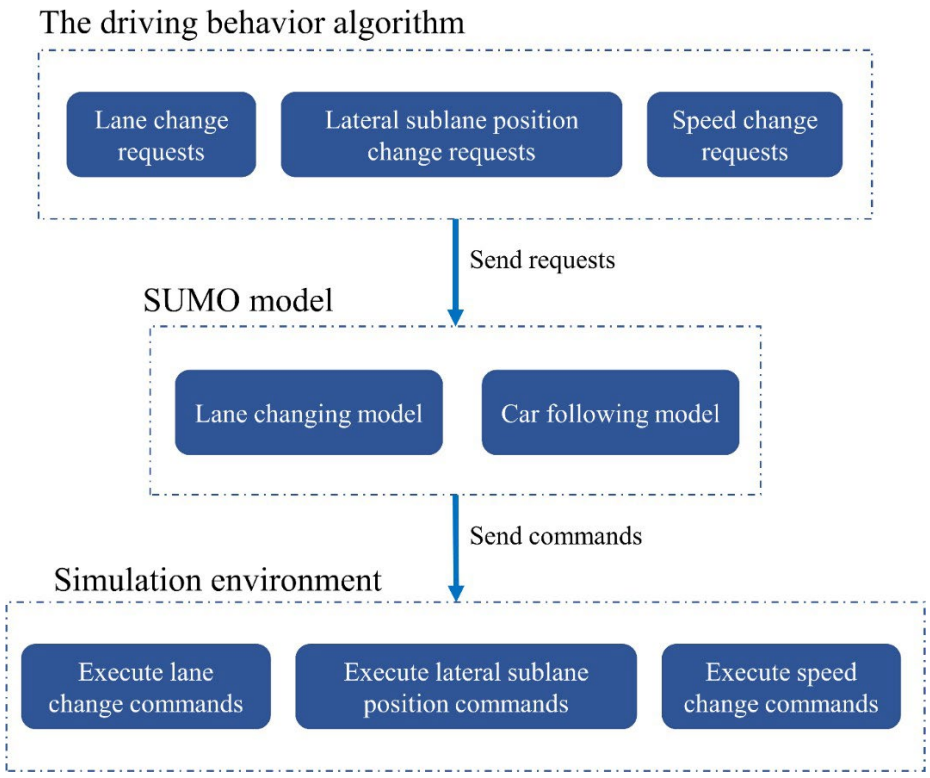

Figure 15. Process of checking the driving behavior algorithm requests in SUMO

In Figure 16, a two-lane one-way road segment is depicted. Figure 16 (a) shows that there are two CAVs in front of the EV in the left lane. There are also five CAVs in the right lane. Figure 16 (b) illustrates turn signal for the CAVs in the left lane indicating that the driving behavior algorithm induced lane-changes for these CAVs. Also, four of the five CAVs in the right lane have pulled over and stopped implying that they are in the stopping area. In Figure 16 (c), the lane changes are completed, and the left lane is free for the passage of EV. The fifth CAV in the right lane has stopped indicating that it is now in the stopping area. Also, two of the CAVs behind the EV have started moving meaning that they have come back to the normal driving behavior.

A road segment with an exclusive left-turn lane is shown in Figure 17. The same behavior as shown in Figure 16 is observed here for the CAVs in the right and left lanes. The only difference is the behavior of the CAV that is in the exclusive left-turn lane. In Figure 17 (a and b), this CAV has not entered the stopping area. In Figure 17 (c), the CAV is in the stopping area and has stopped.

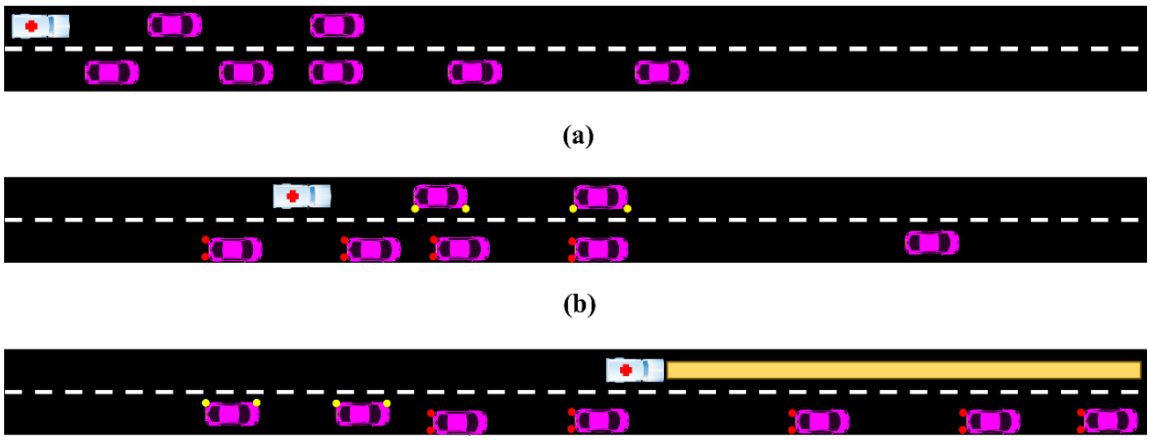

Figure 16. An example of CAVs' response to an EV in a two-lane road segment

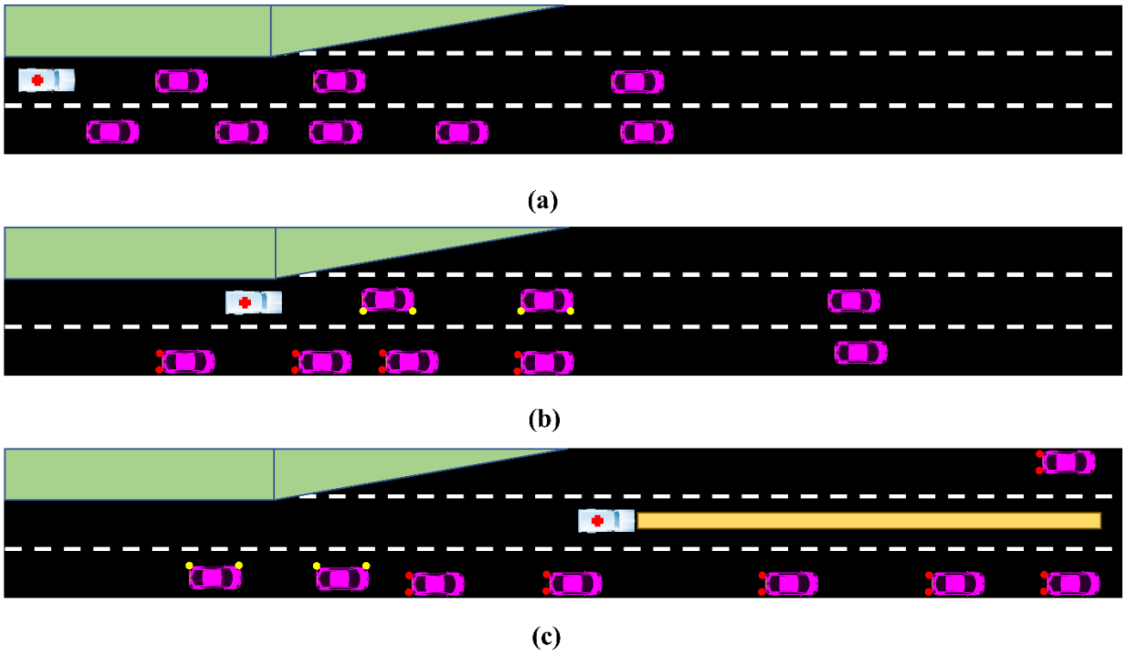

Figure 17. An example of CAVs' response to an EV in a two-lane road segment with an exclusive left-turn lane

4.2.3 The preemption algorithm

The delay of vehicles in a traffic network consists of two components: road segment delay and control delay (C. Cheng et al., 2016). The presented driving behavior algorithm was developed to decrease the road segment delay of EV. In order to reduce or, if applicable, eliminate control delay, a preemption strategy was utilized to prioritize EV's approach in signal timing. The signal planning was shown in Figure 10. The new variables used in the preemption algorithm are defined in Table 4.2.

Table 4.2. Variables used in the preemption algorithm

Variable symbol	Definition
n(t)	The number of CAVs in the left lane between the EV and the intersection at time step *t*.
pt(t)	The calculated preemption threshold at time step *t*. When the distance between the EV and the intersection reaches to this threshold, the preemption should start.
ed(t)	The distance between the EV and the intersection at time step *t* (Positive when the EV has not passed the intersection and negative when the EV has passed the intersection).
y	Yellow time.
h	Saturation headway.
es	The desired speed of EV.
ss(j)	The signal state at signal step *j*. The signal step (*j*) increases when the state of signal changes. Since phases 1, 2, and 3 occurs the same time as phases 4, 5, and 6, respectively, only phases 1, 2, and 3 are considered in preemption. Signal states are provided in Table 4.3.

Table 4.3. Signal states

Signal state name	Definition
g1	The signal state in which the signal color is green for phase 1.
y1	The signal state in which the signal color is yellow for phase 1.
g2	The signal state in which the signal color is green for phase 2.
y2	The signal state in which the signal color is yellow for phase 2.
g3	The signal state in which the signal color is green for phase 3.
y3	The signal state in which the signal color is yellow for phase 3.

Noori et al. developed an EVP strategy for connected vehicle environments (Noori et al., 2016). Their method was adapted in our research with the addition of using the yellow time in transition between other phases to the EV's phase. The algorithm presented in Figure 18 was developed for signal preemption.

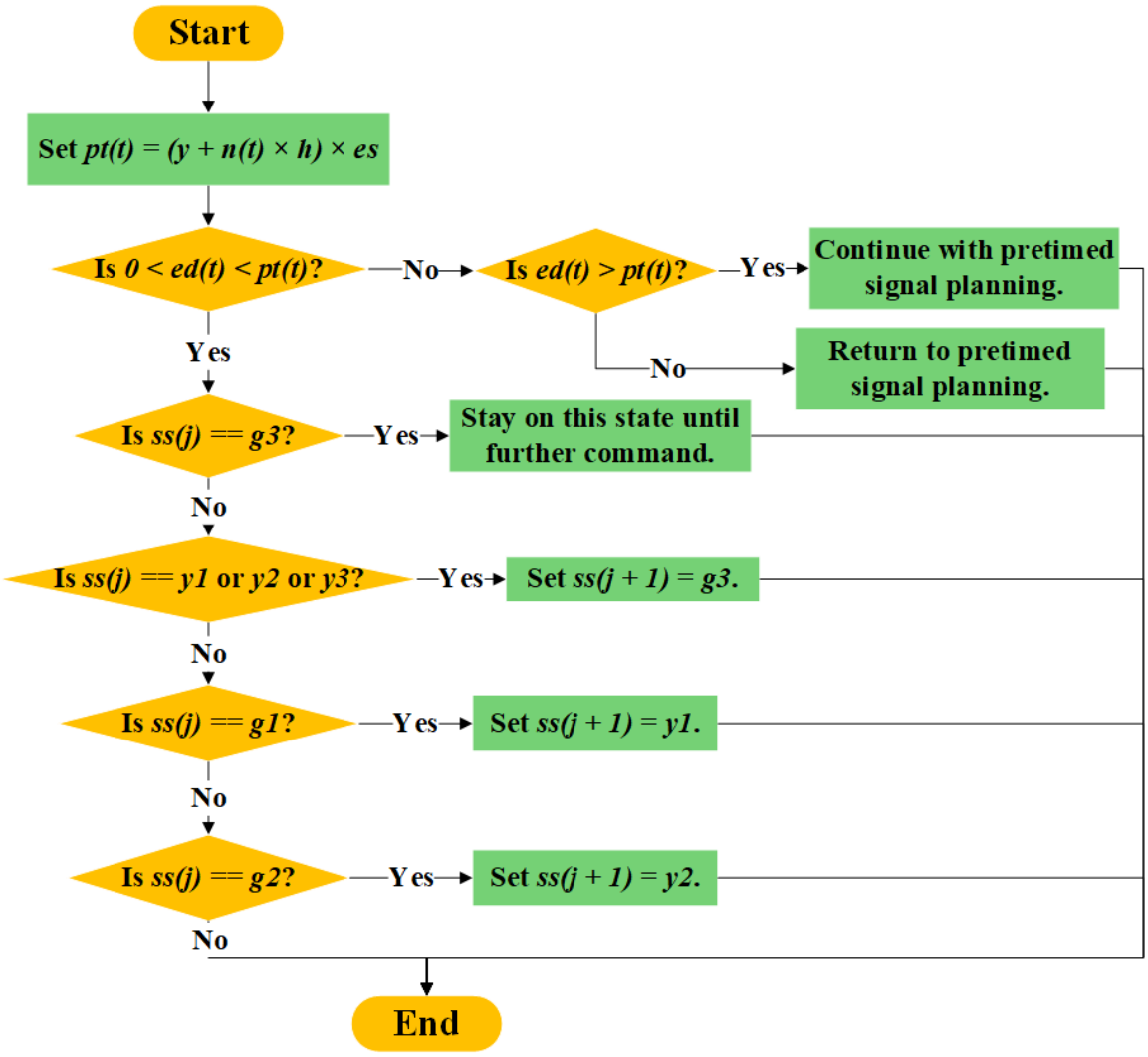

Figure 18. Preemption algorithm

Based on Figure 9, first, the preemption threshold is calculated based on the number of CAVs between the EV and the intersection in the left lane. The preemption was activated based on the amount of time it will take the existing queue and the approaching EV to clear the intersection. The distance at which the preemption activates was calculated based on the desired speed of the EV, the yellow time, the number of vehicles in the queue, and the saturation headway. This algorithm is checked every simulation time step and when the EV crosses the intersection, the signal timing returns to the original timing plan.

The signal timing is generally controlled by SUMO internal model. If a signal state change request is sent from the preemption algorithm, the priority is with the preemption algorithm request. If there is no request from the preemption algorithm, the next signal state is determined by SUMO signal control model. When the preemption ends, SUMO signal control model starts controlling the signal timing from where it was left by the preemption.

4.2.4 Simulation parameters

The desired driving behavior and preemption strategy were written in algorithms using Python (Guido Van Rossum & Drake Jr, 2009). To implement the developed algorithms, traffic control interface (TraCI) module was used as a connection between Python and SUMO. The SUMO's default car following model, Krauss model, was utilized. To simulate the behavior of CAVs, the default parameters of Krauss model were adjusted as shown in Table 4.4 based on the literature review (Atkins, 2016; Qiong Lu et al., 2018). The CAVs used in this research were considered to have the level 5 of autonomation according to SAE J3016 (Standard, 2018). The simulation time step was 0.5 seconds. A warm-up time of 600 seconds was used. Therefore, in each simulation run, one EV entered northbound approach 600 seconds after the start of simulation.

Table 4.4. Adjusted Krauss car following model parameters

Minimum gap (m)	Acceleration (m/s^2)	Deceleration (m/s^2)	Emergency deceleration (m/s^2)	Driver imperfection	Reaction time (s)
0.5	3.8	4.5	8	0	0.6

4.2.5 Design of experiments

To investigate the sensitivity of the relationship between the threshold values and the delay on the arterial segment, several traffic levels were defined and used in simulation scenarios. Different traffic levels and their traffic distributions at intersections are shown in Table 4.5.

Table 4.5. Distribution of intersection movements at different traffic levels (vehicles per hour)

Traffic level	EB/WB through	EB/WB right-turn	EB/WB left-turn	EB/WB total	NB/SB through	NB/SB right-turn	NB/SB left-turn	NB/SB total
1	960	120	120	1200	120	120	120	360
2	1600	200	200	2000	200	200	200	600
3	2240	280	280	2800	280	280	280	840

In the first, second and third traffic levels, 600, 1000, and 1400 vehicles per hour per lane entered the network in the EV's approach, EB/WB. 9 simulation scenarios were defined by considering three threshold settings and three traffic levels. For each simulation scenario, 40 runs with different random seeds were implemented. The value of lane-changing threshold varied in different simulation runs to cover the range of 10 to 400 meters with 10 meters intervals.

4.3 Results and discussion

4.3.1 The proposed model

360 simulation runs were implemented in total. The delay of EV and the average delay of the CAVs influenced by EV in each run were extracted for further analysis. The influenced CAVs were the vehicles that moved in the same approach as EV and has been in the stopping or lane-changing areas. Then, the delay of EV and the average delay of influenced CAVs were plotted versus the lane-changing threshold and provided in Figure 19. To

compare the relationship between the delay and the lane-changing threshold in different scenarios, regression functions were fitted to this relationship. The statistical process was performed using ordinary least squares (OLS) in R programming language (R Core Team, 2019).

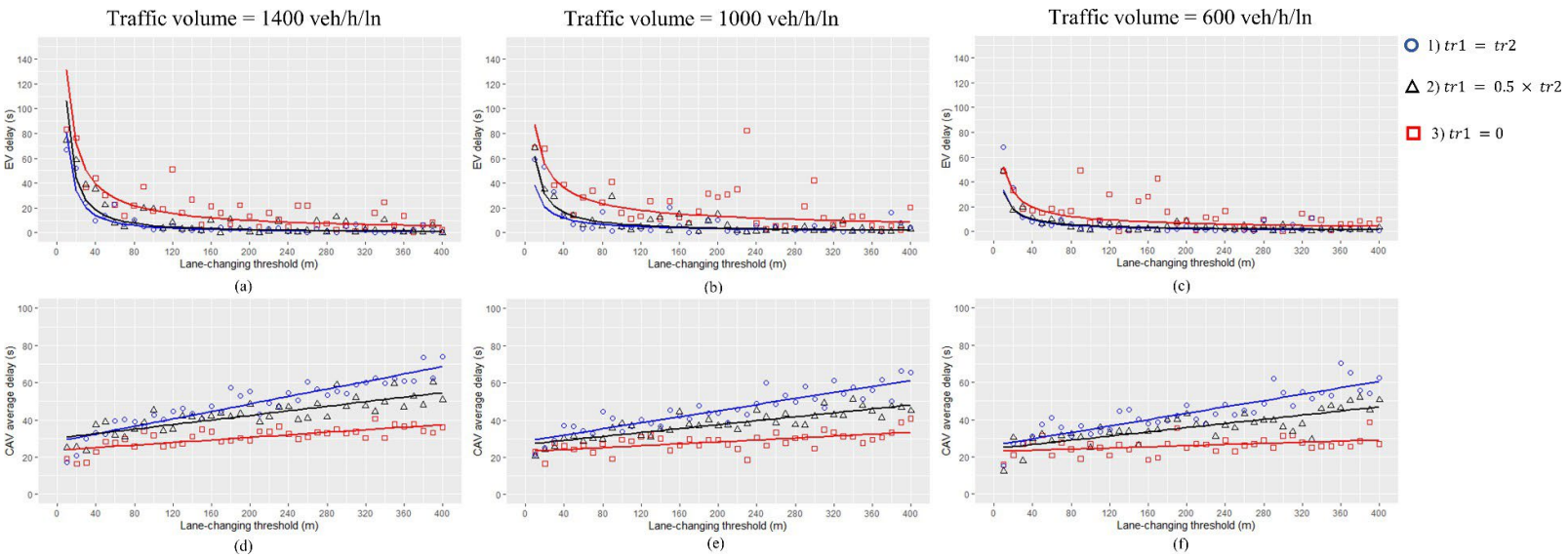

Figure 19. Delay of EV and CAVs versus lane-changing threshold in different simulation scenarios

In Figure 19 (a, b, and c), the relationship between the EV delay and the lane-changing threshold was fitted using a regression function that converges to a horizontal and a vertical asymptote. As the lane-changing threshold increased from zero, a sudden drop was observed in the EV delay. Then, the delay became approximately constant indicating additional lane-changing threshold distance does not impact EV delay beyond a certain point. Figure 19 (a, b, and c) shows that the threshold setting in which tr1 is 0 resulted in higher delay for EV compared to other settings. The reason lies in the lane-changing behavior of vehicles. According to this setting, vehicles do not stop within the lane-changing threshold since there is no stopping area. When all the vehicles in the right lane are moving, lane-changing and moving to the right lane is more difficult for the vehicles in the left lane. This is owing to the lower speed differences between the vehicles in the right and left lanes resulting in fewer gaps. Figure 19 (a, b, and c) also illustrates that the setting in which *tr1* is equal to *tr2* and the setting in which *tr1* is half *tr2* did not have considerable difference in terms of EV delay. The fitted regressions for these two settings converge as the lane-changing threshold increases. These findings are observed in all three traffic levels, and no considerable difference is between them. It can be deduced from Figure 19 (a, b, and c) that the presence of stopping area was influential in reducing the EV delay. The absence of stopping area in the setting in which tr1 is 0 was accompanied with higher EV delay. The minimum EV delay was observed to be zero. Meaning that the preemption algorithm worked properly, and, using it, the control delay was eliminated for EVs in some simulation runs.

Figure 19 (d, e, and f) shows that a direct relationship exists between the average delay of CAVs influenced by EV and the lane-changing threshold. A linear regression was fitted to this relationship. Figure 19 (d, e, and f) illustrates that the highest delays for CAVs, between the three threshold settings, were observed in the setting in which tr1 is equal to tr2 and only stopping area was used. In the setting in which tr1 is 0.5 x *tr2*, lower delays were observed compared to the setting in which *tr1* is equal to *tr2*. The lowest delays were observed when *tr1* = 0 and the stopping area was not utilized. Therefore, as the stopping area became smaller from the setting in which *tr1* is equal to *tr2* to the setting in which *tr1* is 0, the CAV average delay decreased. This direct relationship between the size of stopping area and the CAV average delay is because CAVs had to pull over and stop within the stopping area. The stopped delay in the stopping area increased the average delay of CAVs. As the stopping area became smaller (the setting in which *tr1* is half *tr2*) or eliminated (the setting in which *tr1* is 0), the stopped delay and, as a result, the CAV average delay decreased. These findings are observed in all the traffic levels. Based on the fitted regressions presented in Figure 19 (d, e, and f), the steepest regression line, between the three settings, was obtained in the setting in which tr1 is equal to tr2. And the smallest slope was observed in the setting in which tr1 is 0. According to this observation, the slope of the fitted regression line reduced as the stopping area became smaller. With this observation, it can be inferred that as the stopping area became smaller, the CAV delay became less sensitive to the lane-changing threshold. In Figure 19 (f), the slope is close to zero for the scenario in which tr1 is 0, meaning that by changing the lane-changing

threshold, approximately no variation is observed in the CAV delay. These trends are observed in all three traffic levels.

In general, the fits of the regression curves are worse at higher traffic volumes and lower stopping threshold distances. This is due to failure of requests sent by the behavior algorithm to turn into immediate action, due to interference from other traffic. When the vehicles did not have to stop, fewer gaps were created by changing speeds between lanes. Appendix B shows the individual regression curves.

When comparing the CAV and EV families of curves, there is an apparent tradeoff between total delay. The cases with the highest CAV delay consistently have the lowest EV delay and vice versa. Applications that focus on pre-clearing the EV's lane approach a horizontal asymptote between 40-120 m in front of the EV, depending on the conditions. This information can be fine-tuned and used to select a threshold for connected EVs to request a lane change from CAVs in advance and ensure little delay while only minimally impacting CAV delay.

4.3.2 Comparing the proposed model with an existing model

The proposed algorithm was compared to an existing algorithm to illustrate the advantage of our strategy. Based on Weinert and Düring's behavior algorithm, CAVs change lane when their distances to an EV reach to 150 m and CAVs speeds are higher than 10 m/s to create a rescue lane for the EV. Based on the results presented in Figure 19, the proposed algorithm with *tr1* equal to half *tr2* was used since it reduced the delay for both EV and CAV. Therefore, the proposed algorithm with *tr1* of 75 m and *tr2* of 150 m was used. The

same simulation network and preemption strategy was used for both algorithms. 40 simulation runs were performed for each algorithm and each traffic level (240 runs totally). EV and CAV delay are presented as boxplots for two algorithms in different traffic levels in Figure 20.

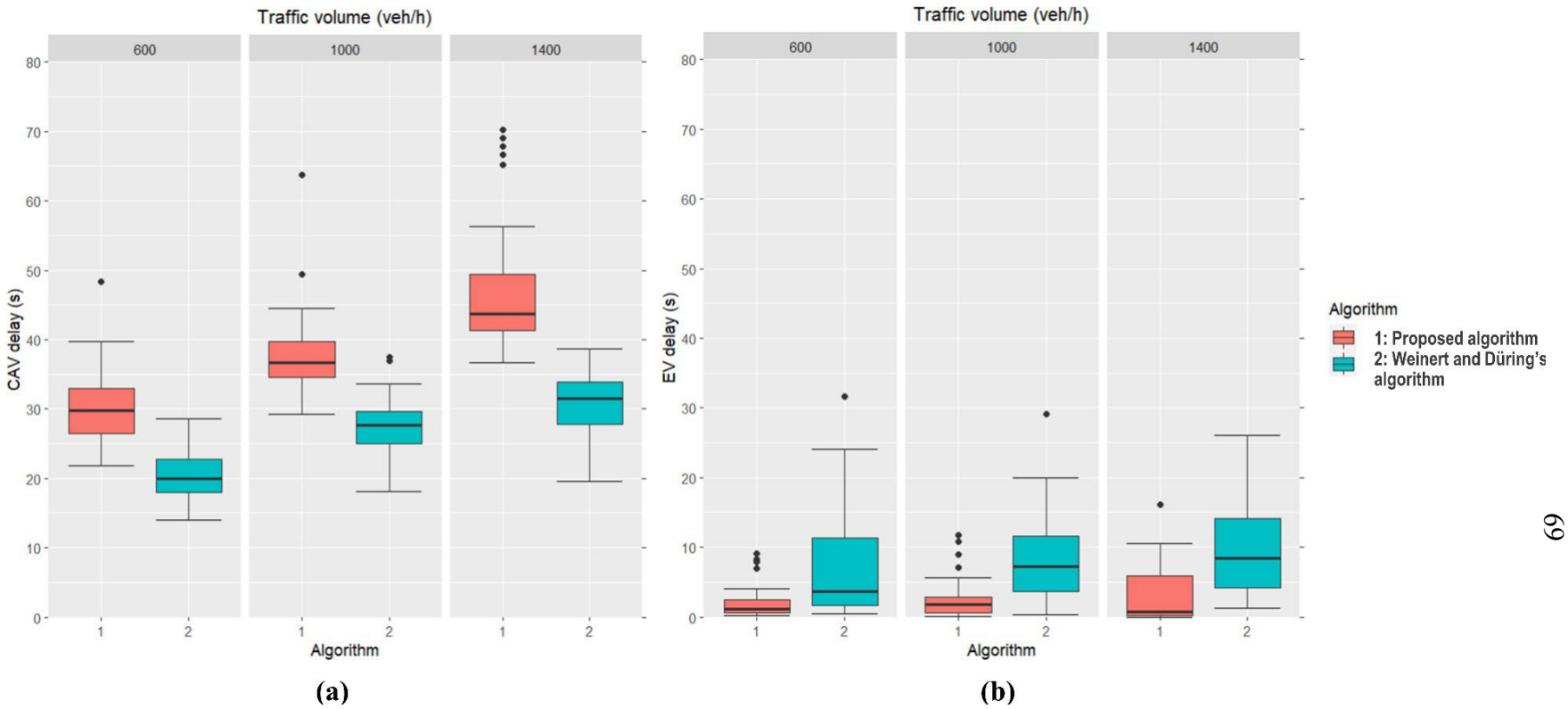

Figure 20. Delays of EVs and CAVs for proposed and Weinert and Düring 's algorithms in different traffic volumes

Based on Figure 20 (a), using the proposed algorithm resulted in higher delay for CAVs compared to Weinert and Düring's algorithm in all traffic levels. Figure 20 (b) shows lower EV delay in the proposed algorithm compared to Weinert and Düring's algorithm. Weinert and Düring's algorithm is similar to our proposed algorithm with *tr1* of zero. The obtained results in Figure 20 are in consistency with the results provided in Figure 19 when comparing the scenario in which *tr1* is zero (similar to Weinert and Düring's algorithm) and the scenario in which *tr1* is half *tr2*. Since stopping behavior was not used in Weinert and Düring's algorithm, CAVs experienced lower delays using their algorithm. Our proposed algorithm was more successful in reducing the delay of EV as using both stopping and lane-changing behaviors reached in faster CAV lane-changing and lane pre-clearing for EV. Appendix C provides the summary statistics of EV and CAV delay for different algorithms and traffic volumes.

4.4 Conclusions

In this research, the lane-changing and stopping behaviors of CAVs were explored on an arterial corridor to investigate how different combinations of these behaviors influence the delays of EV and surrounding traffic which was lacked in the literature. As the objective was to study CAVs behavior to prioritize EV, an algorithm was written to define the desired driving behavior of CAVs, and a preemption algorithm was developed to prioritize the EV's approach at signalized intersections. To obtain the desired lane-changing behavior, two parameters including the stopping and the lane-changing thresholds were introduced. 9 simulation scenarios were defined considering different traffic volumes and different threshold combinations. The delay of EV and the average delay of influenced CAVs were extracted from simulation results and plotted against the lane-changing threshold. Regression functions were fitted to the data to better compare the performance of different scenarios with each other.

The results showed that the use of stopping area was accompanied by reducing the delay of EV while it resulted in increasing the delay of CAVs influenced by EV. The intermediate setting where the stopping threshold is half the lane-changing threshold is more favorable regarding the delays of both EVs and CAVs. The reason is that a considerable difference was not observed in the EV delay between the setting in which only the stopping area was used and the setting in which both areas were used based on the fitted curves. However, lower delays were obtained for the CAVs in the setting in which both areas were used compared to the other setting. Therefore, using the setting in which both areas were used was observed to reduce the CAV delay while not considerably increase the EV delay.

Hence, this setting resulted in better outcomes in terms of the delays of both EVs and CAVs compared to the other two settings. Also, according to the fitted curves, the EV delay was observed to reduce and become constant as the lane-changing threshold increased. It can be deduced that there was an optimum lane-changing threshold after which the EV delay variation was not considerable. On the other hand, a linear regression was fitted to the relationship between the CAV delay and the lane-changing threshold. Therefore, using the optimum lane-changing threshold would be accompanied by the minimum delay for EV and prevent the increasing of CAV delay. Hence, the main goal which was obtaining desired CAV lane-changing and stopping behavior was addressed. The proposed behavior algorithm was compared to an existing algorithm to evaluate its performance.

The results of this research will serve as a benchmark for future research into more complex or cooperative behavior algorithms. Since several traffic levels were simulated in this research, the sensitivity of the developed algorithm was evaluated in response to traffic volume. Hence, in new scenarios with different traffic volumes, the variation of delay can be anticipated according to the results obtained in this research. Also, as different combinations of lane-changing and stopping thresholds were tested in simulations, the results of this study can be generalized to new threshold combinations. Further studies are required to evaluate the generalization of the results to other scenarios. A preemption algorithm was developed in this research with the objective of eliminating control delay for the EV. Preemption algorithms could be developed in future research to optimize the transition between the preemption state and normal state. Hence, the delay of EV could be minimized without having considerable influence on the delays of vehicles in

perpendicular approaches. One ability of CAVs is that their trajectories could be controlled by a processing center. Therefore, their trajectories could be optimized by a model to minimize a specific objective function. A future topic could be optimizing the trajectories of CAVs to minimize the response time of EV. Very little is known about human behaviors during EV encounters. Most of our cited work makes assumptions about behaviors (e.g. compliance to messages or uniform actions). In future research, the human aspect of behaviors could be studied to enable the simulation of human drivers in emergencies so that the improvement of CAVs can be measured compared to human drivers. The algorithms developed in this research were tested in a fully connected and autonomous traffic environment. The cooperative behavior of CAVs in emergencies could be investigated in mixed traffic environments with different market penetration rates in future studies.

CHAPTER 5

COOPERATIVE BEHAVIOR FOR CONNECTED AND AUTONOMOUS VEHICLES TO PRIORITIZE EMERGENCY VEHICLES

5.1 Objective

The objectives of this research are two-fold. The first objective is to establish a methodology for optimizing CAVs trajectories when an EV enters a freeway segment. The optimized trajectories are obtained to minimize the delay of the EV and surrounding CAVs by minimizing a lane-changing cost function. The second objective is to develop a control algorithm to facilitate CAV movements during emergencies using the optimization results. The trajectory optimization method and the control algorithm together form a proposed cooperative behavior framework for CAVs to facilitate EV passage of the segment. The developed framework was evaluated in traffic microsimulation on a three-lane freeway with a right shoulder. The same methodology could be implemented in freeway segments with different number of lanes.

5.2 Methodology

In this research, a cooperative behavior framework was established to identify optimal trajectories for CAVs and order CAVs to move based on the trajectories to clear a lane for an EV. The optimal trajectories were estimated recursively using binary linear programming, implemented in the Gurobi module of Python (Gurobi Optimization, 2021; G Van Rossum & Drake, 2009). Traffic simulations were performed in SUMO software (Lopez et al., 2018). SUMO and its associated TraCI were used to send and receive CAVs information to Python, control CAVs based on optimization results and measure the effectiveness of optimization methodology. A control algorithm was defined to specify the behavior of CAVs and order them to move based on the optimized trajectories. The control

algorithm sends lane change and speed change requests to SUMO. These requests are checked by SUMO's car following model, Krauss (Krauß, 1998) and lane-changing model, SL2015 (Erdmann, 2015). Then, the requests are executed if they are recognized safe and feasible by SUMO. The simulation framework is shown in Figure 21. The optimization was implemented in simulation on a 1-mile (1609 m) segment of a three-lane freeway with a shoulder on the right side. The freeway and shoulder lanes widths were 13 ft (3.96 m) and 10 ft (3.05 m), respectively. The freeway speed limit was 55 mile/h (24.59 m/s). EVs were granted permission to move 10 mile/h (4.47 m/s) faster than regular traffic could move in the travel lane (Henchey et al., 2014; Weinert & Düring, 2015). It was assumed that shoulder could be used in emergencies by EVs and CAVs with the speed limit of 35 mile/h (15.65 m/s). The simulation network is illustrated in Figure 22. The car-following parameters provided in Table 5.1 were used to adjust Krauss model in SUMO for the behavior of CAVs (Atkins, 2016; Qiong Lu et al., 2018). CAVs were assumed to have level 5 of autonomation according to SAE J3016 (Standard, 2018).

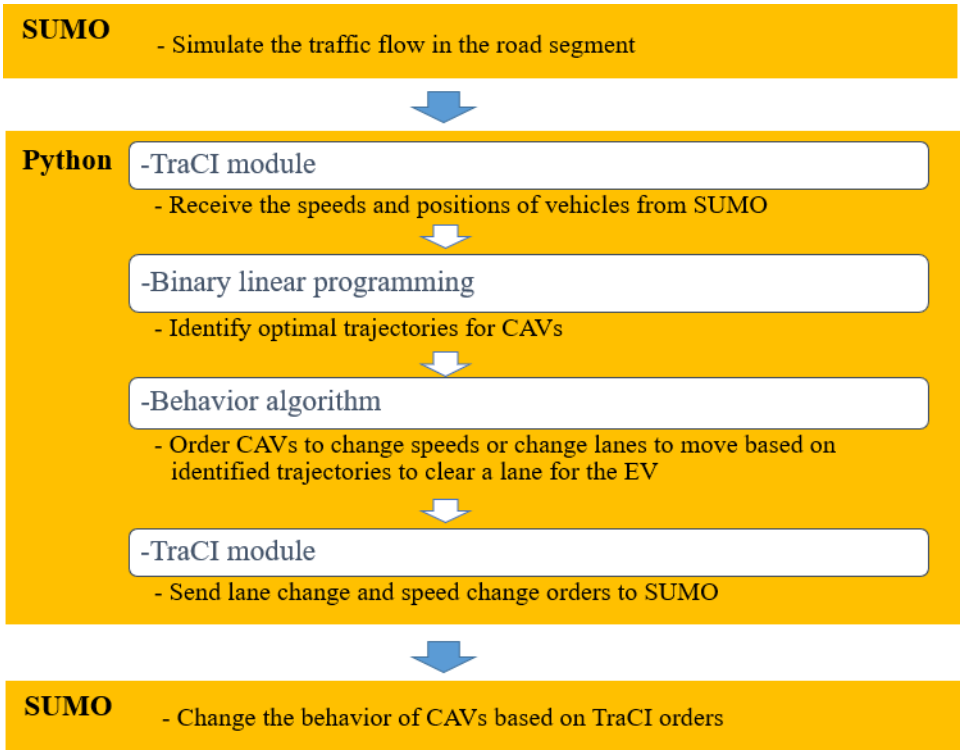

Figure 21. Simulation framework

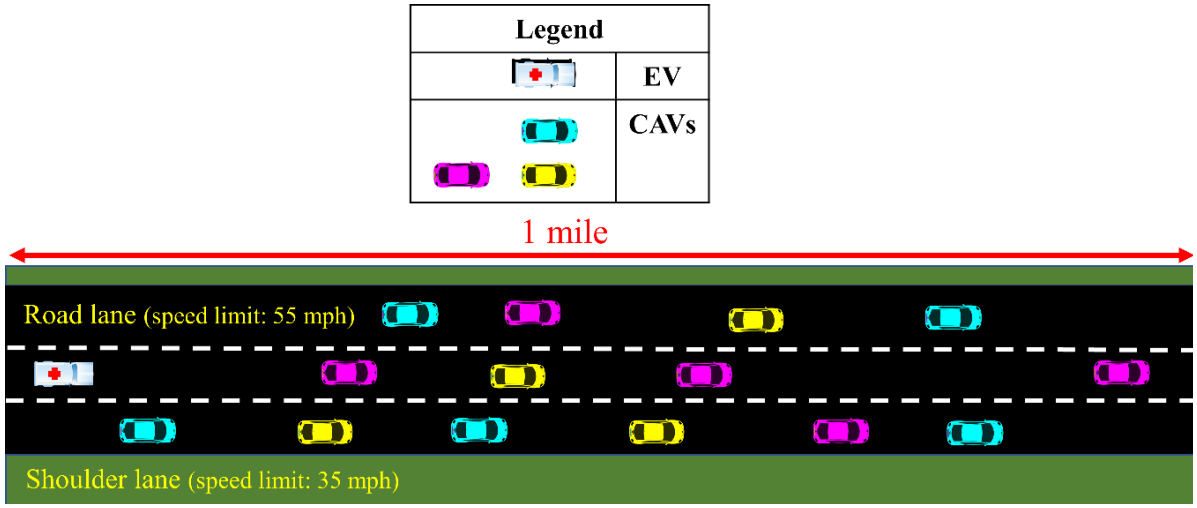

Figure 22. Simulation network

Table 5.1. Adjusted Krauss car following model parameters for CAVs.

Minimum gap (m)	Acceleration (m/s^2)	Deceleration (m/s^2)	Emergency deceleration (m/s^2)	Driver imperfection	Reaction time (s)
0.5	3.8	4.5	8	0	0.6

5.2.1 Optimization

The optimization method developed in this research is based on optimization approaches implemented by (Hannoun et al., 2018) and (J. Wu et al., 2020). As discussed in the literature review, microsimulation driving behavior models have not been considered in the cooperative behavior algorithms developed in discrete cell simulations (Hannoun et al., 2018; J. Wu et al., 2020). Hence, our study focused on developing a cooperative behavior framework applicable in microsimulation. The optimization approach implemented in this study aimed to minimize the costs associated with CAVs following optimized trajectories in microsimulation. A new cost function was developed to minimize the lane-changing cost of traffic when clearing lane for EV. Several new constraints were added to eliminate infeasible trajectories and reduce the lane-changing conflicts. A control algorithm, provided in the next section, was developed to order CAVs to move based on the optimized trajectories which was absent previously.

The proposed optimization algorithm identifies the fastest approach to clear an EV's lane recursively during simulation. For this goal, the positions of CAVs and gaps are identified and parameterized. Then, the algorithm optimizes the assignment of CAVs to gaps with the aim of reducing CAV's lane-changing conflicts. The algorithm also identifies the necessity of using shoulder and allow use of shoulder when CAVs outnumber gaps in freeway lanes. The following assumptions were considered in this research:

1. The EV could enter from any lane and does not change lane after entering the road segment. CAVs should clear EV's lane as soon as possible so the EV does not reduce speed.
2. The positions and speeds of EV and CAVs are transmitted to a central processing unit in real-time.
3. All CAVs apply the optimized trajectories whenever the trajectories are safe and feasible.
4. The shoulder is empty of obstacles.

The objective of optimization is to minimize the cost of lane-changing for the CAVs and provide an organized approach to clearing the right of way to the EV as a group, rather than individually. The cost of lane-changing is defined as a function of the time required for a CAV to reach an assigned gap and complete a lane change. To this end, the positions and speeds of CAVs are transmitted to a central processor. In this application, Python acts as the central processor. Based on CAVs' positions, the central processor calculates the positions of eligible gaps between CAVs. Then, each CAV is assigned to an eligible gap using binary linear programming. The following parameters are utilized to identify the optimization zone and eligible gaps:

L = *Rolling buffer zone length*. The CAVs that are in front of the EV and within this zone are included in the optimization. Figure 23 illustrates the rolling buffer zone length.

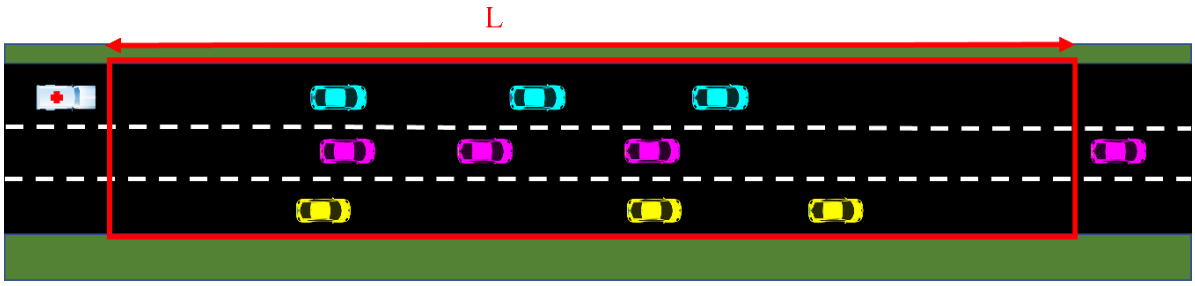

Figure 23. Rolling buffer zone length

g^{min} = *Minimum eligible gap length*. When the distance between two CAVs is more than or equal to the minimum eligible gap length, the open area between them is identified as one or multiple eligible gaps. An eligible gap should be long enough so a CAV can change lane and move to it. Figure 24 illustrates the minimum eligible gap length.

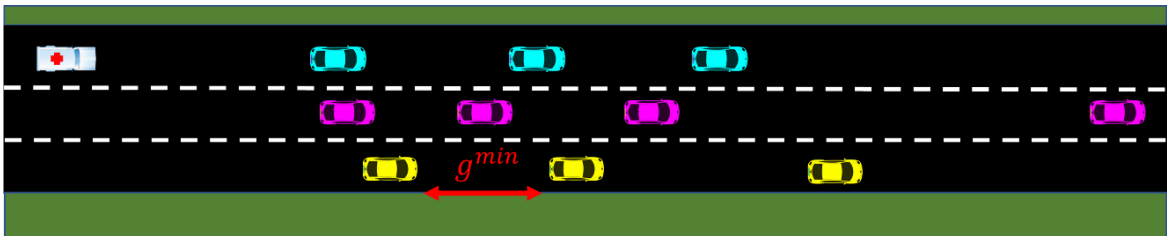

Figure 24. Minimum eligible gap length

All the variables and parameters implemented in optimization are shown in Table 5.2 and Table 5.3.

Table 5.2. Optimization variables

Variable	Definition
w_i^j	*Assignment variable*: A binary variable that shows whether CAV *I* is assigned to gap *j* or not. The value is 1 when it is assigned; otherwise, it is 0.

Table 5.3. Optimization parameters

Parameter	Definition
C_i^j	Cost of moving CAV I to gap j.
c_1	A constant showing the cost of a lane change.
c_2	A constant showing the cost of moving forward unit length related to surrounding CAVs in the current lane.
S^{avg}	Average speed of CAVs.
$x_i^{CAV}(t)$	Longitudinal distance between rear bumper of CAV *I* and front bumper of the EV at time step *t*. An example is provided in Figure *25*.
$x_j^{GAP}(t)$	Longitudinal distance between rear side of gap *j* and front bumper of the EV at time step *t*. An example is provided in Figure *25*.
$y_i^{CAV}(t)$	Lane index of CAV *I* at time step *t*. An example of lane indices is shown in Figure *26*.
$y_j^{GAP}(t)$	Lane index of gap *j* at time step *t*.
$x^{EV}(t)$	Longitudinal distance of EV from segment's starting point at time step *t*.
x^{OPT}	Optimization repetition threshold. Its default value is 0 at the start of simulation. Whenever the EV crosses this threshold, optimization is repeated.
n	Number of CAVs in the buffer zone.
m	Number of eligible gaps in the buffer zone.
g^a	Length of the available gap between two CAVs
n^g	Number of eligible gaps in the available gap.
g^e	Length of eligible gap.
$CAVs^{BUFF}(t)$	A list containing the IDs of CAVs which are inside the buffer zone at time step *t*.

An example of longitudinal distances of CAVs and gaps to the EV is illustrated in Figure 25.

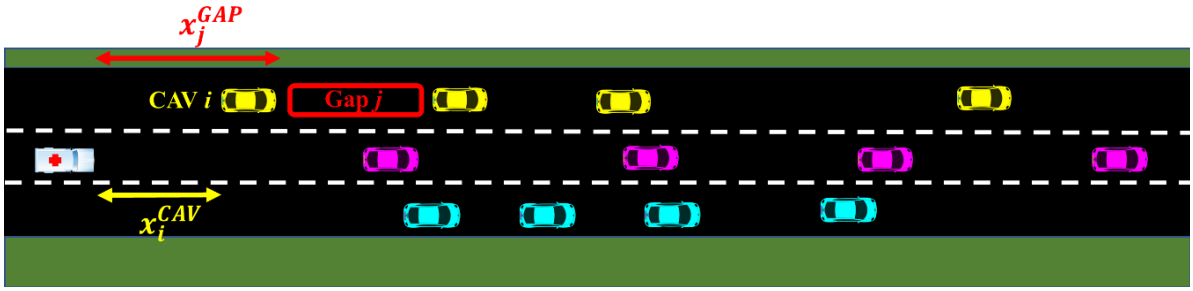

Figure 25. Longitudinal distances between CAVs and the EV and between gaps and the EV.

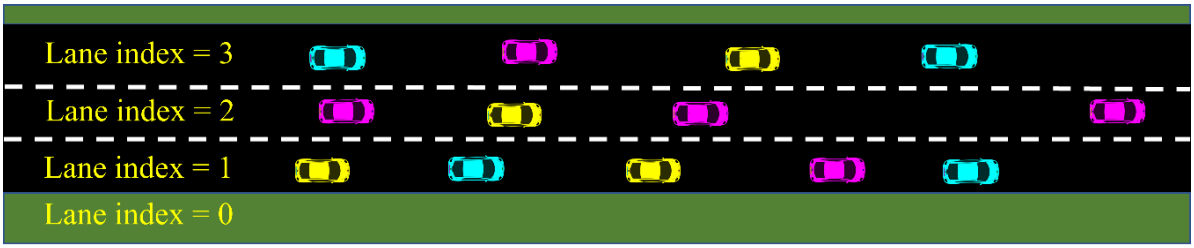

Figure 26. Lane indices

As it is illustrated in Figure 26, lane index starts from 0 in shoulder and increases as it gets closer to center of road's cross section. Lane index can be higher than 3 if there are more than 3 road lanes.

Hannoun et al. and Wu et al. divided road segment to identical cells and positioned vehicles and gaps inside these cells (Hannoun et al., 2018; J. Wu et al., 2020). As this approach is not possible in microsimulation where vehicle movements are continuous, gaps are defined based on vehicle positions in this study. First, the length of available gap between any two CAVs are identified. Then, Equations 5.1 and 5.2 identifies number and length of eligible gaps in this available gap. Based on Equation 5.1, the available gap length is divided by minimum eligible gap length, and number of eligible gaps is obtained by flooring the division result. Then, the available gap length is divided by the obtained number of eligible gaps, and floor of division give us the length of eligible gaps according to Equation 5.2. It is derived that eligible gap length is equal or higher than minimum gap length and less than twice minimum gap length.

$$n^g = \lfloor \frac{g^a}{g^{min}} \rfloor \quad 5.1$$

$$g^e = \lfloor \frac{g^a}{n^g} \rfloor \quad 5.2$$

Figure 27 illustrates an example of eligible gap identification. In this example, the available gap is divided into two eligible gaps.

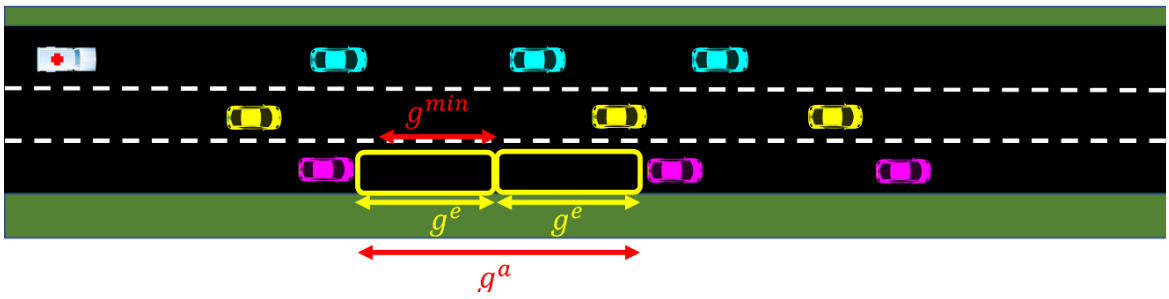

Figure 27. An example of eligible gap identification

Optimization is only performed for the CAVs and eligible gaps that are inside the buffer zone. Once the optimization is completed, the assigned trajectories are transmitted to CAVs using TraCI. If the EV enters from the right or left lanes, the CAVs in the middle lane may be required to change lanes to create gaps for other CAVs in the EV's lane. Hence, the positions of CAVs are also defined as eligible gaps except for the CAVs in the EV's lane. The optimization then decides whether the CAVs in other lanes should change lane or not. All CAVs and eligible gaps are numbered to be used in optimization. An example of numbering is illustrated in Figure 28. The numbers of CAVs and gaps are shown with parameters I and j, respectively.

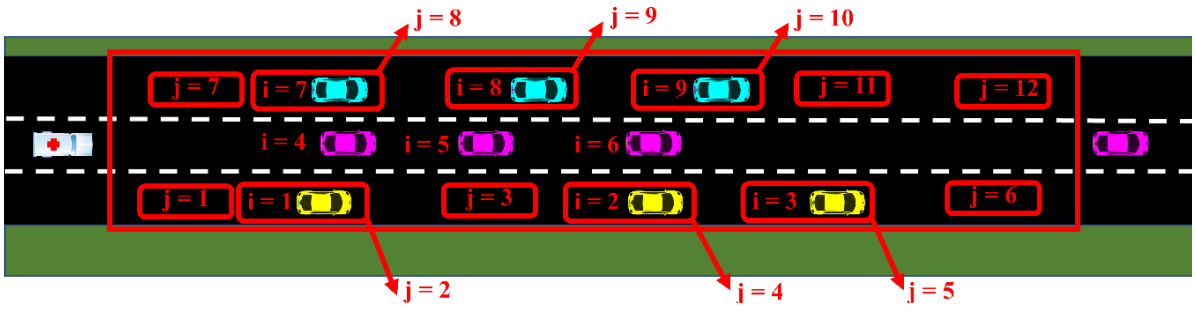

Figure 28. An example of the numbering of CAVs and gaps

The objective function is defined considering the cost of lane-changing. The cost of lane-changing is estimated using two parameters including the time required to continue moving in the current lane to reach the assigned gap and the time required to perform lane-changing and enter the target lane. Therefore, the cost function had two components: a term dependent on the longitudinal distance between a CAV and its assigned gap and the speed difference between the CAV and other CAVs and another term related to the lane-changing process.

Binary linear programming was used to minimize the objective function. Generally, linear programming minimizes or maximizes a linear function of variables limited by a set of linear constraints. When only one binary variable is used, the optimization problem becomes binary linear programming (Soudi & Tomsovic, 1998). The objective and cost functions are provided in Equations 5.3 and 5.4, respectively.

$$minimize \sum_{i=1}^{n} \sum_{j=1}^{m} C_i^j \tag{5.3}$$

$$C_i^j = (c_1 |y_j^{GAP}(t) - y_i^{CAV}(t)| + c_2 (x_j^{GAP}(t) - x_i^{CAV}(t)))w^j{}_i \tag{5.4}$$

The parameters of c_1 and c_2 should be calibrated for any application based on the average time required to complete a lane change and the difference between the speed of a CAV and the average speed of CAVs when the CAV needs to move forward and reach its assigned gap. In our simulation setting, it was observed that, on average, it took 2 seconds for a CAV to complete a lane change. Therefore, c_1 was set to 2 seconds. The value of c_2 was dependent on the speed difference between a CAV and its surrounding CAVs. In our

control algorithm, it was assumed that when a CAV needs to move forward to reach its assigned gap, it can increase its speed up to 20 percent. Hence, the value of c_2 was calculated as the time required to move forward a unit length related to surrounding CAVs according to Equation 5.5.

$$c_2 = \frac{1}{S^{avg} \times 0.2} \tag{5.5}$$

Five constraints were defined in the optimization process as follows. The first two constraints are based on (Hannoun et al., 2018) and (J. Wu et al., 2020). The next constraints were added to eliminate infeasible trajectories and reduce lane-changing conflicts.

1) *One CAV per gap:* The first constraint, shown in Equation 5.6, ensured that each gap was assigned to a maximum of one CAV. In other words, at each gap, the sum of assignment variables for CAVs should be equal to 0 or 1.

$$\sum_{i=1}^{n} w_i^j \leq 1;\ \forall j = 1,2,\dots,m \tag{5.6}$$

2) *One gap per CAV*. This constraint, provided in Equation 5.7, checked that each CAV was assigned to a single gap. Based on this constraint, for each CAV, the sum of assignment variables at different gaps should be equal to 1.

$$\sum_{j=1}^{m} w_i^j = 1;\ \forall i = 1,2,\dots,n \tag{5.7}$$

3) *Forward movement*. Using to this constraint, CAVs were assigned to the gaps that were in front of them. This ensured that they did not need to decrease their speeds to reach the assigned gaps behind them. Therefore, the EV is not required to decrease its speed due to the speed reductions of CAVs. Equation 5.8 shows the forward movement constraint.

$$\sum_{j=1}^{m}(x_j^{GAP}(t) - x_i^{CAV}(t))w_i^j \geq 0;\ \forall i = 1,2,\dots,n \quad 5.8$$

4) *One lane change limitation*. This constraint, formulated in Equation 5.9, ensured lane changes were feasible. If a CAV required two lane changes to reach its assigned gap, there might be another CAV in the middle lane, between the CAV and its assigned gap, making the lane change infeasible. Therefore, lane changes were limited to one lane change.

$$\sum_{j=1}^{m}|y_j^{GAP}(t) - y_i^{CAV}(t)|w_i^j \leq 1;\ \forall i = 1,2,\dots,n \quad 5.9$$

5) *No relative forward movement without lane change*. To reduce the conflict between CAVs, the assignment of CAVs to other gaps in the same lane were restricted. Hence, only the CAVs required to change lane may move forward relative to CAV platoon to reach their assigned gaps and other CAVs do not change speed. This constraint is formulated in Equation 5.10.

$$\sum_{j=1}^{m}(x_j^{GAP}(t) - x_i^{CAV}(t))w_i^j z_i^j \geq 0;\ \forall i = 1,2,\dots,n \quad 5.10$$

Where z_i^j is defined in Equation 5.11.

$$z_i^j = \begin{cases} 1 \; if |y_j^{GAP}(t) - y_i^{CAV}(t)| = 0 \\ 0 \; if |y_j^{GAP}(t) - y_i^{CAV}(t)| > 0 \end{cases} ; \forall i = 1,2,\dots,n ; \forall j = 1,2,\dots,m \quad 5.11$$

Optimization is performed based on the algorithm provided in Figure 29. This algorithm is performed at every simulation step and first checks if the conditions for optimization are met. Optimization is repeated at intervals of $L/2$ to ensure that CAVs had time to reach their assigned gap before receiving a new assignment.

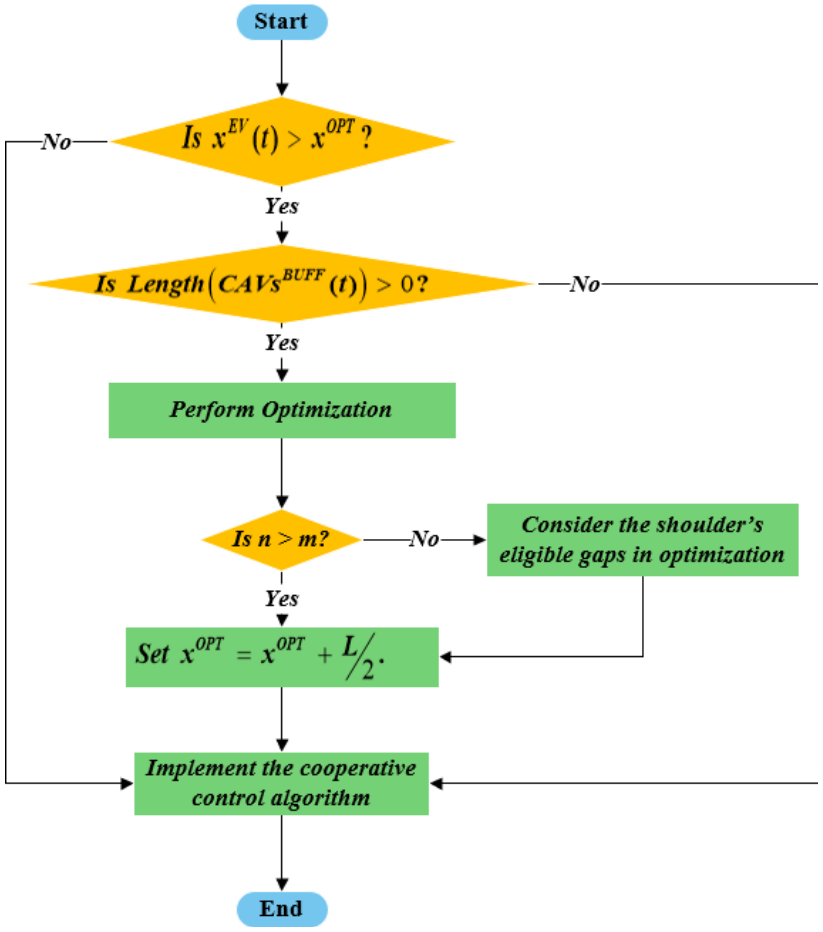

Figure 29. Optimization algorithm

According to Figure 29, there is a check if the EV's longitudinal position is higher than the optimization repetition threshold. If so, the number of CAVs in the buffer zone are checked. If there are any CAVs in the buffer zone, optimization is performed. When there are more CAVs than eligible gaps in the buffer zone, the optimization is infeasible. In this condition optimization cannot meet "one gap per CAV" constraint, provided in Equation 5.7,since the optimization cannot find available gaps for all CAVs. If optimization is infeasible using three freeway lanes, the shoulder is used to add additional gaps to the buffer zone, and optimization is repeated. At the end, half buffer length is added to the repletion threshold. The output of the optimization process is a set of assigned gaps for CAVs. The control algorithm, described in the next section, will be used to meet those assignments.

5.2.2 Cooperative control algorithm

To specify the cooperative behavior in SUMO, a control algorithm was written in Python and added to SUMO through the TraCI module. The proposed cooperative control algorithm is provided in Figure 31. The parameters utilized in the cooperative algorithm are presented in Table 5.4. In the previous section, optimized trajectories were obtained based on the positions of CAVs and gaps relative to the EV, x_i^{CAV} and x_j^{GAP}. However, these relative positions cannot be used by CAVs to follow optimized trajectories, as the EV moves faster than CAV traffic. Hence, a CAV which moves with the same speed as traffic should be used as the origin of positioning. Positioning origin for every CAV i and its assigned gap j was defined the lag CAV which is behind gap j in the same lane. An example of positioning relative to the lag CAV is provided in Figure 30.

Table 5.4. Parameters used in the cooperative algorithm.

Parameter	Definition
$S_i^{CAV}(t)$	Speed of CAV *i* at time *t*.
c	A constant that is used to increase the speed of a CAV to reach its assigned gap which is 1.2.
$x_i^{CAV\_LAG}(t)$	Longitudinal distance between rear bumper of CAV *i* and front bumper of the lag CAV at time *t*. This variable can be negative when CAV *i* is behind the lag CAV. An example is provided in Figure 30.
$x_{(i,j)}^{ASSIGN\_GAP}(t)$	Longitudinal distance between rear side of gap *j* assigned to CAV *i* and front bumper of the lag CAV at time *t*. An example is provided in Figure 30.
$y_{(i,j)}^{ASSIGN\_GAP}(t)$	Lane index of gap *j* assigned to CAV *i* at time *t*.
$S_{(i,j)}^{LAG}(t)$	Speed of the lag CAV. If the lag CAV needs to change speed or there is no lag CAV behind gap *j*, then the closest CAV to gap *j* that does need to change speed is selected as the lag CAV.

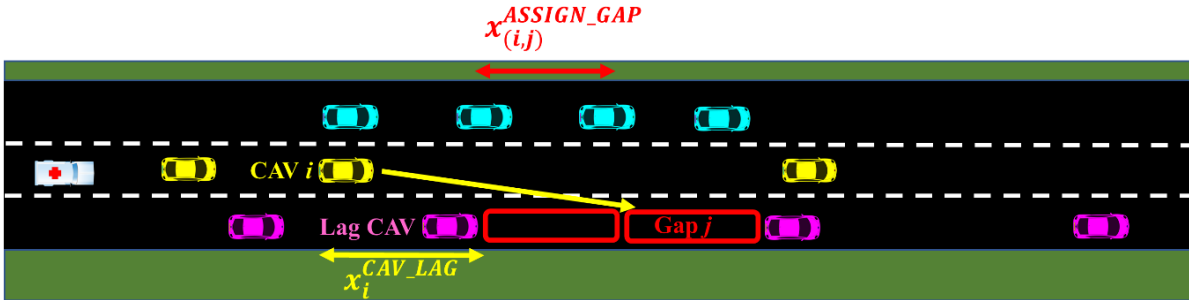

Figure 30. Longitudinal distances between CAVs and the lag CAV and between gaps and the lag CAV.

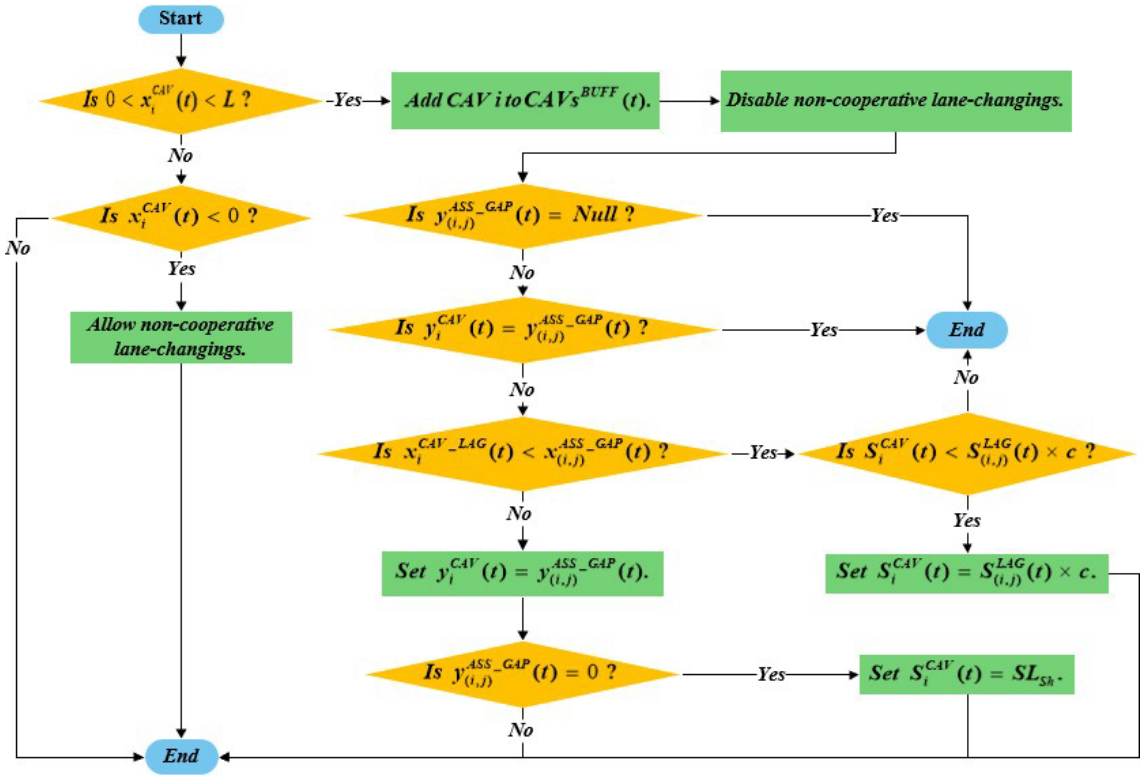

Figure 31. Cooperative control algorithm

The algorithm provided in Figure 31 is performed for every CAV at every simulation step. The first step checks the distance between the CAV and the EV. If the CAV is in front of the EV and within the buffer zone, the CAV should be added to the buffer list of CAVs, and all non-cooperative lane changes are disabled. Non-cooperative lane changes are defined as lane changes that are not required based on optimized trajectories. Hence, CAVs in the buffer zone only perform lane changes requested by the cooperative algorithm. Only the CAVs that are in the buffer list are considered for the optimization process. Then, the algorithm checks whether a gap was assigned to this CAV by optimization. If the CAV has an assigned gap, the lane index of the assigned gap and the CAV are compared. If they have different lane indices, the CAV should perform a lane change. Before performing the

lane change, the longitudinal positions of the CAV and the assigned gap are compared. If the assigned gap is in front of the CAV, the CAV may need to increase speed to reach the assigned gap. Due to safety concerns, the CAV is only allowed to increase its speed up to 20 percent higher than the lag CAV's speed. When the CAV reaches to the longitudinal position of its assigned gap, the CAV changes lanes. If the assigned gap is in the shoulder lane, the CAV is ordered to reduce its speed to observe the shoulder's speed limit. When the EV passes the CAV, non-cooperative lane changes become allowed. The developed cooperative algorithm is applicable to freeway segments with more than 3 road segments.

5.2.3 Non-cooperative and base control algorithms

To evaluate the extent of improvement achieved by the cooperative control algorithm, a non-cooperative control algorithm was implemented. In the non-cooperative algorithm, CAVs act individually without optimization to clear the EV's lane. As optimization is not used, the positions of eligible gaps are unknown. Hence, all the CAVs which are in the EV's lane and inside the buffer zone are ordered to move to their right. If a CAV is ordered to move to shoulder, it should observe the shoulder's speed limit. The non-cooperative algorithm is provided in Figure 32 and performed for every CAV in every simulation step.

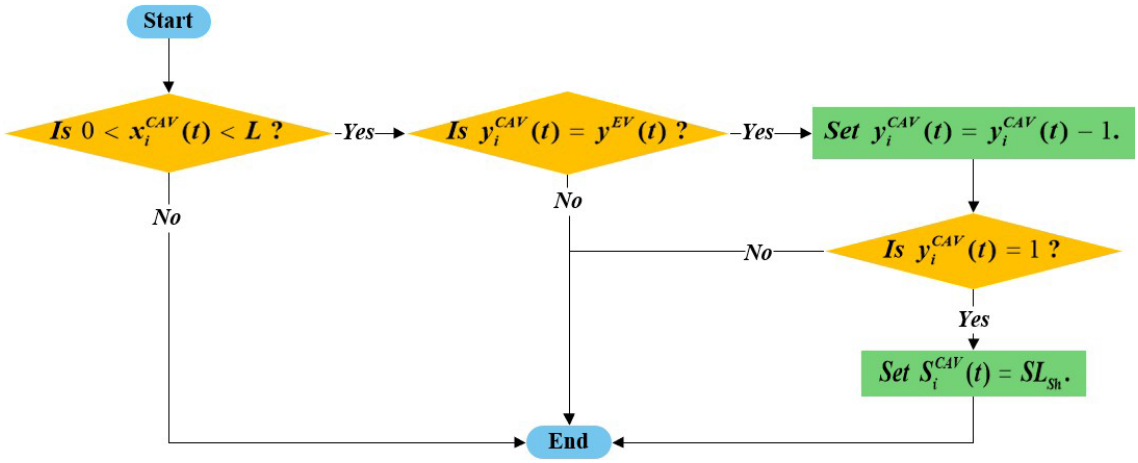

Figure 32. Non-cooperative control algorithm

Additionally, a base algorithm was used in which the EV utilizes the shoulder under the shoulder's speed limit, and CAVs are not disturbed or ordered to perform any lane change or speed change.

5.2.4 Design of experiments

EV travel time reliability was investigated to evaluate algorithms performances (Z. Zhang et al., 2016). As the buffer zone length is an important parameter in the cooperative behavior framework, the sensitivity of EV travel time to buffer length was investigated in different traffic densities and EV entrance lanes. To illustrate the extent of shoulder use in the cooperative framework, shoulder use percentage was calculated by dividing shoulder use duration by EV travel time. Shoulder use duration values were normalized by EV travel time to better compare simulation runs with different EV travel times. The results are provided in Figure 33.

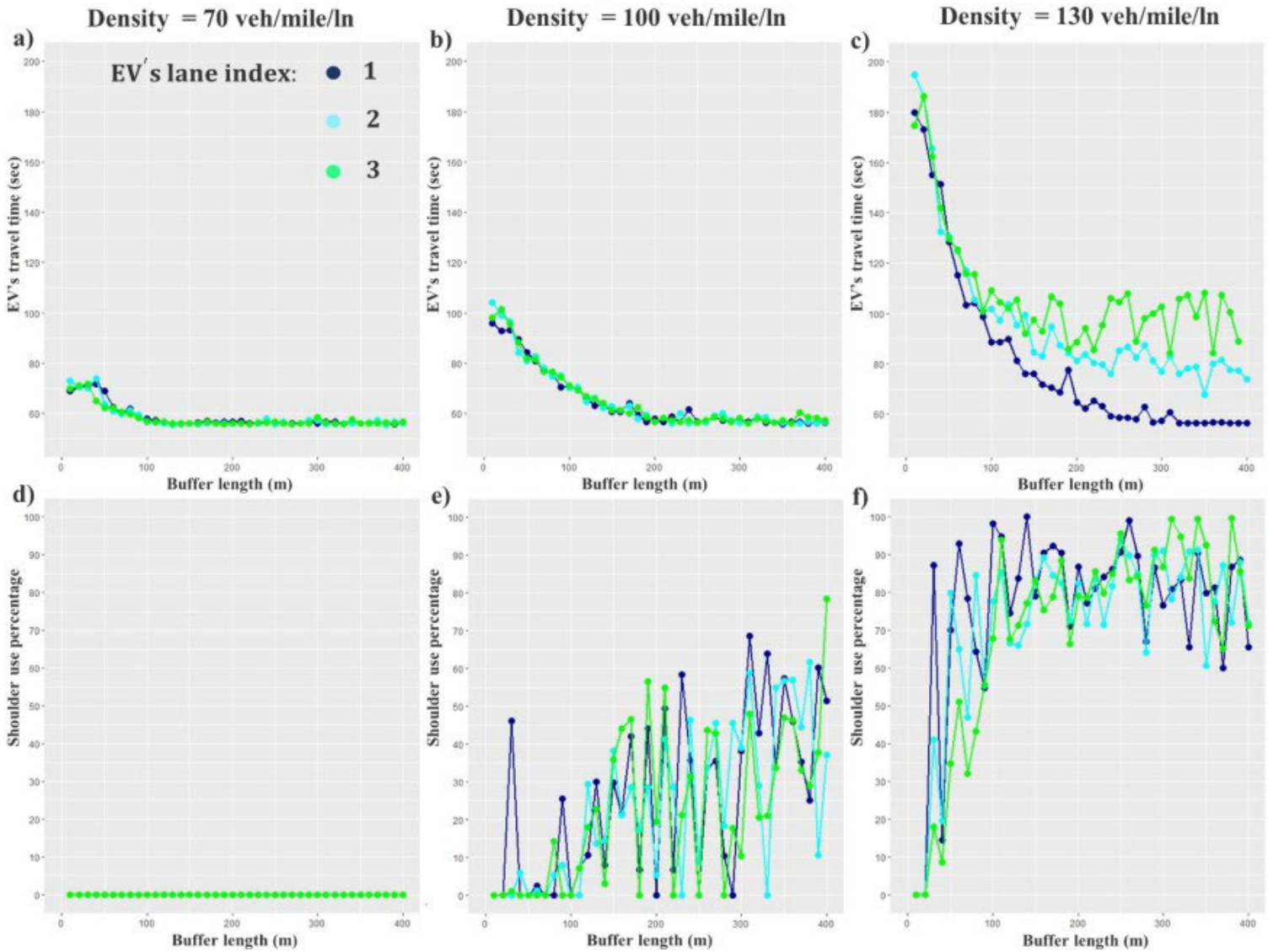

Figure 33. Sensitivity of EV travel time to buffer length.

Figure 33 (a), (b), and (c) illustrates as buffer length increases, the EV's travel time reduces toward a minimum travel time which is the free flow travel time at the EV's speed limit. Comparing Figure 33 (a), (b), and (c), it is observed that as density increases, EV's travel time increases, and higher buffer lengths are required to reduce the travel time to its minimum. Figure 33 (a), (b) show the EV's lane does not considerably influence the cooperative algorithm's performance in low and medium densities. However, Figure 33 (c) illustrates the lane the EV uses impacts the algorithm's performance in high density. As the optimization without shoulder use becomes infeasible in congested traffic, the cooperative algorithm starts using shoulder to clear the EV's lane. Figure 33 (d), (e), and (f) suggests that as traffic becomes more congested, shoulder use percentage increases. In Figure 33 (f), the buffer lengths of higher than 100 meters resulted in the cooperative algorithm using shoulder over more than half of EV's travel time. Thus, the cooperative algorithm is very dependent on using shoulder to clear EV's lane in high density. Additionally, if the EV's lane is not adjacent to the shoulder's lane, it takes more time clear the EV's lane.

Based on Figure 33, EV's travel time reaches its minimum at the buffer length of around 300 meters in all scenarios expect when EV moves on the lanes not adjacent to shoulder in high traffic density. Hence, 300 meters was chosen to evaluate the EV's travel time reliability of developed algorithms. Also, several simulation runs were performed using different minimum gap lengths in the cooperative algorithm, and the gap length of 10 meters reached in lowest EV travel time in our simulation settings. 18 simulation scenarios

were chosen based on control algorithm, traffic density and EV's lane index. Defined simulation scenarios are provided in Table 5.5.

Table 5.5. Simulation scenarios

Scenario	Algorithm	Density (veh/mi/ln)	EV's lane index	Buffer length (meters)	Minimum gap (meters)
BL0	Base	70 (Low)	0	-	-
NL1	Non-cooperative	70 (Low)	1	300	-
CL1	Cooperative	70 (Low)	1	300	10
NL2	Non-cooperative	70 (Low)	2	300	-
CL2	Cooperative	70 (Low)	2	300	10
NL3	Non-cooperative	70 (Low)	3	300	-
CL3	Cooperative	70 (Low)	3	300	10
BM0	Base	100 (Medium)	0	-	-
NM1	Non-cooperative	100 (Medium)	1	300	-
CM1	Cooperative	100 (Medium)	1	300	10
NM2	Non-cooperative	100 (Medium)	2	300	-
CM2	Cooperative	100 (Medium)	2	300	10
NM3	Non-cooperative	100 (Medium)	3	300	-
CM3	Cooperative	100 (Medium)	3	300	10
BH0	Base	130 (High)	0	-	-
NH1	Non-cooperative	130 (High)	1	300	-
CH1	Cooperative	130 (High)	1	300	10
NH2	Non-cooperative	130 (High)	2	300	-
CH2	Cooperative	130 (High)	2	300	10
NH3	Non-cooperative	130 (High)	3	300	-
CH3	Cooperative	130 (High)	3	300	10

5.3 Results and discussion

50 simulation runs with different random seeds were performed for each scenario provided in Table 5.5. Figure 34 shows the variability of EV travel time and CAV delay in different scenarios provided in Table 5. Shoulder use percentage was averaged for the scenarios with the cooperative algorithm and provided in Table 5.6. Also, ANOVA tests were performed for EV travel time and CAV delay considering three factors including traffic density, EV

lane index and control algorithm. The results of ANOVA tests are provided in Table 5.7, Table 5.8 and Table 5.9.

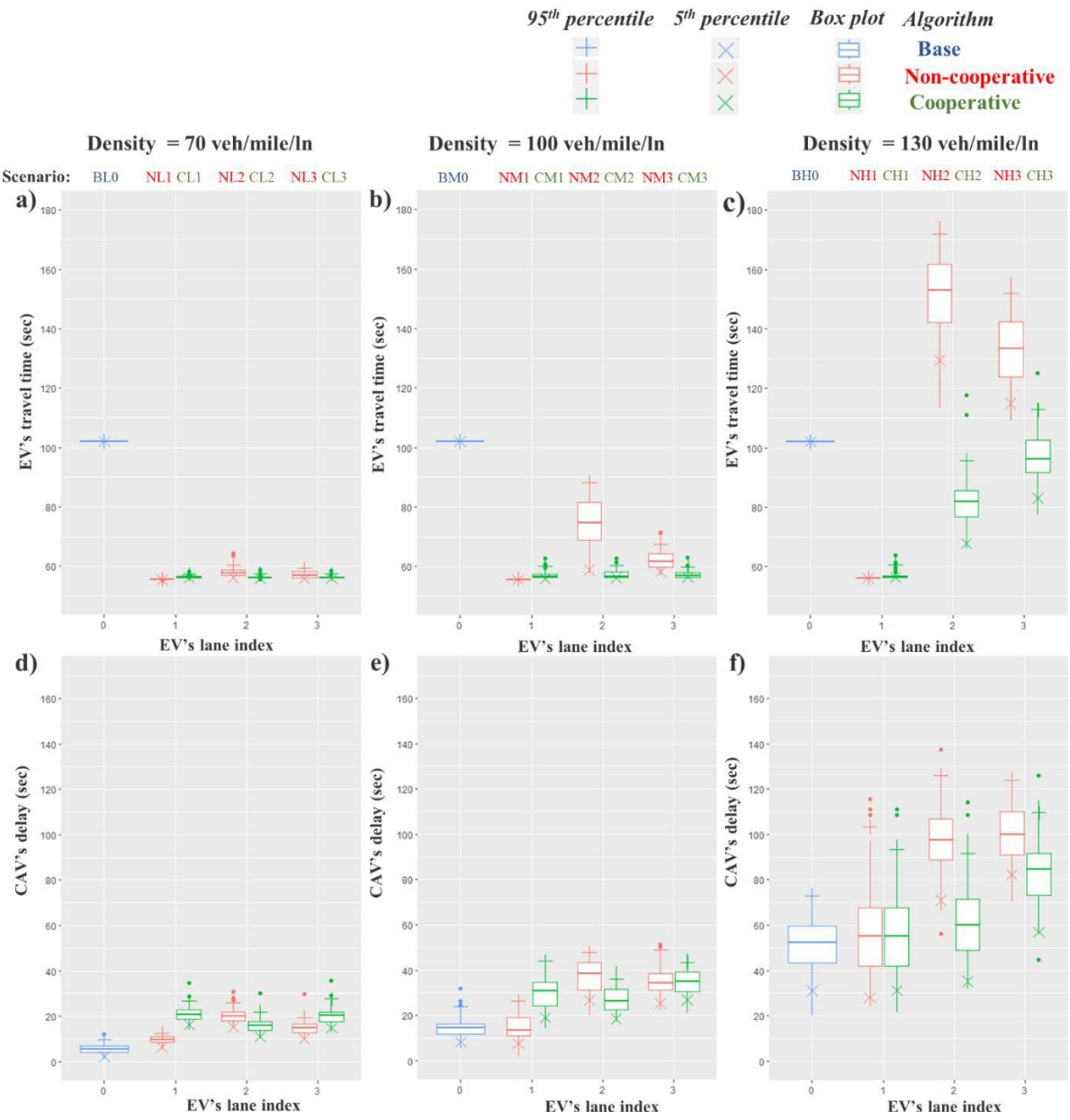

Figure 34. EV travel time and CV delay in different scenarios.

Table 5.6. Mean shoulder use percentage in the scenarios with the cooperative algorithm.

Algorithm	Density (veh/mi/ln)	EV's lane index	Mean shoulder use percentage
Cooperative	70 (Low)	1	0
Cooperative	70 (Low)	2	0
Cooperative	70 (Low)	3	0
Cooperative	100 (Medium)	1	37
Cooperative	100 (Medium)	2	32
Cooperative	100 (Medium)	3	36
Cooperative	130 (High)	1	84
Cooperative	130 (High)	2	84
Cooperative	130 (High)	3	83

Table 5.7. ANOVA results for EV travel time

Factor	F value	P value
Density (Low, medium & high)	442.1	<0.01
Lane index (1, 2 & 3)	156.0	<0.01
Algorithm (Cooperative & non-cooperative)	139.3	<0.01

Table 5.8. ANOVA results for CAV delay

Factor	F value	P value
Density (Low, medium & high)	1361.51	<0.01
Lane index (1, 2 & 3)	105.25	<0.01
Algorithm (Cooperative & non-cooperative)	19.41	<0.01

Table 5.9. ANOVA results for EV travel time with EV lane index as factor

Density	Algorithm	Factor	F value	P value
Low	Cooperative	Lane index (1, 2 & 3)	1.83	0.16
Medium	Cooperative	Lane index (1, 2 & 3)	0.67	0.52
High	Cooperative	Lane index (1, 2 & 3)	344.8	<0.01
Low	Non-cooperative	Lane index (1, 2 & 3)	57.09	<0.01
Medium	Non-cooperative	Lane index (1, 2 & 3)	138.1	<0.01
High	Non-cooperative	Lane index (1, 2 & 3)	1131	<0.01

Table 5.7 and Table 5.8 verifies that, in general, averages of EV travel time and CAV delay are statistically not equal in scenarios with different traffic densities and EV lane indices. It is also verified that using cooperative algorithm reached in statistically different average EV travel time and CAV delay compared to the non-cooperative algorithm. According to Figure 34 (a), (b) and (c), the cooperative algorithm is successful in significantly reducing EV travel time in the scenarios with EV on the lanes not adjacent to shoulder. Also, the size of boxplots and the difference between 95^{th} and 5^{th} percentiles illustrates using the cooperative algorithm results in lower EV travel time variance in these scenarios. This indicates that, in the mentioned scenarios, the cooperative algorithm is successful in reducing EV travel time and improving the travel time reliability of EV compared to other algorithms. In the scenarios with EV on the lane adjacent to shoulder, EV travel time of cooperative algorithm is slightly higher than travel time of non-cooperative algorithm. This is a trade-off for intelligent use of shoulder in cooperative algorithm which will be discussed in detail in the following.

Comparing the scenarios with cooperative and non-cooperative algorithms in Figure 34 (a), (b) and (c), the cooperative algorithm results in lower EV travel time in all lanes except lane 1. Non-cooperative algorithm has slightly lower EV travel time in lane 1 since this algorithm blindly uses shoulder when the EV is in lane 1 in all traffic densities. However, the cooperative algorithm uses shoulder only when required in congested traffic. Using shoulder enable CAVs to clear EV's lane as fast as possible. On the other hand, using shoulder reduces safety due to lower width, potential blockage by obstacles, and reentry to the travel lane being a challenge. Shoulder lanes are not designed to be used by a CAV

platoon and should be considered as a last resort when there is no other available solution. Hence, an intelligent algorithm like our developed cooperative algorithm should be implemented to identify the necessity of shoulder use.

The same trend observed for the difference between EV travel time of cooperative algorithm in different lanes in Figure 33 is also observed in Figure 34 (a), (b) and (c). Table 5.9 also verifies this trend as it shows, among all scenarios, mean EV travel time is not dependent on EV lane index in the cooperative scenarios with low and medium densities. Comparing scenarios CL1, CL2 and CL3 in Figure 34 (a), the EV lane index does not considerably impact EV travel time when the cooperative algorithm is used in low traffic densities. The results of scenarios CM1, CM2 and CM3 in Figure 34 (b) also illustrate the independence of EV travel time to EV lane index in medium density. However, the increasing trend of EV travel time from scenario CH1 to CH3 in Figure 34 (c) shows a direct relationship between EV travel time and lane index in high densities with the cooperative algorithm. According to Table 5.6, the cooperative algorithm uses the shoulder in more than 80 percent of EV travel time in high density. Therefore, as the EV's lane become farther from the shoulder's lane, CAVs need more time to clear the EV's lane.

Comparing the scenarios with the non-cooperative algorithm in Figure 34 (a), (b) and (c) shows that lowest EV travel times are observed in lane 1 (scenarios NL1, NM1 and NH1). This is due to the advantage of using the shoulder when the EV is in lane 1 for non-cooperative scenarios. When the EV is in lane 1, the CAVs in lane 1 are directed to move to the shoulder which has enough eligible gaps. In Figure 34 (a), no considerable difference is observed between scenarios NL2 and NL3. However, comparing scenarios NM2 and

NH2 with scenarios NM3 and NH3, respectively, in Figure 34 (b) and (c), it is observed that higher EV travel times are observed in lane 2 compared to lane 3. The reason for this is that when the EV is in lane 3, the CAVs in lane 2 can move to lane 1 and help the lane-changing of the CAVs in lane 3. Hence, the eligible gaps in both lanes 1 and 2 can be used to clear lane 3 for the EV. Figure 34 (a), (b) and (c) also shows increasing density leads in an increase in EV travel time as it was expected for lanes 2 and 3 with the non-cooperative algorithm.

According to Figure 34 (a), (b) and (c), the same travel time is observed in the base algorithm in all scenarios and all simulation runs with similar 95^{th} and 5^{th} percentiles (scenarios BL0, BM0 and BH0). This is to be expected as the EV moves on the shoulder, observing the shoulder speed limit and has no conflict with CAV traffic in the base algorithm. Figure 34 (a), (b) and (c) illustrates that EV travel times in all scenarios with cooperative algorithm are lower than the travel time in the scenarios with the base algorithm. Only the 95^{th} percentile travel time of scenario CH3 is higher than EV travel time of scenario BH0 in Figure 34 (c). However, even in scenario CH3, the box plot's upper quartile, is lower than the base algorithm travel time.

According to Figure 34 (d), CAV delay is lower for scenario CL2 compared to scenarios CL1 and CL3. Based on Figure 31, in the cooperative algorithm, when the EV is in lane 2, the CAVs in this lane have access to all eligible gaps in lanes 1 and 3. However, when the EV is in lane 1, CAVs in lane 1 only have access to the eligible gaps in lane 2, and the cooperative algorithm can order the CAVs in lane 2 to move to lane 3 to aid the lane-changing of the CAVs in lane 1. The same situation happens when the EV is in lane 3.

Therefore, when the EV is in lane 2, less CAVs are engaged in the lane-changing process. This results in reducing the lane-changing cost and as the CAVs in lane 2 have access to all eligible gaps, they can clear EV's lane sooner with lower average delay. The same trend is observed for lanes 2 and 3 in Figure 34 € and (f), and CAV delays in scenarios CM2, CH2 are lower compared to scenarios CM3 and CH3, respectively. It is shown as density increases, from Figure 34 (d) to (f), the difference between the CAV delays of lanes 1 and 2 becomes smaller for the cooperative algorithm. In Figure 34 (f), there is no considerable difference between the CAV delays of scenarios CH1 and CH2. This is the result of shoulder use percentage rise as traffic density increases according to Table 5.6. When the cooperative algorithm uses shoulder to clear lane 1 for EV, the CAVs in lane 1 have access to the eligible gaps in shoulder and have less conflict with the CAVs in lanes 2 and 3. This reduces CAV average delay until CAV delays of scenarios CH1 and CH2 become similar.

According to Figure 34 (d), (e), and (f), lower CAV delays are observed in lane 1 compared to lanes 2 and 3 in the scenarios with the non-cooperative algorithm. This is because using the shoulder, which has enough eligible gaps for CAVs in lane 1, eliminates the conflict with CAVs in lanes 2 and 3. Comparing scenarios NL2 and NL3 in Figure 34 (d), the CAV delay in lane 2 is higher than the CAV delay in lane 3. Unlike the cooperative algorithm, the positions of eligible gaps are unknown in the non-cooperative algorithm. Hence, the lane-changing of a CAV in the EV's lane depends on the presence of an eligible gap in the vicinity of CAV or on the CAVs in other lanes to create a new gap when there is not an available gap. When the EV is in lane 2, the CAVs in lane 2 only have access to the gaps in lane 1. However, when the EV is in lane 3, the CAVs in lane 3 have access to the gaps

in lane 2, and the potential lane changing of CAVs from lane 2 to lane 1 can help creating new gaps in lane 2. The faster lane changing of CAVs results in faster clearance of EV‘s lane and reducing the average delay of CAVs. Moving from Figure 34 (d) to (f), the difference between CAV delay of lanes 2 and 3 becomes smaller for the non-cooperative algorithm. In Figure 34 (f), similar CAV delay is observed for scenarios NH2 and NH3. The reason is that as density increases, the number of eligible gaps reduces. Hence, in high traffic density of Figure 34 (f), when EV is in lane 3, higher number of CAVs in lanes 2 and 1 should engage in speed adjustment to make new gaps for CAVs in lane 3. As a result, higher CAV average delay is observed in scenario NH3.

Delays of scenarios BL0, BM0 and BH0 shows a baseline for the delay of CAVs which are not disturbed by EV. As observed in Figure 34 (d), (e) and (f), the base algorithm has lowest CAV delay compared to the non-cooperative and cooperative algorithms. Comparing scenarios NL1 and CL1 in Figure 34 (d), it is illustrated that, when EV is on lane 1 with low traffic density, the non-cooperative algorithm reached a lower CAV delay compared to the cooperative algorithm. The reason is that the non-cooperative algorithm always uses shoulder in lane 1. However, the cooperative algorithm only results in shoulder use when it is required. According to Table 5.6, the cooperative algorithm does not use shoulder in low density as there are enough eligible gaps in lanes 2 and 3 in scenario CL1. In this situation, the CAVs in lanes 2 and 3 are also integrated in the lane changing process which increases average CAV delay. Based on Figure 34 (a) and (d), while there is a small difference in CAV delay, there is not a considerable difference in EV travel time of scenario CL1 compared to scenario NL1. It is worth mentioning that scenario CL1 reached the same

EV travel time without using shoulder. As density increases, from Figure 34 (d) to (f), CAV delay of cooperative algorithm decreases in lane 1. It can be observed in Figure 34 (f) that there is no considerable difference between the CAV delays of scenarios NH1 and CH1. This is likely because of high shoulder use percentage in scenario CH1 based on Table 5.6. Hence, the cooperative and non-cooperative algorithms perform similarly regarding CAV delay in high densities when EV is on lane 1.

Comparing scenarios NL2, NM2, and NH2 with scenarios CL2, CM2 and CH2, respectively, in Figure 34 (d), (c), and (f), it is shown that the non-cooperative algorithm results in higher CAV delay compared to the cooperative algorithm when the EV is in lane 2. This is expected as the positions of eligible gaps are known and the CAVs in lane 2 have access to the eligible gaps in both lanes 1 and 3 in the cooperative algorithm compared to the non-cooperative algorithm in which gaps are unknown and the CAVs in lane 2 only have access to the gaps in lane 1. As density increases, from Figure 34 (d) to (f), it is observed that CAV delay of the non-cooperative algorithm in lane 3 increases until, in scenario NH3, it becomes higher than the CAV delay of the cooperative algorithm, scenario CH3. This is likely because of the increasing percentage of shoulder use in the cooperative algorithm in higher densities based on Table 5.6. Based on Figure 34 (b), (c), (e) and (f), the cooperative algorithm reached in lower EV travel time and CAV delay in all scenarios with EV on lanes 2 or 3, except scenario CL3, compared to the non-cooperative algorithm.

5.4 Conclusions

The goal of this research was to create a cooperative framework for CAVs to minimize the lane-changing disruption while clearing EV's way on multi-lane freeways which was a gap

in the literature. Binary linear programming, an optimization approach was used to optimize the trajectory of CAVs in the buffer zone of EV. The objective function aims to minimize lane-changing conflict. To prevent creation of infeasible lane-changes, gap assignments were limited to requiring only one lane-change. Also, to prevent CAV maneuvers causing EV speed reduction, CAVs were only assigned to the gaps in front of them. A cooperative control algorithm was developed to control CAV gap assignments and lane-changing directives based on optimized trajectories to clear EV's lane. In the cooperative algorithm, the shoulder could be used by CAVs if optimization becomes infeasible using freeway road lanes. A non-cooperative algorithm in which CAVs act independently, and a base algorithm in which the EV moved on the shoulder were both defined to evaluate the performance of the cooperative algorithm. The developed algorithms were implemented in traffic simulation on a three-lane freeway with a right shoulder.

The results showed using the cooperative algorithm reduced EV travel time and improved travel time reliability compared to other tested algorithms in the scenarios in which EV was on the lanes not adjacent to shoulder. The cooperative algorithm was successful in reducing CAV delay compared to the non-cooperative algorithm in most of scenarios with EV on the lane not adjacent to shoulder. It was illustrated that the cooperative algorithm resulted in slightly higher EV travel time and CAV delay when EV moved on the lane adjacent to shoulder. Small increases in travel time and delay were a trade-off for the intelligent use of shoulder in the cooperative algorithm intending to minimize shoulder use. The average shoulder uses of cooperative algorithm were 0, 35 and 84 percent of EV travel

time in low, medium, and high densities, respectively, while this measure was 100 percent for the non-cooperative algorithm in all densities. Hence, with lower shoulder use percentage, the cooperative algorithm reached in approximately the same EV travel time compared to non-cooperative algorithm. The results indicate that if EVs move on the rightmost road lane, adjacent to shoulder, the cooperative algorithm can clear EV's lane and have minimal adverse impact on CAV delay as it can wisely open shoulder to CAVs when required which addresses the goal of this research. The developed cooperative framework is not limited to freeway segments with 3 road lanes and could be applied to freeways segments with different number of lanes.

The developed framework could be implemented to enhance EV movement in traffic networks and reduce the negative impact of EV prioritization on traffic. Intelligent use of shoulder enables the cooperative algorithm to avoid using shoulder when there are obstacles in shoulder which was not considered in the scenarios of this research. The developed cooperative framework could be adopted in future research to identify shoulder use feasibility through obstacle detection to improve the safety and performance. This study focused on prioritizing EV on freeway segments. Future studies could consider extending this framework to optimize the behavior of CAVs in emergencies in arterial road segments with various geometries. Our cooperative approach was developed and tested in fully connected and autonomous traffic. This approach could be adopted to consider human driving behavior in mixed traffic with different market penetration rates. Some of the implemented optimization constraints including "one lane-change limitation," "only forward movements" and "no relative forward movements in the same lane" were

limitations of this research. These constraints were used to prevent the generation of infeasible trajectories in optimization. Future studies can focus on improving infeasible trajectory identification methods to include a larger set of feasible trajectories to enhance the algorithm's performance. As EV was assumed moving on the same lane in our methodology, future research can adopt the cooperative framework considering EV lane-changing to increase degree of freedom in optimization and improve its performance.

CHAPTER 6

SUMMARY, CONTRIBUTIONS, AND FUTURE DIRECTION

In this thesis, EV prioritization was investigated in CAV traffic to develop frameworks able to reduce EV response time while minimizing negative influence on general traffic. To this end, three main research objectives were followed. Firstly, creation and dissipation of the disruption included by EV in a corridor was studied to recommend solutions to eliminate this disruption. Secondly, lane-changing and stopping behavior of CAVs were studied when clearing a lane for EV in a corridor to identify the best lane-changing behavior to minimize the delay of EV and traffic. Thirdly, a cooperative behavior framework was developed for CAVs to optimize their trajectories when preclearing EV's lane to minimize lane-changing disruption.

In chapter 1, the importance of EV response time was provided, and it was illustrated why it was important to reduce EV response time and the disruption created by EV on general traffic. In chapter 2, the related literature review was provided, and the research gaps were identified. In chapter 3, the disruption created by EVP in arterial cross streets at signalized intersections was investigated to facilitate discharging the disruption. A queue estimation model was developed based on shockwave theory and was validated though simulating EVP at an isolated signalized intersection in SUMO. Simulation results showed by increasing the traffic flow of cross street in uncongested traffic, maximum and minimum queue lengths of the preemption cycle increased with a constant slope. It was also observed that increasing preemption time reached in increased maximum and minimum queue lengths of preemption cycle. The results verified the model was able to quantify how the disruption created by EVP should be counteracted by adjusting signal timing in transition cycles. This research shows that shockwave theory can quantify the disruption created by

EVP and investigate solutions to counteract the disruption. The influence of different parameters including preemption, transition, signal timing, and traffic can be investigated on the disruption. Using the developed model, the strategies to prevent the disruption can be designed, and if the disruption is not preventable, the solutions to aid the approaches recover quickly after EVP can be investigated.

In chapter 4, the lane-changing and stopping behaviors of CAVs were explored on an arterial corridor to investigate how behavior of CAVs influenced the delays of EV and surrounding traffic. To this end, a driving behavior algorithm was developed to define desired behavior of CAVs when an EV approaches, and a preemption method was developed to prioritize the EV's approach at signalized intersections. Two parameters including stopping and lane-changing thresholds were introduced. It was concluded using both lane-changing and stopping behaviors was more favorable as it resulted in lower CAVs delay. An optimum lane-changing threshold was recognized which was accompanied by minimum EV delay. At the end, the proposed behavior algorithm was compared to an existing algorithm to evaluate its performance. The proposed algorithm proved its ability to induce more reduction in EV delay compared to the existing algorithm. The results of this research will serve as a benchmark for future research into more complex or cooperative behavior algorithms. One ability of CAVs is that their trajectories could be controlled by a processing center. Therefore, their trajectories could be optimized by a model to minimize the response time of EV.

In Chapter 5, a cooperative behavior framework was developed for CAVs to minimize the lane-changing disruption while clearing EV's way on multi-lane freeways. Binary linear

programming was used to optimize the trajectory of CAVs in the buffer zone of EV through minimizing lane-changing conflict. A cooperative control algorithm was developed to control CAV gap assignments and lane-changing directives based on optimized trajectories to clear EV's lane. The cooperative algorithm can direct CAVs to use shoulder when required. The cooperative algorithm was evaluated in comparison to a non-cooperative algorithm in which CAVs acted independently, and a base algorithm in which the EV moved on the shoulder in microsimulation. The results showed using the cooperative algorithm reduced EV travel time and improved EV travel time reliability compared to other tested algorithms in the scenarios in which EV was on the lanes not adjacent to shoulder. The cooperative algorithm was successful in reducing CAV delay compared to the non-cooperative algorithm in most of scenarios with EV on the lane not adjacent to shoulder. Small increases in EV travel time and CAV delay when EV moved on the lane adjacent to shoulder was a trade-off for the intelligent use of shoulder in the cooperative algorithm intending to minimize shoulder use. The results indicate that if EVs move on the rightmost road lane, adjacent to shoulder, the cooperative algorithm can clear EV's lane and have minimal adverse impact on CAV delay as it can wisely open shoulder to CAVs when required. The developed framework could be implemented to enhance EV movements in traffic networks and reduce the negative impact of EV prioritization on traffic. Intelligent use of shoulder enables the cooperative algorithm to avoid using shoulder when there are obstacles in shoulder which can be studied in future research. As very little is known about human behaviors during EV encounters, in future research, the human aspect of behaviors could be studied to enable the simulation of human drivers in emergencies so that the improvement of CAVs can be measured compared to human

drivers. Our cooperative approach was developed and tested in fully connected and autonomous traffic. This approach could be adopted to consider human driving behavior in mixed traffic with different market penetration rates.

In summary, using the cooperative framework developed in chapter 5, EVs can be prioritized on freeway segments by providing optimized trajectories for CAV traffic with the aim of minimizing lane-changing conflict to ensure non-stop movements for EV and CAVs. On the other hand, on urban arterials, vehicles may be required to stop along their way. Hence, stopping behavior should be considered in CAV control algorithm. The developed lane-changing and preemption algorithms, provided in chapter 4, can be used to prioritize EV movement on urban arterials. As a result of using EVP on signalized corridors, cross streets may face huge disruptions which require several cycles to be discharged. The queue estimation model developed in chapter 3 could be implemented to evaluate preemption and transition strategies in aiding cross streets recover sooner from EVP disruption. Hence, this dissertation provides a comprehensive framework able to prioritize EV in CAV traffic on different road types and reduce the disruption induced on traffic.

The developed framework could be implemented in transportation management systems to ensure transportation systems can provide prioritization for EVs while minimizing the created disruption. In future research, the developed EV prioritization framework could be extended to become adoptable for more complex scenarios including different road types and geometries along a corridor. The developed framework could be implemented in EV routing algorithms to evaluate different routing options and choose the best one which

ensure unimpeded EV movement, minimize the induced disruption on general traffic and eliminate the residual disruption as fast as possible. Future studies can extend the developed cooperative behavior framework to provide instructions for human driven vehicles with the aim of harmonizing autonomous and non-autonomous vehicles in clearing EV's way.

REFERENCES

Afdhal, A., & Elizar, E. (2015). Enhanced route guidance and navigation for emergency vehicle using V2I-based cooperative communication. (Ed.),^(Eds.). 2015 International Electronics Symposium (IES), Surabaya, Indonesia.

Akdoğan, M. A., Bayındır, Z. P., & Iyigun, C. (2018). Locating emergency vehicles with an approximate queuing model and a meta-heuristic solution approach. *Transportation Research Part C: Emerging Technologies*, *90*, 134-155.

An, C., Wu, Y.-J., Xia, J., & Huang, W. (2018). Real-time queue length estimation using event-based advance detector data. *Journal of Intelligent Transportation Systems*, *22*(4), 277-290.

Atkins, W. (2016). Research on the Impacts of Connected and Autonomous Vehicles (CAVs) on Traffic Flow. Department for Transport London, UK.

Bai, Y., Zhang, Y., Li, X., & Hu, J. (2022). Cooperative weaving for connected and automated vehicles to reduce traffic oscillation. *Transportmetrica A: transport science*, *18*(1), 125-143.

Ban, X. J., Hao, P., & Sun, Z. (2011). Real time queue length estimation for signalized intersections using travel times from mobile sensors. *Transportation Research Part C: Emerging Technologies*, *19*(6), 1133-1156.

Bieker-Walz, L., Behrisch, M., & Junghans, M. (2018). Analysis of the traffic behavior of emergency vehicles in a microscopic traffic simulation. *EPiC Series in Engineering*, *2*, 1-13.

Blackwell, T. H., & Kaufman, J. S. (2002). Response time effectiveness: comparison of response time and survival in an urban emergency medical services system. *Academic Emergency Medicine*, *9*(4), 288-295.

Blanchard, I. E., Doig, C. J., Hagel, B. E., Anton, A. R., Zygun, D. A., Kortbeek, J. B., Powell, D. G., Williamson, T. S., Fick, G. H., & Innes, G. D. (2012). Emergency medical services response time and mortality in an urban setting. *Prehospital Emergency Care*, *16*(1), 142-151.

Buckman, N., Schwarting, W., Karaman, S., & Rus, D. (2021). Semi-Cooperative Control for Autonomous Emergency Vehicles. (Ed.),^(Eds.). 2021 IEEE/RSJ International Conference on Intelligent Robots and Systems (IROS).

Cetin, M. (2012). Estimating queue dynamics at signalized intersections from probe vehicle data: Methodology based on kinematic wave model. *Transportation research record*, *2315*(1), 164-172.

Chang, J., Talas, M., & Muthuswamy, S. (2013). Simple methodology for estimating queue lengths at signalized intersections using detector data. *Transportation research record*, *2355*(1), 31-38.

Chang, Y., & Edara, P. (2017). AReBIC: Autonomous reservation-based intersection control for emergency evacuation. (Ed.),^(Eds.). 2017 IEEE Intelligent Vehicles Symposium (IV).

Chang, Y., & Edara, P. (2018). Evaluation of a reservation-based intersection control algorithm for hurricane evacuation with autonomous vehicles. *International journal of disaster risk reduction*, *31*, 1152-1158.

Cheng, C., Du, Y., Sun, L., & Ji, Y. (2016). Review on theoretical delay estimation model for signalized intersections. *Transport Reviews*, *36*(4), 479-499.

Cheng, Y., Qin, X., Jin, J., Ran, B., & Anderson, J. (2011). Cycle-by-cycle queue length estimation for signalized intersections using sampled trajectory data. *Transportation research record*, *2257*(1), 87-94.

Chowdhury, A. (2016). Priority based and secured traffic management system for emergency vehicle using IoT. (Ed.),^(Eds.). 2016 International Conference on Engineering & MIS (ICEMIS), Agadir, Morocco.

Cleal, P. (1982). Priority for Emergency Vehicles at Traffic Signals (No. 1445-4467

Ekram, A.-A., & Rahman, M. S. (2018). Effects of connected and autonomous vehicles on contraflow operations for emergency evacuation: a microsimulation study. (Ed.),^(Eds.). Transportation Research Board 97th Annual Meeting.

Erdmann, J. (2015). SUMO's lane-changing model (*Modeling Mobility with Open Data* (pp. 105-123). Springer.

Fujii, H., Yoshimura, S., & Seki, K. (2010). Multi-agent based traffic simulation at merging section using coordinative behavior model. *Computer Modeling in Engineering & Sciences(CMES)*, *63*(3), 265-282.

Gomes, G. (2022). A framework for hybrid simulation of transportation networks. *Journal of Simulation*, *16*(2), 166-181.

Gurobi Optimization, L. (2021). Gurobi optimizer reference manual.

Haghani, M., Hosseinzadeh, A., & Kluger, R. (2023). A lane-changing behaviour algorithm for connected and autonomous vehicles to facilitate emergency vehicle movements on urban arterials in microsimulation. *Journal of Simulation*, 1-15.

Hannoun, G. J., & Menendez, M. (2022). Modular vehicle technology for emergency medical services. *Transportation Research Part C: Emerging Technologies*, *140*, 103694.

Hannoun, G. J., Murray-Tuite, P., Heaslip, K., & Chantem, T. (2018). Facilitating emergency response vehicles' movement through a road segment in a connected vehicle environment. *IEEE Transactions on Intelligent Transportation Systems*, *20*(9), 3546-3557.

Hassannayebi, E., Memarpour, M., Mardani, S., Shakibayifar, M., Bakhshayeshi, I., & Espahbod, S. (2020). A hybrid simulation model of passenger emergency evacuation under disruption scenarios: A case study of a large transfer railway station. *Journal of Simulation*, *14*(3), 204-228.

Henchey, M. J., Batta, R., Blatt, A., Flanigan, M., & Majka, K. (2014). A simulation approach to study emergency response. *Journal of Simulation*, *8*(2), 115-128.

Humayun, M., Almufareh, M. F., & Jhanjhi, N. Z. (2022). Autonomous Traffic System for Emergency Vehicles. *Electronics*, *11*(4), 510. https://www.mdpi.com/2079-9292/11/4/510

Kang, W., Xiong, G., Lv, Y., Dong, X., Zhu, F., & Kong, Q. (2014). Traffic signal coordination for emergency vehicles. (Ed.),^(Eds.). 17th International IEEE Conference on Intelligent Transportation Systems (ITSC), Qingdao, China.

Karmakar, G., Chowdhury, A., Kamruzzaman, J., & Gondal, I. (2020). A smart priority-based traffic control system for emergency vehicles. *IEEE Sensors Journal*, *21*(14), 15849-15858.

Khayatian, M., Mehrabian, M., Andert, E., Dedinsky, R., Choudhary, S., Lou, Y., & Shirvastava, A. (2020). A survey on intersection management of connected autonomous vehicles. *ACM Transactions on Cyber-Physical Systems*, *4*(4), 1-27.

Khayatian, M., Mehrabian, M., & Shrivastava, A. (2018). RIM: Robust intersection management for connected autonomous vehicles. (Ed.),^(Eds.). 2018 IEEE Real-Time Systems Symposium (RTSS).

Krauß, S. (1998). Microscopic modeling of traffic flow: Investigation of collision free vehicle dynamics.

Lenné, M. G., Triggs, T. J., Mulvihill, C. M., Regan, M. A., & Corben, B. F. (2008). Detection of emergency vehicles: Driver responses to advance warning in a driving simulator. *Human Factors*, *50*(1), 135-144.

Lighthill, M. J., & Whitham, G. B. (1955). On kinematic waves II. A theory of traffic flow on long crowded roads. *Proceedings of the Royal Society of London. Series A. Mathematical and Physical Sciences*, *229*(1178), 317-345.

Liu, H. X., Wu, X., Ma, W., & Hu, H. (2009). Real-time queue length estimation for congested signalized intersections. *Transportation Research Part C: Emerging Technologies*, *17*(4), 412-427.

Liu, Y., Li, Z., Liu, J., & Patel, H. (2016). A double standard model for allocating limited emergency medical service vehicle resources ensuring service reliability. *Transportation Research Part C: Emerging Technologies*, *69*, 120-133.

Lopez, P. A., Behrisch, M., Bieker-Walz, L., Erdmann, J., Flötteröd, Y.-P., Hilbrich, R., Lücken, L., Rummel, J., Wagner, P., & Wießner, E. (2018). Microscopic traffic simulation using sumo. (Ed.),^(Eds.). 2018 21st International Conference on Intelligent Transportation Systems (ITSC), Maui, HI, USA.

Lu, Q., & Kim, K.-D. (2017). A genetic algorithm approach for expedited crossing of emergency vehicles in connected and autonomous intersection traffic. *Journal of Advanced Transportation*, *2017*.

Lu, Q., & Kim, K.-D. (2019). Autonomous and connected intersection crossing traffic management using discrete-time occupancies trajectory. *Applied Intelligence*, *49*, 1621-1635.

Lu, Q., Tettamanti, T., & Varga, I. (2018). Impacts of autonomous vehicles on the urban fundamental diagram.

Mell, H. K., Mumma, S. N., Hiestand, B., Carr, B. G., Holland, T., & Stopyra, J. (2017). Emergency medical services response times in rural, suburban, and urban areas. *JAMA surgery*, *152*(10), 983-984.

Michalopoulos, P. G., Stephanopoulos, G., & Stephanopoulos, G. (1981). An application of shock wave theory to traffic signal control. *Transportation research part B: methodological*, *15*(1), 35-51.

Miculescu, D., & Karaman, S. (2019). Polling-systems-based autonomous vehicle coordination in traffic intersections with no traffic signals. *IEEE Transactions on Automatic Control*, *65*(2), 680-694.

Mirjalili, R., Barati, H., & Yazici, A. (2023). Resilience Analysis of New York City Transportation Network After Snow Storms. *Transportation research record*, *2677*(1), 694-707.

Moussa, N. (2009). Evacuation Model for Emergency Vehicles in Highways. *International Journal of Modern Physics C*, *20*(01), 59-69.

Mu, H., Liu, L., & Li, X. (2018). Signal preemption control of emergency vehicles based on timed colored petri nets. *Discrete Dynamics in Nature and Society*, *2018*.

Nageshrao, S., Tseng, H. E., & Filev, D. (2019). Autonomous highway driving using deep reinforcement learning. (Ed.),^(Eds.). 2019 IEEE International Conference on Systems, Man and Cybernetics (SMC).

Nellore, K., & Hancke, G. P. (2016). Traffic management for emergency vehicle priority based on visual sensing. *Sensors*, *16*(11), 1892.

Nelson, E. J., & Bullock, D. (2000). Impact of emergency vehicle preemption on signalized corridor operation: An evaluation. *Transportation research record*, *1727*(1), 1-11.

Noori, H. (2013). Modeling the impact of vanet-enabled traffic lights control on the response time of emergency vehicles in realistic large-scale urban area. (Ed.),^(Eds.). 2013 IEEE International Conference on Communications Workshops (ICC), Budapest, Hungary.

Noori, H., Fu, L., & Shiravi, S. (2016). A connected vehicle based traffic signal control strategy for emergency vehicle preemption. (Ed.),^(Eds.). Transportation Research Board 95th Annual Meeting, Washington, DC, USA.

O'Keeffe, C., Nicholl, J., Turner, J., & Goodacre, S. (2011). Role of ambulance response times in the survival of patients with out-of-hospital cardiac arrest. *Emergency medicine journal*, *28*(8), 703-706.

Obenauf, A. W., Souleyrette, R. R., Kluger, R. M., & Pratelli, A. (2019). Impact of self-driving and connected vehicles on emergency response: the case of the USA and implications for ITALY. *WIT Transactions on The Built Environment*, *189*, 101-112.

Olaverri-Monreal, C., Errea-Moreno, J., & Díaz-Álvarez, A. (2018). Implementation and evaluation of a traffic light assistance system based on V2I communication in a simulation framework. *Journal of Advanced Transportation*, *2018*.

Papadoulis, A., Quddus, M., & Imprialou, M. (2019). Evaluating the safety impact of connected and autonomous vehicles on motorways. *Accident Analysis & Prevention*, *124*, 12-22.

Parada, L., Candela, E., Marques, L., & Angeloudis, P. (2023). Safe and efficient manoeuvring for emergency vehicles in autonomous traffic using multi-agent proximal policy optimisation. *Transportmetrica A: transport science*, 1-29.

Park, H., Waddell, D., & Haghani, A. (2019). Online optimization with look-ahead for freeway emergency vehicle dispatching considering availability. *Transportation Research Part C: Emerging Technologies*, *109*, 95-116.

Qin, X., & Khan, A. M. (2012). Control strategies of traffic signal timing transition for emergency vehicle preemption. *Transportation Research Part C: Emerging Technologies*, *25*, 1-17.

R Core Team. (2019). R: A language and environment for statistical computing. R Foundation for Statistical Computing, Vienna, Austria, 2019.

Richards, P. I. (1956). Shock waves on the highway. *Operations research*, *4*(1), 42-51.

Robertson, W., & Glassbrook, G. (1979). The centrally integrated traffic control system (CITRAC)(A) studies and objectives (B) control principles. *Public Lighting*, *44*(HS-030 127).

Sahebi, S., Heshami, S., Khojastehpour, M., Rahimi, A., & Mollajani, M. (2024). Assessing Public Perception of Car Automation in Iran: Acceptance and Willingness to Pay for Adaptive Cruise Control. *arXiv preprint arXiv:2401.17329*.

Sanderson, L. B., & Lord, J. (1978). Computers: Microcomputers promise less stop, more go: Designers off urban traffic-control systems propose hierarchical schemes to enhance local control, reliability, and maintainability. *IEEE spectrum*, *15*(11), 30-32.

Sharma, A., Bullock, D. M., & Bonneson, J. A. (2007). Input–output and hybrid techniques for real-time prediction of delay and maximum queue length at signalized intersections. *Transportation research record*, *2035*(1), 69-80.

Shelby, S. G., Bullock, D. M., & Gettman, D. (2006). Transition methods in traffic signal control. *Transportation research record*, *1978*(1), 130-140.

Shelke, M., Malhotra, A., & Mahalle, P. N. (2019). Fuzzy priority based intelligent traffic congestion control and emergency vehicle management using congestion-aware routing algorithm. *Journal of Ambient Intelligence and Humanized Computing*, 1-18.

Shen, L., Liu, J., Yao, Z., Wu, W., & Yang, H. (2022). A new queue shock wave theory based on platoon dispersion modeling. *Physica A: Statistical Mechanics and its Applications*, *603*, 127725.

So, J., Kang, J., Park, S., Park, I., & Lee, J. (2020). Automated emergency vehicle control strategy based on automated driving controls. *Journal of Advanced Transportation*, *2020*, 1-11.

Soudi, F., & Tomsovic, K. (1998). Optimized distribution protection using binary programming. *IEEE transactions on power delivery*, *13*(1), 218-224.

Standard, S. (2018). J3016-Taxonomy and Definitions for Terms Related to Driving Automation Systems for on-Road Motor Vehicles. June.

Stephanopoulos, G., Michalopoulos, P. G., & Stephanopoulos, G. (1979). Modelling and analysis of traffic queue dynamics at signalized intersections. *Transportation Research Part A: General*, *13*(5), 295-307.

Strong, D. W., Nagui, M., & Courage, K. (2006). New calculation method for existing and extended HCM delay estimation procedure. (Ed.),^(Eds.). Proceedings of the 87th Annual Meeting Transportation Research Board.

Su, H., Zhong, Y. D., Chow, J. Y., Dey, B., & Jin, L. (2023). EMVLight: A multi-agent reinforcement learning framework for an emergency vehicle decentralized routing and traffic signal control system. *Transportation Research Part C: Emerging Technologies*, *146*, 103955.

Su, H., Zhong, Y. D., Dey, B., & Chakraborty, A. (2022). Emvlight: A decentralized reinforcement learning framework for efficient passage of emergency vehicles. (Ed.),^(Eds.). Proceedings of the AAAI Conference on Artificial Intelligence.

Sun, D., & Elefteriadou, L. (2014). A driver behavior-based lane-changing model for urban arterial streets. *Transportation science*, *48*(2), 184-205.

Van Rossum, G., & Drake, F. (2009). Python 3 Reference Manual CreateSpace. *Scotts Valley, CA*.

Van Rossum, G., & Drake Jr, F. L. (2009). *Python 3 Reference Manual, Scotts Valley, CA: CreateSpace.* (Vol. 620). Centrum voor Wiskunde en Informatica Amsterdam.

Vigos, G., Papageorgiou, M., & Wang, Y. (2008). Real-time estimation of vehicle-count within signalized links. *Transportation Research Part C: Emerging Technologies*, *16*(1), 18-35.

Virdi, N., Grzybowska, H., Waller, S. T., & Dixit, V. (2019). A safety assessment of mixed fleets with connected and autonomous vehicles using the surrogate safety assessment module. *Accident Analysis & Prevention*, *131*, 95-111.

Viriyasitavat, W., & Tonguz, O. K. (2012). Priority management of emergency vehicles at intersections using self-organized traffic control. (Ed.),^(Eds.). 2012 ieee vehicular technology conference (vtc fall).

Wang, J., Yun, M., Ma, W., & Yang, X. (2013). Travel time estimation model for emergency vehicles under preemption control. *Procedia-social and behavioral sciences*, *96*, 2147-2158.

Wang, R., Xu, Z., Zhao, X., & Hu, J. (2019). V2V-based method for the detection of road traffic congestion. *IET Intelligent Transport Systems*, *13*(5), 880-885.

Wang, Z., Cai, Q., Wu, B., Zheng, L., & Wang, Y. (2017). Shockwave-based queue estimation approach for undersaturated and oversaturated signalized intersections using multi-source detection data. *Journal of Intelligent Transportation Systems*, *21*(3), 167-178.

Webster, F. V. (1958). *Traffic signal settings* (

Weinert, F., & Düring, M. (2015). Development and assessment of cooperative v2x applications for emergency vehicles in an urban environment enabled by behavioral models (*Modeling Mobility with Open Data* (pp. 125-153). Springer.

Wu, J., Kulcsár, B., Ahn, S., & Qu, X. (2020). Emergency vehicle lane pre-clearing: From microscopic cooperation to routing decision making. *Transportation research part B: methodological*, *141*, 223-239.

Wu, X., & Liu, H. X. (2011). A shockwave profile model for traffic flow on congested urban arterials. *Transportation research part B: methodological*, *45*(10), 1768-1786.

Xu, X., Yang, L., Gao, Z., & Long, J. (2017). Simulations for train traffic flow on single-track railways with speed limits and slopes. *Journal of Simulation*, *11*(4), 346-356.

Ye, L., & Yamamoto, T. (2019). Evaluating the impact of connected and autonomous vehicles on traffic safety. *Physica A: Statistical Mechanics and its Applications*, *526*, 121009.

Yu, C., Sun, W., Liu, H. X., & Yang, X. (2019). Managing connected and automated vehicles at isolated intersections: From reservation-to optimization-based methods. *Transportation research part B: methodological*, *122*, 416-435.

Yun, I., Lee, C. K., & Oh, Y. T. (2011). Investigation on the exit phase controls for emergency vehicle preemption. *KSCE Journal of Civil Engineering*, *15*(8), 1419-1426.

Yun, I., Park, B. B., Lee, C. K., & Oh, Y. T. (2012). Comparison of emergency vehicle preemption methods using a hardware-in-the-loop simulation. *KSCE Journal of Civil Engineering*, *16*(6), 1057-1063.

Zhang, H., Liu, H. X., Chen, P., Yu, G., & Wang, Y. (2019). Cycle-based end of queue estimation at signalized intersections using low-penetration-rate vehicle trajectories. *IEEE Transactions on Intelligent Transportation Systems*, *21*(8), 3257-3272.

Zhang, Z., He, Q., Gou, J., & Li, X. (2016). Performance measure for reliable travel time of emergency vehicles. *Transportation Research Part C: Emerging Technologies*, *65*, 97-110.

Zheng, L., Zhu, C., He, Z., & He, T. (2021). Safety rule-based cellular automaton modeling and simulation under V2V environment. *Transportmetrica A: transport science*, *17*(1), 81-106.

Zhou, W., Chen, D., Yan, J., Li, Z., Yin, H., & Ge, W. (2022). Multi-agent reinforcement learning for cooperative lane changing of connected and autonomous vehicles in mixed traffic. *Autonomous Intelligent Systems*, *2*(1), 5.

APPENDIX A

The process of driving Equations 3.5, 3.6, 3.7 and 3.8 to calculate Q^n_{max}, T^n_{max}, Q^n_{min} and T^n_{min} are provided in details in this appendix. Based on the right triangles created by v_1 and v_2, the vertical line at T^n_{max} and the horizontal axis in Figure 1 (b), the following equation can be derived.

$$T^n_{max} = \frac{Q^n_{max}}{v_1} + T^n_a = \frac{Q^n_{max}}{v_2} + T^n_g \qquad \text{A.1}$$

Then, Q^n_{max} can be written in the following form.

$$Q^n_{max} = \frac{T^n_g - T^n_a}{(\frac{1}{v_1} - \frac{1}{v_2})} \qquad \text{A.2}$$

Based on the right triangles created by v_1 and v_4, the vertical line at T^{n-1}_{min} and the horizontal axis in Figure 1 (b), the following equation is derived.

$$T^{n-1}_{min} = \frac{Q^{n-1}_{min\_obs}}{v_1} + T^n_a = \frac{Q^{n-1}_{min\_obs}}{v_4} + T^n_r \qquad \text{A.3}$$

The following equation is derived from Equation A.3 by substituting v_4 with v_2 since they have the same magnitude.

$$T^n_r - T^n_a = Q^{n-1}_{min\_obs}(\frac{1}{v_1} - \frac{1}{v_2}) \qquad \text{A.4}$$

Using the term obtained in Equation A.4, Equation A.2 can be rewritten in the following form.

$$Q^n_{max} = \frac{(T^n_g - T^n_r) + (T^n_r - T^n_a)}{(\frac{1}{v_1} - \frac{1}{v_2})} = \frac{(T^n_g - T^n_r) + Q^{n-1}_{min\_obs}(\frac{1}{v_1} - \frac{1}{v_2})}{(\frac{1}{v_1} - \frac{1}{v_2})} \qquad \text{A.5}$$

By substituting the term $(T_g^n - T_r^n)$ with the red time, R, in Equation A.5, Q_{max}^n can be calculated with the following equation.

$$Q_{max}^n \quad \frac{R+Q_{min\_obs}^{n-1}\left(\frac{1}{v_1}-\frac{1}{v_2}\right)}{\left(\frac{1}{v_1}-\frac{1}{v_2}\right)} \qquad \text{A.6}$$

Based on the right triangle created by v_1, the vertical line at T_{max}^n and the horizontal line at $Q_{min\_obs}^{n-1}$ in Figure 1 (b), the following equation can be derived to calculate T_{max}^n.

$$T_{max}^n = T_{min}^{n-1} + \frac{\left(Q_{max}^n - Q_{min\ obs}^{n-1}\right)}{v_1} \qquad \text{A.7}$$

With substituting T_{min}^{n-1} with its equivalent from Equation A.3 and substituting v_4 with v_2, T_{max}^n can be written based on the cycle start time, T_r^n.

$$T_{max}^n = T_r^n + \frac{Q_{min\ obs}^{n-1}}{v_2} + \frac{\left(Q_{max}^n - Q_{min\ obs}^{n-1}\right)}{v_1} \qquad \text{A.8}$$

Based on the right triangles created by v_3 and v_4, the vertical line at T_{min}^n and the horizontal axis in Figure 1 (b), the following equation can be derived.

$$T_{min}^n = T_b^n - \frac{Q_{min}^n}{v_3} = T_r^{n+1} + \frac{Q_{min}^n}{v_4} \qquad \text{A.9}$$

Then, Q_{min}^n can be written in the following form.

$$Q_{min}^n = \frac{T_b^n - T_r^{n+1}}{\left(\frac{1}{v_3}+\frac{1}{v_4}\right)} \qquad \text{A.10}$$

Based on the right triangle created by v_3, the vertical line at T_{max}^n and the horizontal axis in Figure 1 (b), T_b^n can be derived in the following equation.

$$T_b^n = T_{max}^n + \frac{Q_{max}^n}{v_3} \qquad \text{A.11}$$

By substituting T^n_{max} with its equivalent from Equation A.8, Equation A.11 can be rewritten in the following form.

$$T^n_b = T^n_r + Q^n_{max}\left(\frac{1}{v_1} + \frac{1}{v_3}\right) - Q^{n-1}_{min\_obs}\left(\frac{1}{v_1} - \frac{1}{v_2}\right) \qquad \text{A.12}$$

By substituting T^n_b from Equation A.12 in Equation A.10 and substituting v_4 with v_2, Q^n_{min} can be rewritten as.

$$Q^n_{min} \quad \frac{Q_{max}\left(\frac{1}{v_1}+\frac{1}{v_3}\right) - Q_{min\_obs}\left(\frac{1}{v_1}-\frac{1}{v_2}\right) - (T_{r}^{n+1} - T_{r}^{n})}{\left(\frac{1}{v_2}+\frac{1}{v_3}\right)} \qquad \text{A.13}$$

By substituting the term $(T^{n+1}_r - T^n_r)$ with the cycle length, $(R + G)$, in Equation A.13, the following equation is resulted to calculate Q^n_{min}.

$$Q^n_{min} \quad \frac{Q^n_{max}\left(\frac{1}{v_1}+\frac{1}{v_3}\right) - Q^{n-1}_{min\_obs}\left(\frac{1}{v_1}-\frac{1}{v_2}\right) - (\quad)}{\left(\frac{1}{v_2}+\frac{1}{v_3}\right)} \qquad \text{A.14}$$

Based on the right triangle created by v_3, the vertical line at T^n_{max} and the horizontal line at Q^n_{min} in Figure 1 (b), the following equation can be derived to calculate T^n_{min}.

$$T^n_{min} = T^n_{max} + \frac{(Q^n_{max} - Q^n_{min})}{v_3} \qquad \text{A.15}$$

APPENDIX B

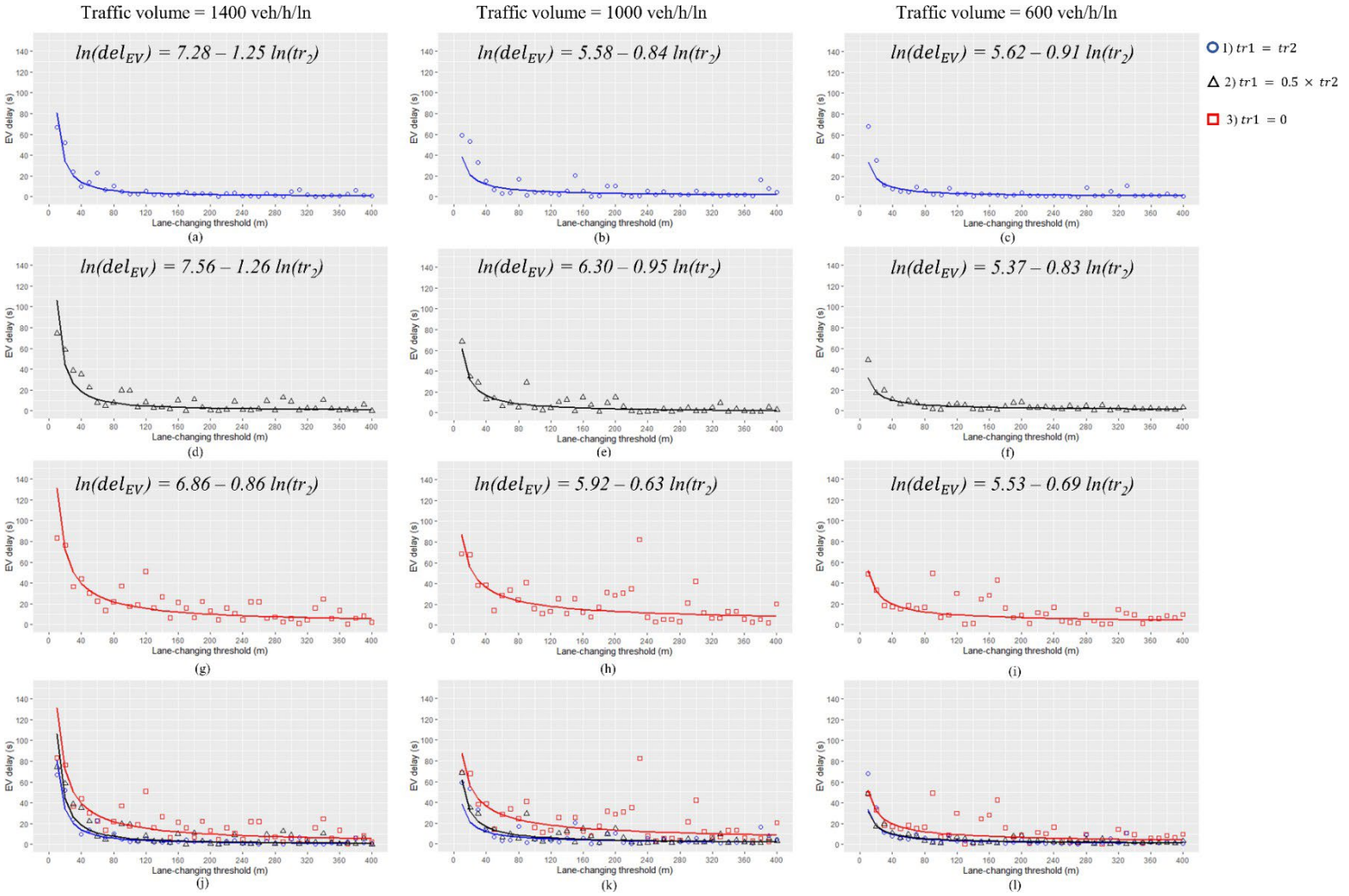

Figure B.1. The delay of EV versus lane-changing threshold in simulation scenarios with preemption

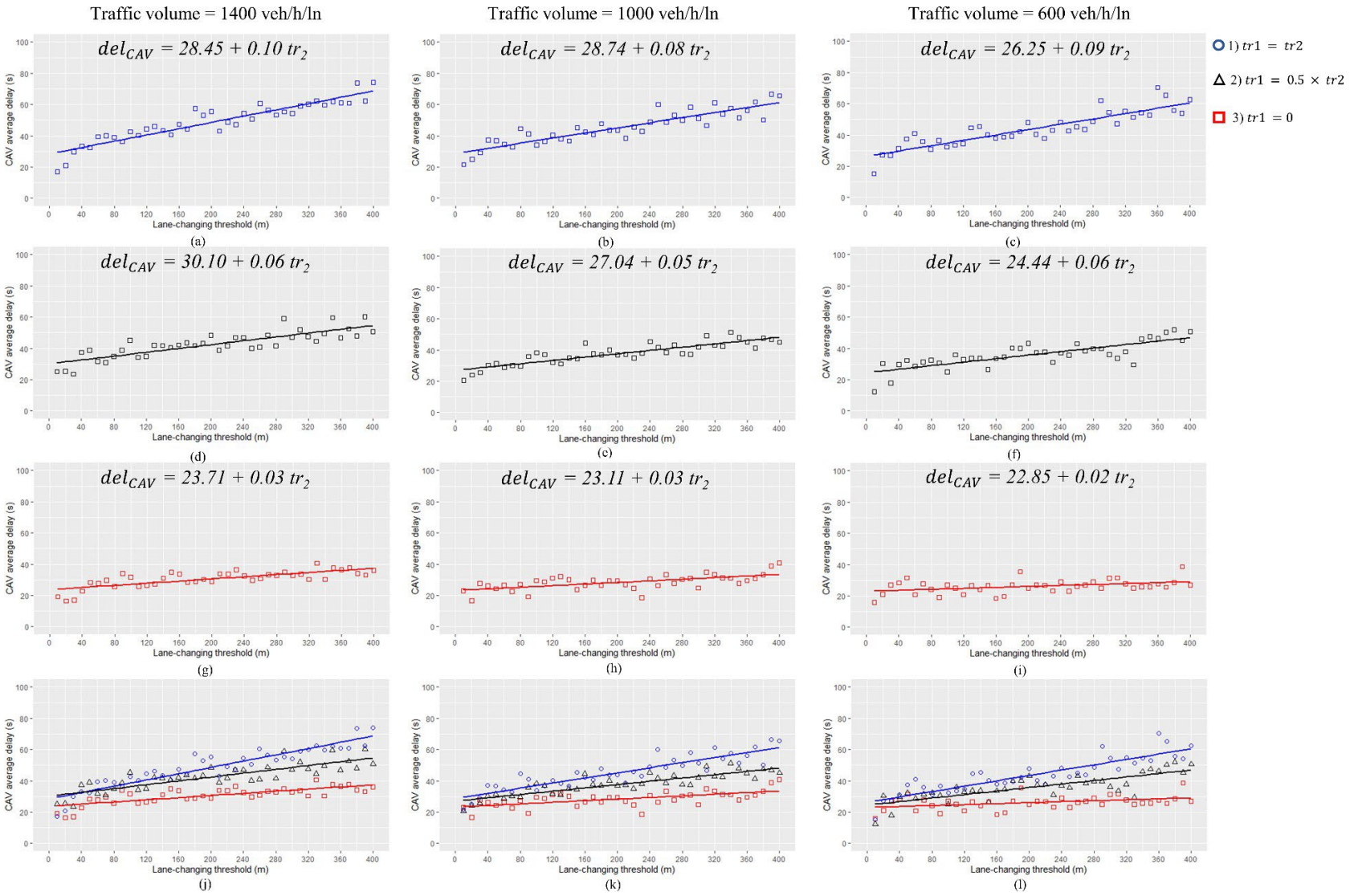

Figure B.2. The average delay of influenced CAVs versus lane-changing threshold in simulation scenarios with preemption

APPENDIX C

Table C.1. Summary statistics for CAV delay for proposed and Weinert and Düring's algorithms in different traffic volumes

		Traffic volume (veh/h)		
		600	1000	1400
Algorithm	Proposed	Mean: 29.97 SD: 5.22	Mean: 37.64 SD: 5.88	Mean: 46.75 SD: 9.01
	Weinert and Düring's	Mean: 20.42 SD: 3.76	Mean: 27.65 SD: 4.02	Mean: 30.77 SD: 4.11

Table C.2. Summary statistics for EV delay for proposed and Weinert and Düring's algorithms in different traffic volumes

		Traffic volume (veh/h)		
		600	1000	1400
Algorithm	Proposed	Mean: 2.14 SD: 2.38	Mean: 2.43 SD: 2.78	Mean: 3.14 SD: 3.84
	Weinert and Düring's	Mean: 6.77 SD: 7.12	Mean: 8.30 SD: 6.49	Mean: 9.87 SD: 6.9

CURRICULUM VITAE

NAME: Mohamadreza Haghani

ADDRESS: Department of Civil and Environmental Engineering, University of Louisville, W.S. Speed, Louisville, KY, 40292, USA

EDUCATION:

Ph.D., Civil and Environmental Engineering
University of Louisville, Louisville, KY, 2024
M.S., Civil and Environmental Engineering
Iran University of Science and Technology, Tehran, Iran, 2016
B.S., Civil and Environmental Engineering
Shahid Bahonar University of Kerman, Kerman, Iran, 2013

JOURNAL PUBLICATIONS:

M Haghani, A Hosseinzadeh, and R Kluger. "A Lane-changing Behaviour Algorithm for Connected and Autonomous Vehicles to Facilitate Emergency Vehicle Movements on Urban Arterials in Microsimulation." Journal of Simulation (2023): 1-15.

N Navid, R Camporeale, M Khaleghi, **M Haghani**, A Sheykhfard, and K Shaaban. "A Method to Determine an Equity Score for Transportation Systems in the Cities." Sustainability 15, no. 7 (2023): 5818.

M Haghani, R Jalalkamali, and H Haghani "Calibration of Highway Safety Manual's Crash Prediction Model for Rural Two-Lane Two-Way Roads in a Developing Country: A Case Study" Computational Research Progress in Applied Science & Engineering, CRPASE: Transactions of Civil and Environmental Engineering 7 (2021): 1-9.

M Haghani, R Jalalkamali, and M Berangi "Assigning Crashes to Road Segments in Developing Countries" In Proceedings of the Institution of Civil Engineers-Transport, vol. 172, no. 5, pp. 299-307. Thomas Telford Ltd, 2019.

A Mansourkhaki, M Berangi, M Haghiri, and **M Haghani** "A Neural Network Noise Prediction Model for Tehran Urban Roads." Journal of Environmental Engineering and Landscape Management 26, no. 2 (2018): 88-97.

CONFERENCE PROCEEDINGS:

M Haghani, and R Kluger "Developing a Shockwave-Based Queue Estimation Model to Quantify the Disruption Created by Emergency Vehicle Preemption in Perpendicular Approaches" Transportation Research Board 103rd Annual Meeting, 2024.

M Haghani, O Kresse, and R Kluger "Investigating the Recovery of a Coordinated Urban Arterial after Emergency Vehicle Preemption" Transportation Research Board 102nd Annual Meeting, 2023.

A Hosseinzadeh, **M Haghani**, R Kluger "Exploring Influencing Factors on Crash-related Emergency Response Time: A Machine Learning Approach" Transportation Research Board 100th Annual Meeting, 2021.